

INFORMATION TO USERS

This manuscript has been reproduced from the microfilm master. UMI films the text directly from the original or copy submitted. Thus, some thesis and dissertation copies are in typewriter face, while others may be from any type of computer printer.

The quality of this reproduction is dependent upon the quality of the copy submitted. Broken or indistinct print, colored or poor quality illustrations and photographs, print bleedthrough, substandard margins, and improper alignment can adversely affect reproduction.

In the unlikely event that the author did not send UMI a complete manuscript and there are missing pages, these will be noted. Also, if unauthorized copyright material had to be removed, a note will indicate the deletion.

Oversize materials (e.g., maps, drawings, charts) are reproduced by sectioning the original, beginning at the upper left-hand corner and continuing from left to right in equal sections with small overlaps.

Photographs included in the original manuscript have been reproduced xerographically in this copy. Higher quality 6" x 9" black and white photographic prints are available for any photographs or illustrations appearing in this copy for an additional charge. Contact UMI directly to order.

**Bell & Howell Information and Learning
300 North Zeeb Road, Ann Arbor, MI 48106-1346 USA
800-521-0600**

UMI[®]

**RELATIONSHIP OF CLOUDINESS TO NEAR SURFACE TEMPERATURE
OVER LAND AREAS OF THE NORTHERN HEMISPHERE**

A Dissertation Presented

by

BOMIN SUN

**Submitted to the Graduate School of the
University of Massachusetts Amherst in partial fulfillment
of the requirements for the degree of**

DOCTOR OF PHILOSOPHY

February 2001

Department of Geosciences

UMI Number: 3000350

UMI[®]

UMI Microform 3000350

Copyright 2001 by Bell & Howell Information and Learning Company.

**All rights reserved. This microform edition is protected against
unauthorized copying under Title 17, United States Code.**

**Bell & Howell Information and Learning Company
300 North Zeeb Road
P.O. Box 1346
Ann Arbor, MI 48106-1346**

© Copyright by Bomin Sun 2001

All Rights Reserved

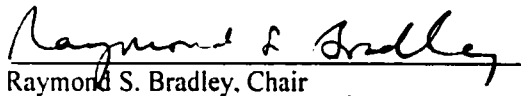
RELATIONSHIP OF CLOUDINESS TO NEAR SURFACE TEMPERATURE
OVER LAND AREAS OF THE NORTHERN HEMISPHERE

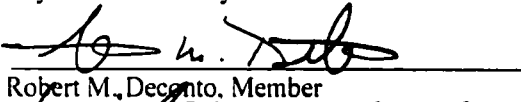
A Dissertation Presented

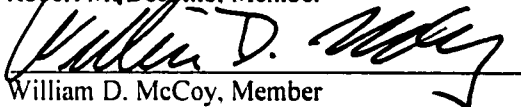
by

BOMIN SUN

Approved as to style and content by:

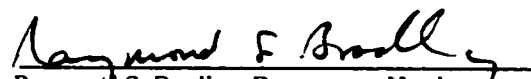

Raymond S. Bradley, Chair


Robert M. Deconto, Member


William D. McCoy, Member


Thomas T. Arny, Member


Pavel Ya. Groisman, Member


Raymond S. Bradley, Department Head
Department of Geosciences

DEDICATION

To my parents and wife

ACKNOWLEDGEMENTS

It is with my deepest gratitude that I thank my advisor Professor Ray Bradley for providing the opportunity to pursue the Ph.D. study here at University of Massachusetts, Amherst. I admire very much Ray's wisdom, scientific vision and broad knowledge, and appreciate greatly his generous mentorship. I also extend my heartfelt gratitude to Dr. Pasha Groisman, with whom I worked closely on cloud-related climate variability and change where my thesis focuses. I am impressed very much by Pasha's determined and efficient research style, and admire very much his expertise in climate research. I believe I shall always be grateful for their guidance and shall always appreciate the opportunity of working with them.

I also would like to express my gratitude to my other committee members for their reviews of the dissertation and helpful commentaries.

I like to take this opportunity to thank all the people in the Climate System Research Center for their continuous help and encouragement on both my study and life. Special thanks to Frank Keimig for his patient instruction on my English writing and pronunciation, and to Caspar Ammann for many stimulating discussions and conversations on various topics we are interested in.

I am also deeply thankful for the assistance and kindness provided by the people at National Climatic Data Center in Asheville, North Carolina, where I worked three summers as a visiting graduate student.

ABSTRACT

RELATIONSHIP OF CLOUDINESS TO NEAR SURFACE TEMPERATURE OVER LAND AREAS OF THE NORTHERN HEMISPHERE

FEBRUARY 2001

BOMIN SUN, B.S., HANGZHOU UNIVERSITY

M.S., INSTITUTE OF ATMOSPHERIC PHYSICS, CHINESE ACADEMY OF SCIENCES

Ph.D., UNIVERSITY OF MASSACHUSETTS AMHERST

Directed by: Professor Raymond S. Bradley

Relationship of cloudiness to near surface temperature over land areas of the Northern Hemisphere for the past several decades is assessed using the data from surface meteorological weather stations, satellite observations, and the NCEP reanalysis project.

The overall cloud relationship to near surface temperature is well represented by near surface humidity and surface conditions. Nighttime cloud-related surface warming decreases with the increase in near surface specific humidity. After cloud longwave-related temperature change and snow cover information are removed, one unit of cloud cover is empirically associated with a surface cooling of 0.59 K. The AMIP-1 models generally were able to reproduce the cold season cloud-temperature relationship, but not for the warm season and for the diurnal cycle.

The daytime cloud-related surface cooling over China and the contiguous U.S. generally strengthened, but slightly weakened over Canada and the former USSR during the post WWII period. Since the 1970s a prominent increase in atmospheric humidity has weakened cloud longwave effect on surface temperature (best seen at nighttime) over the extratropical land areas. Significant changes and a general redistribution of cloudiness occurred over the contiguous U.S. and the former USSR (south of 60°N) during the past forty to fifty

years. Low cloudiness increased over the contiguous U.S. while it decreased over the former USSR (south of 60°N). Total cloud amount and convective cloud frequency increased in both countries.

TABLE OF CONTENTS

	Page
ACKNOWLEDGEMENTS	v
ABSTRACT	vi
LIST OF TABLES	x
LIST OF FIGURES	xi
CHAPTER	
1. INTRODUCTION	1
2. OBSERVATIONAL DATA AND GCM RUNS.....	3
2.1 Observational Data	3
2.2 GCM Runs	6
3. METHODOLOGIES	7
3.1 Definition of the Cloud-Related Near Surface Temperature Change.....	7
3.2 Area Averaging Approach	8
4. RECENT CHANGES IN CLOUD TYPE FREQUENCY	10
4.1 Introduction.....	10
4.2 Cloudiness Observing Practice	11
4.2.1 GTS Reports versus National Archive Data.....	12
4.2.2 Characteristics of National Observing Practice.....	13
4.3 Cloud Type Data and Frequency Calculation.....	15
4.3.1 Cloud Type Data Description	15
4.3.2 Cloud Type Frequency Calculation	18
4.4 Recent Changes in Cloud Type Frequency.....	22
4.4.1 The Former USSR (south of 60°N).....	22
4.4.2 The Contiguous United States	29
4.4.3 Cloud Cover Intercomparison.....	41
4.5 Changes in Atmospheric Hydrological Cycle	45
4.6 Conclusions and Discussions.....	52

5.	CLIMATOLOGY OF THE CLOUD-RELATED NEAR SURFACE TEMPERATURE CHANGE: COMPARISON OF GCM SIMULATIONS WITH EMPIRICAL DATA.....	60
5.1	Extratropical Land Areas.....	61
5.1.1	Near Surface Temperature in the Presence of Clouds.....	61
5.1.2	Near Surface Humidity in the Presence of Clouds.....	65
5.2	Tropical Land Areas.....	67
5.3	Conclusions.....	71
6.	TEMPORAL VARIATIONS IN THE CLOUD-RELATED TEMPERATURE CHANGE.....	73
6.1	Introduction.....	73
6.2	Data Pre-processing.....	75
6.3	Parameterizations of the Cloud-Related Temperature Change.....	76
6.3.1	Nighttime.....	76
6.3.2	Daytime.....	88
6.3.3	General Model of the Cloud-Related Temperature Change.....	98
6.4	Trends of Temporal Variations in the Cloud-Related Temperature Change.....	99
6.5	Conclusions.....	105
7.	SUMMARY AND CONCLUSIONS.....	107
APPENDICES		
A.	AN INTERPOLATION SCHEME FOR DIURNAL VARIATION OF CLOUD TYPE FREQUENCY.....	111
B.	RELATIONSHIP BETWEEN THE TWO DEFINITIONS OF THE CLOUD-RELATED TEMPERATURE CHANGE.....	113
C.	EFFECTS OF THE ACCURACY OF THE NIGHTTIME CLOUD OBSERVATIONS ON THE ESTIMATES OF THE CLOUD-TEMPERATURE RELATIONSHIP.....	121
D.	CONTRIBUTION OF SURFACE AIR TEMPERATURE VARIATIONS TO NOCET CHANGES.....	124
E.	METHOD OF INSTRUMENTAL VARIABLE.....	125
	REFERENCES.....	127

LIST OF TABLES

Table		Page
4.1	Changes in components of the atmospheric hydrological cycle over the Asian part of Russia in summer during the period of 1936-1990. Statistically significantly trends are marked with * (0.05 level) and ** (0.01) level respectively	51
5.1	Specific humidity, q (g/kg) and cloud-related near surface temperature change, $OCET_1$ (K), in tropical regions based on observational data	70
6.1	Estimates of derivate $dNOCET/dq_{clear}$ for night- and daytime over four different countries and seasons.....	90
6.2	NOCET variance, D , and the variance of residual terms in Eqs. (6.5.1) and (6.5.2) ($K/tenth\ of\ cloud\ cover$) ² . ϵ are the residual terms of the monthly countrywide averaged NOCET estimates over the four countries under considerations; $\bar{\epsilon}$ are long-term time averaged values of ϵ	98

LIST OF FIGURES

Figure	Page
2.1 Map of surface weather stations used in this study	4
4.1 Nighttime cloudiness comparison between all observations and observations with good illumination. (A) high level cloud type frequency and (B) low level cloud amount.....	17
4.2 (A) 187 stations with at least 36-year records throughout 1949-1994 over the contiguous U.S. and (B) a subset of 127 stations with temporally homogeneous records throughout 1952-1992.....	20
4.3 (A) 223 stations over the FUSSR over the period 1936-1990 and (B) a subset of 55 stations with temporally homogeneous records throughout 1945-1990.....	21
4.4 Seasonal variations of total and low cloud amounts over the FUSSR south of 60°N. Linear trend at or above the 0.05 significance level is marked with a thin line	23
4.5 Seasonal frequency of stratiform clouds over the FUSSR south of 60°N. Any linear trend at or above the 0.05 significance level is denoted as a percentage change (relative to the mean over the period 1945-1990) per decade	24
4.6 Same as Fig. 4.5 except for (A) <i>Stratocumulus</i> and (B) <i>Stratus</i>	25
4.7 Same as Fig. 4.5 except for convection clouds (<i>Cu&Cb</i>).....	26
4.8 Same as Fig. 4.5 except for high level clouds	26
4.9 Same as Fig. 4.6 except from the frozen network (Fig. 4.3B).....	28
4.10 Changes in daytime annual mean total cloud amount (black line) and low cloud frequency (red line) over the contiguous U.S. The correlation coefficient (after the removal of linear trends) is 0.80	30

4.11	Changes in daytime seasonal low cloud amount and low cloud frequency. r is the correlation coefficient (after the removal of seasonal cycle).	31
4.12	Seasonal frequency of the occurrence of stratiform clouds over the contiguous U.S.. Any linear trend at or above the 0.05 significance level is denoted as a percentage change (relative to the mean over the period 1949-1994) per decade. The threshold of 2 tenths of total cloud cover is used to select cloud type records.....	32
4.13	Same as Fig. 4.12 except for (A) <i>Stratocumulous</i> and (B) <i>Stratus</i>	33
4.14	(A) seasonal frequency of occurrence of daytime <i>Cumulonimbus</i> area-averaged over the contiguous U.S. (B) same as A, except for the occurrence which was counted with total cloud cover greater than 2 tenths	34
4.15	Same as Fig. 4.12 except for high level clouds	36
4.16	Annual mean daytime frequencies of <i>Cumulonimbus</i> and high level clouds over the contiguous U.S.. The correlation coefficient (after the removal of the linear trends), r , is equal to 0.64.....	37
4.17	Same as Fig. 4.12 except from the frozen network (Fig. 4.2B).....	38
4.18	Spatial distribution of linear trend in cloud type frequency over the period 1952-1992. Black circle represents an upward trend while blank circle represents a downward trend. The value of the circle denotes the statistical confidence of the linear trend. For example, " ≥ 95 " indicates that the linear trend is at or above the 0.05 significance level. (A) stratiform and (B) <i>Cumulonimbus</i>	39
4.19	Intercomparison of monthly total cloud cover with daily average of three datasets: GBS00, HW99, and D2. R_{13} (R_{23}) is the correlation coefficient between D2 and GBS00 (HW99) calculated after the removal of the seasonal cycle	42
4.20	Comparison of annual total cloud amount between GBS00 and HW99, and between all observations and light observations in HW99. Light observations are selected based on the moonlight criterion suggested by Hahn et al. (1995)	44

4.21	Changes in annual number of days with precipitation and in frequency of low cloud types area-averaged over the contiguous U.S.. R^2 is the variance ascribed to the linear trend	46
4.22	Changes in the number of spring days with heavy precipitation and <i>Cumulonimbus</i> frequency over the southern U.S. including Texas, Louisiana, Mississippi, Arkansas, Oklahoma, and Kansas	47
4.23	Same as Fig. 4.22 except for the southeastern U.S. and for summer season.....	48
4.24	Changes in frequency of summer days with (heavy) precipitation and various cloud types over the Asian part of the FUSSR	49
4.25	Changes in convective cloud frequency at 1 PM and percent of daily heavy precipitation over the Asian part of Russia. R is the correlation coefficient	50
4.26	Changes in the lower tropospheric static stability over the FUSSR and the contiguous U.S. during spring	54
4.27	Same as Fig. 4.26 except for winter.....	55
4.28	Changes in near surface temperature over the contiguous U.S. and the FUSSR	57
4.29	Changes in daytime total cloud amount and near surface relative humidity over Agana (13.48°N, 144.80°E). The red curve is 12-month running mean. The green band represents El Nino event	58
5.1	Daily mean OCET comparison between the observational data and the AMIP runs. Unit: K. January and April.....	62
5.2	Same as Fig. 5.1 except for July and October	63
5.3	July OCET estimates over land areas from the CCC and the UIUC AMIP model runs and from the empirical data. Unit: K. Nighttime and daytime.....	64

5.4	Same as Fig. 5.1 except for mean daily OCEH (in percentage of the mean daily water vapor pressure: $100\%(H_{ave}-H_{clr})/H_{ave}$)	66
5.5	Regions where cloud-related temperature change shown in Table 5.1 is assessed. Mountainous stations spreading over three continents are not shown	69
6.1	Variations of winter nighttime near surface specific humidity under clear skies and normalized cloud-related temperature change (NOCET) (multiplied by -1) area-averaged over the contiguous U.S., Canada (south of 50°N), the FUSSR (south of 60°N), and china (east of 110°E). Correlation coefficients, R, are statistically significant at the 0.05 level	77
6.2	Same as Fig. 6.1 except for spring	78
6.3	Same as Fig. 6.1 except for summer	79
6.4	Same as Fig. 6.1 except for autumn	80
6.5	Same as Fig. 6.1 except for annual mean	81
6.6	Normalized nighttime cloud-related temperature change (NOCET) as function of near surface specific humidity and its functional approximation. Estimates are based on 2148 individual monthly NOCET values area averaged over the four countries of interest	83
6.7	Same as Fig. 6.6 except for NOCET ₁ on the y-axis and q _{overcast} on the x-axis. Estimates are based on 2688 individual monthly NOCET ₁ values area-averaged over the four countries in Fig. 6.6 and arithmetically averaged over the western tropical Pacific islands	86
6.8	Relationship between NOCET (multiplied by -1) and near surface specific humidity under clear skies area-averaged over the contiguous U.S. during summer for (A) nighttime and (B) daytime	89

6.9	Daytime normalized cloud-related temperature change (NOCET) and its decompositions. The x-axis represents the sine function of monthly mean noontime solar elevation. All the data points in this figure represent long-term (1972-1990) monthly mean area-averaged values over the four countries of interest.....	92
6.10	Relationship between snow cover extent and RT_1 (=daytime NOCET – $(0.16+0.98 (q_{clear})^{0.5})$). All the data points represent monthly mean area-averaged values over the four countries in consideration over the period 1972-1990.....	95
6.11	Relationship between snow cover extent and residual term, RT_1 . The black solid line represents RT_1 (the left y-axis) and the red dotted line represents snow cover extent (the right y-axis)	96
6.12	Residual term, RT_2 , for individual months of 1972-1990 area-averaged over the the four countries of interest. Here $RT_2 = NOCET - (0.98/\sqrt{q_{clr}} - 0.16) - 0.36 *snow$	97
6.13	Annual mean area-averaged time series of daytime (A) OCET and (B) NOCET over the four countries in consideration.....	100
6.14	Same as Fig. 6.13 except for (A) daytime total cloud amount and (B) daytime near surface specific humidity under clear sky condition	101
6.15	Variations of nighttime total cloud amount and OCET over the contiguous U.S. during summer.....	103
A1	A sensitivity test of summer 1 PM cloud cover time series to the change in observational time in 1966. Cloud amount was area-averaged over the former USSR south of 60N. The cloud amount measurements for the period of 1966-1990 were interpolated to the 1 PM observation times (used before 1966) using additional climatological diurnal cloud information. The result of this interpolation (thin solid line) and the original time series (dotted line) from Figure 2 of Sun and Groisman (2000) are shown. The trend in the interpolated time series is $-1.4\%/10$ yrs compared to $-1.1\%/10$ yrs in the original time series. The difference in trends is not statistically significant.....	112
B1	Relationship between various relevant elements of the nighttime cloud-related near surface temperature change in winters at the station Miami of Florida	115

B2	Same as Fig. B1 except for the station Springfield of Illinois.....	116
B3	Same as Fig. B2 except for daytime	117
B4	Example of the relationship between nighttime OCET and OCET ₁ . The formulas below the black solid line are the general conclusions on the relationship between nighttime OCET and OCET ₁	118
B5	Relationship between daytime OCET and OCET ₁	119
C1	Comparison of two sets of long-term nighttime (A) NOCET and (B) OCET estimates. Solid lines represent standard estimates. Dashed lines represent the estimates based only on the data that conform to the moonlight criterion	122

CHAPTER 1

INTRODUCTION

Clouds exert a dominant influence on the energetics of the Earth's climate through their albedo cooling effect and greenhouse warming effect. The interaction of clouds with radiation alters the surface-atmosphere heating distribution, which in turn drives atmospheric motion that is responsible for the redistribution of clouds. The key parameters of clouds within the context of cloud feedback include the macroscopic properties of clouds, such as cloud amount, cloud height, and cloud thickness, and the microphysical properties of clouds, such as number, size, shape, and phase of cloud particles. Due to the complexity of the multiscale nature of cloud formation and cloud-radiation interactions, the details of the interaction of clouds with the state of the climate system remain unclear and constitute one of the major uncertainties in climate modeling and prediction (Cess et al. 1996, 1997; Weare et al. 1996). Observations are therefore critical for a better understanding of the role of cloudiness in present, past, and future climate variations.

Recent field experiments, e.g., the Earth Radiation Budget Experiment (ERBE) (Barkstrom 1984), the International Satellite Cloud Climatology Project (ISCCP) (Rossow and Schiffer 1991), the Atmospheric Radiation Measurement Program (ARM) (Stokes and Schwartz 1994), and the Indian Ocean Experiment (INDOEX) (Ramanathan et al. 1995) have provided detailed information on cloud properties and atmospheric radiation fluxes, thus making important contributions to our understanding of the processes that lead to the present and perturbed cloud properties and of the role of clouds in the climate system (Wielicki et al. 1995). However, field experiments are too short in time for long-term cloud-related climate studies. Also, most of the recent cloud studies have focused on ocean areas (e.g., Weare 1994; Weaver and Ramanathan 1997; Norris 1999), where climate regime and cloud properties are

different from those over land areas (Kiehl 1994). The conventional surface weather station observing network provides a unique opportunity to explore longer-term cloud-climate relationships over the Earth's land areas, where surface warming has really happened. This research aims to understand the spatial distribution and the temporal variations of the cloud-related temperature change and to detect climate change signals through analyzing large scale changes in cloudiness over land areas of the Northern Hemisphere in the past several decades.

A physically based statistical approach is used to assess the portion of the change in near surface temperature that is related to cloud radiative effect. This approach was named in Groisman et al. (1996) as "overall cloud effect on near surface temperature" or OCET. OCET is defined as the difference of near surface temperature (T) between average (all) and clear sky or between overcast and average (all) weather conditions. The outline of this research is as follows. Chapter 2 describes the general characteristics of datasets used in this study, including observational data and seven general circulation model (GCM) runs. Detailed data processing procedures are described in individual chapters of 4-6. Chapter 3 presents the approach for defining the cloud-related near surface temperature change. An area averaging method, frequently used in this study, is also introduced in this chapter. Interdecadal changes in cloudiness, particularly the occurrence of different cloud types over the contiguous U.S. and the former Soviet Union (hereforth FUSSR) (south of 60°N), and their climatic implications are discussed in Chapter 4. Chapter 5 presents the observational climatology of the cloud-related temperature change over land areas of the Northern Hemisphere and its comparison with the simulation of the AMIP-1 GCMs on both seasonal and diurnal time scales. Interdecadal changes in the cloud-related temperature change for nighttime and daytime respectively with the emphasis on the impact of water vapor and snow cover on that temperature change are addressed in Chapter 6. The last chapter gives a summary and conclusions drawn from this research.

CHAPTER 2

OBSERVATIONAL DATA AND GCM RUNS

2.1 Observational Data

The major data set used in this study is from the conventional land surface weather station network (Fig. 2.1). This network has approximately 1,500 first-order meteorological weather stations distributed over land areas of the Northern Hemisphere including tropical islands, with a better than average spatial coverage over the contiguous U.S., southern Canada, Europe, eastern China, and the southern former USSR. This surface based dataset has been used to make the data-model comparison in Groisman et al. (2000) and is hereafter called the GBS00 dataset. In Figure 2.1, the black dots represent the stations with data observed by national meteorological services. So, the data over Canada, the U.S., China, the FUSSR, and some other countries are the conventional national archive records. The red triangles represent the stations with data collected through the Global Telecommunication System (GTS) and other supplementary weather networks. These stations are located mainly over subtropical and tropical regions (except over the western tropical Pacific islands). In general, national archive data have long records (i.e., 40-50 years in length) and contain few errors (national meteorological centers have performed all necessary quality check procedures and verifications before they release the data to the public). The GTS data have records available for scientific use only starting in 1971 over land and generally are considered less reliable than those delivered by national meteorological services in off-line mode (USAFETAC 1986). Also, the practices used to process GTS reports differ in several ways from those for national archive data (see Section 4.2.1 for details).

The time resolution of the GBS00 dataset is hourly/3-hourly/6-hourly, depending on which country the data come from. The meteorological elements of this dataset include total

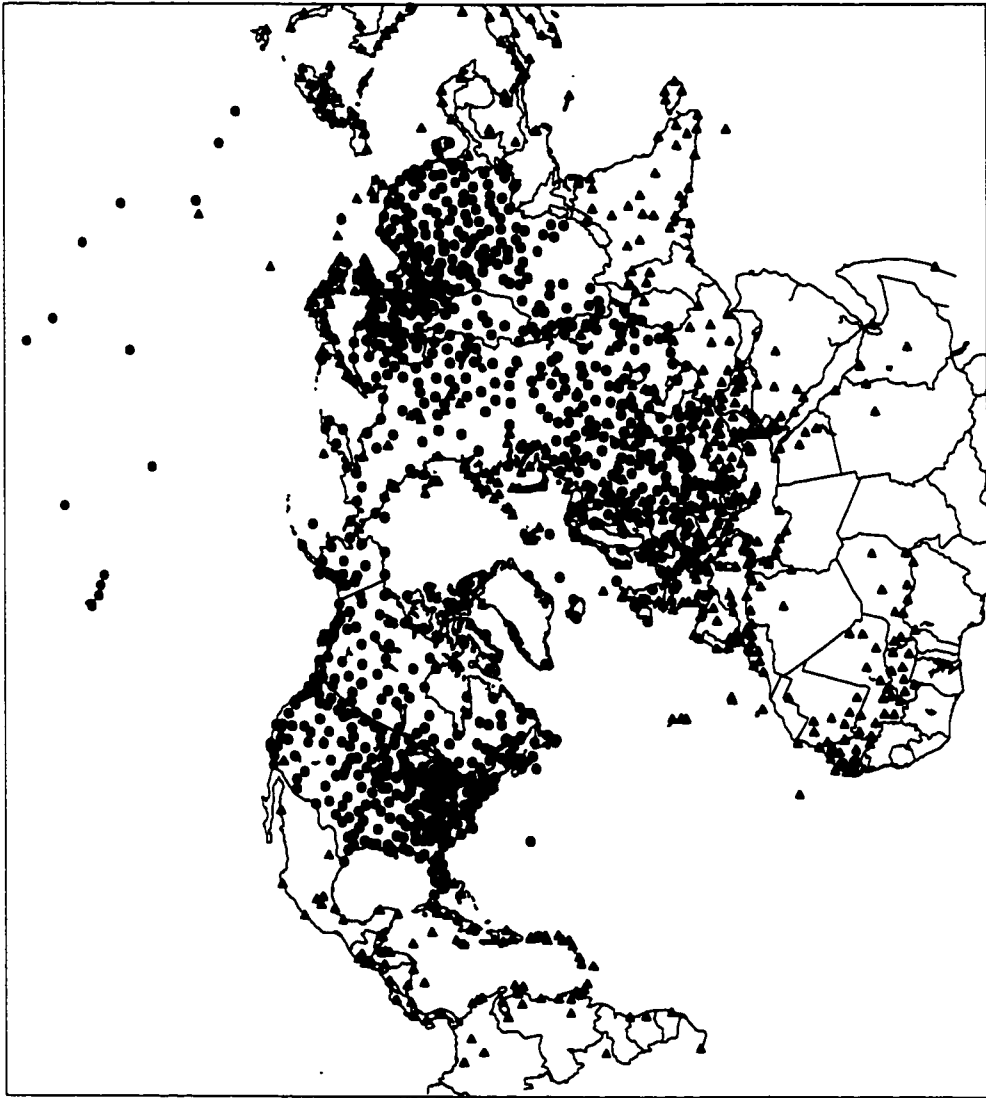


Figure 2.1 Map of surface weather stations used in this study. Dots represent stations with data from national meteorological services. Triangles show the stations with data from the Global Telecommunication System and/or supplementary networks.

and low cloud cover, and low, middle, and high level cloud types, as well as simultaneous measurements of near surface temperature, near surface relative humidity, near surface water vapor pressure, near surface air pressure, and other weather information. In most of the meteorological weather stations, near surface temperature was measured at 1.5 to 2 meters above ground. Currently low cloud amount and cloud type data are available only over the U.S. and the FUSSR (see Chapter 4 for detailed descriptions of cloud type data). The cloud characteristics in this network are human visual observations from the surface. In order to make sure that the national archive data (i.e., the data from the U.S., the FUSSR, and China) in GBS00 are reliable, an intercomparison is made between GBS00 national archive dataset, the Hahn and Warren (1999) dataset (HW99 afterwards), and the International Satellite Cloud Climatology Project (ISCCP) D2 (Rossow and Schiffer 1999) dataset. HW99 dataset is also made up of synoptic surface station records, but was collected through GTS. It covers 44 years (1952-1995) over the ocean but only 26 years (1971-1996) over land areas. ISCCP D2 dataset covers the whole globe but starts in 1983.

Daily rain gauge precipitation data of the U.S. (Easterling et al. 1998) and the FUSSR (Razuvaev et al. 1993) are used to indirectly corroborate the observed interdecadal changes in cloudiness including the frequency of occurrence of cloud types. NOAA satellite-derived gridded monthly snow cover frequency data (1972-1990) (Robinson et al. 1993) are employed to estimate the contribution of snow on the ground to the daytime cloud-temperature relationship. Each grid contains the estimate of snow occurrence frequency in a given month varying from 0 (no snow) to 1 (snow on the ground during the entire month). Lower tropospheric static stability (700 hPa-1000 hPa), calculated from the National Center for Environmental Prediction (NCEP) monthly potential temperature reanalysis data during 1958-1994 (Kalnay et al. 1996), is used to infer the significance of cloudiness changes over the U.S. and the FUSSR. The cloud-related surface air temperature change derived from the synoptic

surface observed dataset (that is, GBS00 dataset) is used to evaluate the performance of seven AMIP-1 climate models described in Section 2.2.

2.2 GCM Runs

The AMIP-1 experiment has been thoroughly described by Gates (1992). Climate models participating in this project were run with the same lower boundary conditions of sea surface temperature and sea ice observed during the period January 1979 through December 1988. The outputs of the following AMIP GCMs are used in this research's data-model comparison: the Goddard Institute for Space Studies (GISS), the Max Plank Institute, Germany (MPI), the University of Illinois at Urbana-Champaign (UIUC), the Main Geophysical Observatory, Russia (MGO), the Canadian Climate Center (CCC), the Laboratoire de Météorologie Dynamique, France (LMD), the U.S. National Meteorological Center (NMC). Which cloud schemes were used and how cloud fractions were determined in each model can be found in Philips (1996) and Weare et al. (1996). Near surface temperature was estimated at 2 meters above ground in the aforementioned AMIP models except in the GISS model, where near surface temperature was estimated at 10 meters above ground. There are some differences in time increments of the model outputs: GISS, UIUC, MGO, LMD, and NMC runs provide daily average data while the CCC output has a 6-hour time increment and the MPI output has 12-hourly average values. So the diurnal relationship between cloud cover and surface meteorological fields in GISS, MGO, LMD, MPI, and NMC model runs cannot be assessed. Thus the analyses of those five model outputs below are restricted to the mean daily relationship. The UIUC modeling group performed a special re-run of their AMIP experiment and stored the 6-hour increments of the July model output at the request of Dr. Pavel Ya. Groisman . The outputs from the CCC and the UIUC models are therefore used to make the data-model comparison of the diurnal cycle regarding the cloud-related temperature change.

CHAPTER 3

METHODOLOGIES

3.1 Definition of the Cloud-Related Near Surface Temperature Change

In this study, a physically based statistical method is used to define the cloud-related near surface temperature change.

$$\text{OCET} = E(T | \text{average sky}) - E(T | \text{clear sky}) \quad (3.1)$$

$$\text{OCET}_1 = E(T | \text{overcast sky}) - E(T | \text{average sky}) \quad (3.2)$$

Where E is a mathematical expectation or arithmetic averaging and T is near surface temperature. The cloud-related near surface temperature change is thus defined as the near surface temperature difference between average (all) and clear sky weather conditions (Eq. 3.1) or between overcast and average (all) weather conditions (Eq. 3.2). Formula (3.1) or (3.2) is similar to the one which Ramanathan (1987) proposed to define cloud radiative forcing:

$$\text{LW CRF} = F(\text{clear sky}) - F(\text{all sky}) \quad (\text{cloud longwave forcing})$$

$$\text{SW CRF} = Q(\text{all sky}) - Q(\text{clear sky}) \quad (\text{cloud shortwave forcing})$$

Where F and Q are longwave and shortwave radiative fluxes at the top of the atmosphere, respectively.

But, here in this study, near surface temperature is used instead of radiative flux. The cloud-related temperature change defined by Eq. 3.1 or 3.2 was named as "overall cloud effect on near surface temperature", or OCET, in Groisman et al. (1996). However, despite the name, OCET characterizes the *non-causal* relationship between total cloud cover and near surface temperature because near surface temperature change can indeed be caused by cloud radiative forcing (a combination of cloud albedo cooling effect and cloud longwave warming effect) but surface temperature change itself also can lead to a change in cloud parameters including cloud cover. Also, other processes or factors, such as surface heat fluxes and precipitation, can affect

OCET through modifying near surface temperature. Therefore, OCET actually represents “overall cloud relationship to near surface temperature”.

In this work, in order to get enough samples from each station, clear sky is defined as the case with cloud sky coverage smaller than or equal to 2 tenths, and overcast is defined as the case with cloud sky coverage equal to or larger than 8 tenths.

In practice, there are two ways to assess daily average OCET for each month. In Method 1, OCET for each hour of a given month is first calculated, and then averaged over the 24-hour period. In Method 2, mean daily values of total cloud amount (CL) and T are first calculated at each day of a given month, and clear or overcast days are then sorted to obtain monthly OCET. Both methods are applicable to the dataset with diurnal resolution, like the GBS00 data set. For the GCM runs with daily mean output, Method 2 is the only choice to estimate OCET. Groisman et al. (2000) indicated that there is no significant difference between these two methods in assessing monthly OCET but the absolute values of monthly OCET produced by Method 2 generally are larger than the one obtained by Method 1, particularly over high latitudes. In the data-model comparison (Chapter 5), Method 1 is used to calculate observational daily OCET while daily OCET in model runs is estimated using Method 2. Also, the different horizontal resolution between the observing network (Fig. 2.1) and the models and among the models makes it inappropriate to compare the details of the spatial OCET patterns. The data-model comparison in Chapter 5 is thus focused primarily on large-scale patterns of monthly OCET estimates.

3.2 Area Averaging Approach

Throughout this work, a polygon area-averaging approach, the Thiessen polygon method (Thiessen 1911; Kagan 1997), is widely used to estimate the countrywide area-averaged values of meteorological variables. To avoid spurious trends in area-averaged time

series due to temporal and/or spatial instability (or inhomogeneity) of station networks, a standard approach (cf., Jones et al. 1986; Kagan 1997) is used in the area-averaging procedure. First, for each station and each meteorological variable, we calculate the mean value for the reference period 1961-1990, which has the best data coverage at most stations. The stations that do not have at least 25-year record during 1961-1990 are excluded from further analyses. Over the contiguous U.S., the number of stations used in the area-averaging procedure increases from approximately 150 in the 1950s to approximately 190 in the 1980s. Over the FUSSR south of 60°N, the number of stations increases from approximately 125 in 1945 to 150 in 1955 and remains practically stable thereafter. Then, the anomaly from the mean of the reference period at each station is calculated, and then the anomalies and means over the country using the Thiessen method (Thiessen 1911; Kagan 1997) are averaged. The averaging weight of the Thiessen method at each datum point is proportional to the area of the blank region surrounding that datum point. Finally, the area-averaged value of a meteorological variable is created by adding the area-averaged anomaly with the area-averaged mean. Thus derived regional or countrywide time series of monthly values are converted into seasonal means: December, January, and February for winter; March, April and May for spring; June, July, and August for summer; and September, October, and November for autumn, and are analyzed in Chapters 4, 5, and 6. As an additional precaution against spurious trends due to temporal and spatial inhomogeneity of station networks, I compare the area-averaged time series from the “frozen” station network with that from the original network. The “frozen” network approach demands that only those stations which have continuous observations throughout the entire study period be used in area averaging.

CHAPTER 4

RECENT CHANGES IN CLOUD TYPE FREQUENCY

4.1 Introduction

Surface based cloud observations (Angell 1990; Henderson-Sellers 1989, 1992; Karl and Steurer 1990) indicate that total cloud cover has increased in many locations of extratropical land areas in the past several decades (except China, where total cloud cover decreased, see Kaiser 1998). The increase in total cloud cover has been cited as one of the major factors responsible for the observed decrease in the diurnal temperature range (Karl et al. 1993). Total cloudiness is composed of a variety of types, which are generated by different dynamic and thermodynamic processes and therefore have different optical properties and radiative effects. For example, different cloud types respond differently even to the same surface forcing (Norris and Leovy 1994; Fu et al. 1996). Moreover, low stratiform clouds tend to decrease while deep convective clouds tend to increase as sea surface temperatures rise in the eastern equatorial Pacific (Fu et al. 1996). A surface reported cloud type, identified by human observers, based on the cloud's specific morphological characteristic, generally is related to a particular atmospheric boundary layer structure (Norris 1998a,b). For example, the presence of deep convective clouds such as *Cumulonimbus (Cb)* indicates an intensive atmospheric upward heat and water vapor transport, and their penetration into a higher tropospheric level can be identified by the presence of high level clouds (*Cirrus, Ci, Cirrocumulus, Cc, and Cirrostratus, Cs*); the presence of low level stratiform clouds, *Stratocumulus, Sc, and/or Stratus (St)*, often reflects a relative stable stratification of the lower troposphere (Klein and Hartmann 1993; Norris 1998a). So, changes in the frequency of occurrence of surface observed cloud types signify intensification or weakening of atmospheric

convection and a change in the atmospheric thermal state, of which the contemporary *in situ* meteorological observational system lacks appropriate tools for a direct long-term monitoring.

This chapter presents estimates of interdecadal changes in cloud type frequency during the past forty to fifty years over the former USSR and the contiguous United States: cloud type changes for these regions and time scales have thus far not been investigated. The results of this chapter are expected to be helpful in detecting and understanding contemporary climate changes, which may manifest themselves in cloud type changes. The results from this chapter also can be used to validate global climate models, in which cloud processes and their effects still constitute one of the largest uncertainties (Cess et al. 1996; Weare et al. 1996; Groisman et al. 2000).

Due to historical reasons, cloudiness reporting practice is different in different data sources and among different countries. Section 1 introduces observing (processing) practices of cloud measurements in national weather services as well as in GTS. Section 2 presents the major characteristics of cloud type datasets for both the U.S. and the FUSSR, and the calculation method used to obtain cloud type frequency. The results of cloud type frequency changes over the United States and the FUSSR are given in Section 3. In this section, a comparison of cloudiness characteristics is shown among three cloud datasets: GBS00, HW99, and ISCCP D2. Section 4 presents changes in the atmospheric hydrological cycle accompanying the changes in cloudiness over both countries being considered. The conclusions and discussions are given in the last section.

4.2 Cloudiness Observing Practice

The practice of reporting/processing cloudiness for national archive data differs in several ways from that for the GTS reports such as HW99. Also, there are differences in cloud type reporting practice between the FUSSR and the U.S. national weather services. Below,

first, the major features of the GTS cloudiness reports are compared with those of the national archive data. Then, the cloudiness observing practice in the U.S. and the FUSSR' national meteorological services is described, respectively.

4.2.1 GTS Reports versus National Archive Data

1. units. Historically, two unit systems were used for quantitative characterization of cloud amounts: octas (eights) were used in most European countries while tenths were used in the U.S., Canada, the FUSSR, China, and several other countries. In 1947, the International Meteorological Organization (IMO) suggested the use of octas for marine ship observations in order to facilitate and unify the vital meteorological information exchange. Thus, from January 1949 most ships (but unfortunately not all, see Bajuk and Leovy 1998; Norris 1999) started to use octas to report cloud cover amount. These ship observations, collected through the International Code for Radio Weather Reports, constitute the major source of Comprehensive Ocean-Atmosphere Data Set (COADS) (Woodruff et al. 1987), from which the Hahn et al. (1986) and the HW99 ocean datasets developed.

However, despite the IMO recommendation to use octas for cloud amount unit, many countries including the U.S. and the FUSSR still used tenths in their national weather services. Over the U.S. station network, tenths were used until the introduction of the Automated Surface Observing System (ASOS) in the 1990s. The digitized GTS reports have been available in the U.S. for scientific use since 1971. These reports constitute the major source of the HW99 land cloud dataset in that country. In the GTS, the standard unit for cloud amount is octas. The GTS cloud amounts from the U.S., the FUSSR, and several other countries were recalculated by observers (often far from the observation sites) from the data in tenths. The total cloud amount comparison between GBS00 and HW99 (Figs. 4.19 and 4.20) suggests that the error from these man-made recalculations is negligible in the U.S. first order station dataset. Over the FUSSR,

HW99 data contains more than 2000 USSR stations for the 1970s and the 1980s, while only 109 stations were transferred *officially* by the USSR Hydrometeorological Service via GTS.

2. Cloud type reporting. In GTS cloud reports, if multiple cloud types were present at low, middle, or high cloud level during the time of observation, only one cloud type was permitted for each cloud layer description. The selection of which cloud type to be reported is made according to a hierarchy set up by the WMO synoptic code (1975). For example, if any *Cb* with anvil, *Cb* without anvil, *Sc* formed from the spreading of *Cu*, *Cu* and *Sc* mixed at different levels, or large *Cu* is present, it is reported as the low cloud type in that order of preference. However, the cloudiness observing practice in the U.S. and the FUSSR national weather services is different from that in the HW99 GTS cloud reports. The national cloudiness archives deliver a much less restricted list of cloud types: more than one cloud type (if present) is permitted for the report for each low, middle, or high cloud level.

4.2.2 Characteristics of National Observing Practice

National Weather Services of major countries have developed their own observational procedures and these procedures also change with time to meet the demands of the society. The cloudiness observing practice (or reporting policy) from different countries or from different time within a country thus may make the cloud type frequency hard to compare. For example, there is a distinctive difference between the cloud type reporting in the FUSSR and the U.S. weather services. Russian observers report all cloud types present in the sky at a given hour without associating them with specific layer heights. U.S. observers, on the other hand, first list up to four cloud layers and then assign to each of them a predominant single cloud type (if there is at least one cloud type present in the sky) using the WMO synoptic code. Thus, the U.S. observers may skip reporting *Cu* with small amount of sky coverage, which happens to be

at the same height as extensive *Sc* and/or deep *Cb*. This reporting practice difference suggests that *Cu* have much less chance of being reported over the U.S. than over the FUSSR.

During 1936-1990, the FUSSR cloud observing practice remained practically unchanged except for the shift in daily observational time schedule in 1966 (see next section for details). In the U.S. National Weather Service, before 1984 up to four cloud layers (not necessarily at different altitudes) were listed, but only one predominant cloud type for each layer was permitted per report. From 1984 to the ASOS introduction in the early 1990s, the U.S. station network applied the Microcomputer-Aided Paperless Surface Observations (MAPSO) to record cloud types. MAPSO is software that allowed observers to insert their observations directly on the digital media. During this process a set of consistency checks were conducted and interactively reported to observers. This quality control reinforces a strict following of manual instructions. In particular, it did not allow cloud layers to be at the same height but still ascribed only one cloud type (if present) to each altitude layer. This change might lead to reported low cloud layers more extensive in spatial coverage but smaller in number by neglecting insignificant cloud types in the WMO synoptic code. This reporting modification thus made it difficult to secure homogeneity of time series of the low cloud layer number and could cause artificial trends in cloud type frequency. In order to avoid this bias in the U.S. cloud type change analysis, only those cloud types that were reported with the total cloud cover greater than 2 tenths (i.e. when at least 30% of the sky dome has clouds) are counted. Thus, the cases with total cloud cover equal to or less than 2 tenths are excluded from the numerator (but not from the denominator) in our frequency calculation. However, the calculations (see, for example, Fig. 4.12) indicate that the use of 2 tenths of total cloud cover does not affect significantly the trend estimates of cloud type frequency but only lowers the value of the cloud type frequency.

4.3 Cloud Type Data and Frequency Calculation

4.3.1 Cloud Type Data Description

In this study, the following data were used: *in situ* cloud type observations from the first order station networks in the U.S. (see internet web site <http://www4.ncdc.noaa.gov/ol/documentlibrary/datasets.html#TD3280>; 272 stations with manual 3-hourly/hourly cloudiness observations during 1948 to 1994) and in the former USSR (Razuvaev et al., 1995, updated, see internet web site <http://cdiac.esd.ornl.gov/newsletr/fall98/ndp48.htm>; 223 stations with manual 3-/6-hourly cloudiness observations for the period from 1936 to 1990). There are two different reasons for not including the most recent U.S. and FUSSR cloud type observations in this analysis. The FUSSR synoptic data are available from the Global Telecommunication System (GTS), but the national archive data are better quality because they were more carefully pre-processed, quality-controlled, and serially complete (Razuvaev et al. 1995, updated). The Russian Meteorological Service routinely updates this archive. Thus in the future, the FUSSR cloud type information for the 1990s will become available for scientific use. After the early 1990s, the U.S. National Weather Service gradually introduced the Automated Surface Observation System (ASOS) into its conventional station network, thus destroying the homogeneity of time series of cloudiness characteristics because ASOS does not report high level cloud cover and cloud type information.

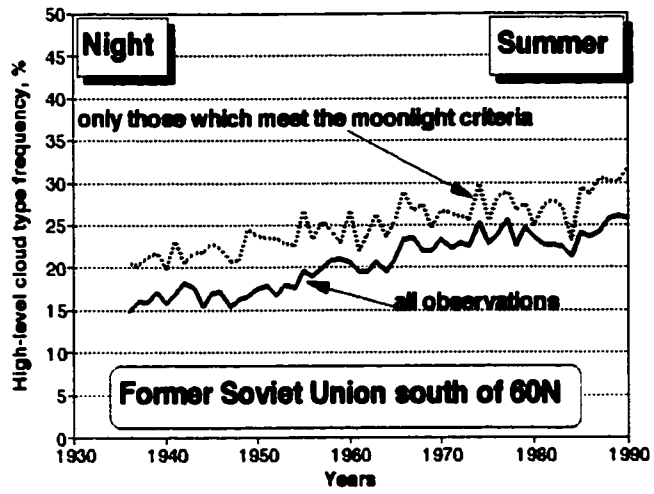
The FUSSR dataset contains information about total and low level cloud cover amounts (measured in tenths), and the occurrence of cloud types but no cloud type sky coverage information is given. In the FUSSR dataset, low cloud types with a base height below 2 kilometers were composed of *Cu*, *Cb*, *Sc*, *St*, *Nimbostratus (Ns)*, *Fractostratus (Fs)*, and *Fractocumulus (Fc)* clouds. Middle level cloud types with a base height between 2 and 6 kilometers include *Altostratus (As)* and *Altostratus (As)* clouds. High level cloud types

include *Ci*, *Cc*, and *Cs* with a base higher than 6 kilometers. These partitions and cloud type definitions are similar to those used in the International Cloud Atlas (WMO 1975) with one exception: *Ns* cloud type was included in low cloudiness (rather than in middle level cloudiness as recommended by the WMO synoptic code 1975). In the FUSSR data set, *Ns* is combined with two other bad-weather related cloud types *Fs* and *Fc*. To be consistent, this exception is preserved in the analysis of the U.S. cloud types.

In the U.S. dataset, 19 types of clouds are present. Before 1984, *Towering Cumulus* was reported as a type of *Cumulus*. Since 1984 it has been reported separately as *Towering Cumulus*. In this analysis these 19 individual types are combined into the following 7 groups: 1. *Cb* (including *Cumulonimbus* and *Cumulonimbus mammatus*), 2. *Cumulus* (including *Cumulus* and *Towering Cumulus*), 3. *Sc*, 4. *St*, 5. *Ns+Fs+Fc*, 6. Middle level cloud types (including *Altostratus*, *Altostratus lenticular*, *Altostratus castellanus*, and *Altostratus mammatus*), and 7. High level cloud types (including *Cirrus*, *Cirrocumulus lenticular*, *Cirrocumulus*, *Cirrocumulus lenticular*, *Cirrocumulus castellanus*, and *Cirrocumulus mammatus*). Total cloud cover (measured in tenths until July 1996) and cloud amount and height by layer are also present in this dataset. In the datasets of both countries, fog is not included in any of these low cloud types but is listed separately as an independent weather phenomenon.

Inappropriate illumination of clouds can bias the nighttime cloud detection, thus affecting the estimate of cloudiness climatology (Hahn et al. 1995). A case study indicates that nighttime cloud detection does not have a significant affect on cloudiness change (Figs. 4.1A and 4.1B). The use of a moonlight criterion largely reduces the sample size of nighttime observations by approximately 50%. This study presents therefore mainly the daytime cloud type frequency changes.

A



B

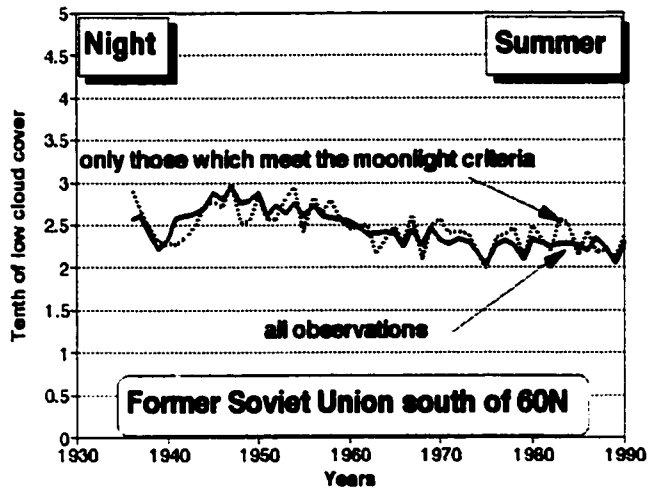


Figure 4.1 Nighttime cloudiness comparison between all observations and observations with good illumination. (A) high level cloud type frequency and (B) low level cloud amount.

4.3.2 Cloud Type Frequency Calculation

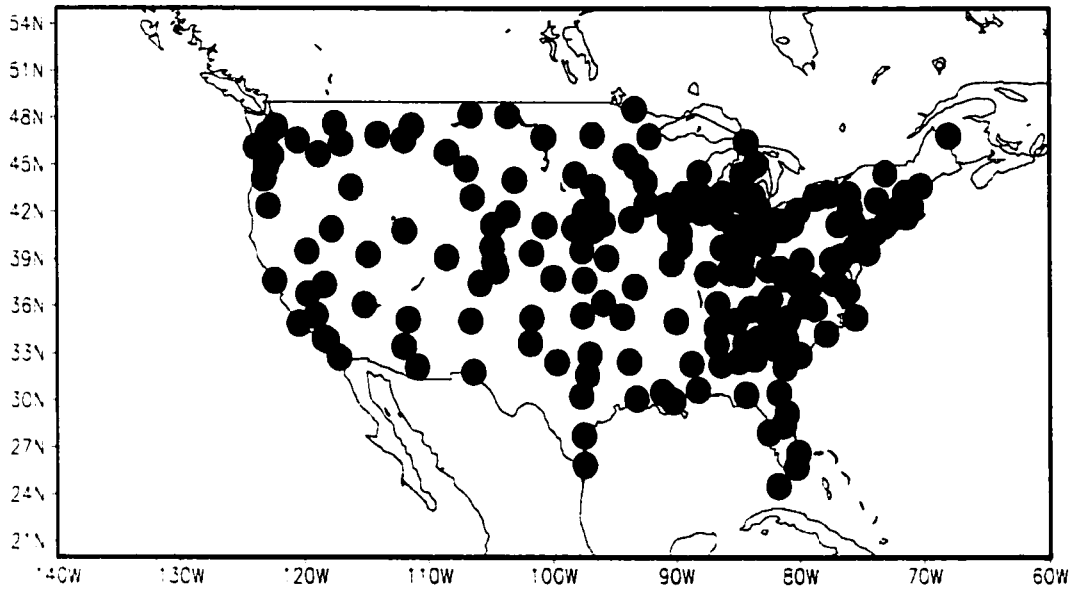
In this study, the frequency of occurrence of each cloud type at a given hour of the day is defined as a ratio ($\times 100\%$) of the number of days/observations with a given cloud type to the total number of days/observations with available cloud information including fog and clear sky (if present). If more than one cloud type was recorded during the time of an observation, each type is counted equally in the frequency calculation. Using this method, the frequency of occurrence of each individual cloud type as well as of a group of cloud type (i.e., low stratiform cloud type including *Sc* and *Sr*; middle level cloud type including *As* and *Ac*, and high level cloud type including *Ci*, *Cs*, and *Cc*) is calculated. The aforementioned seven cloud types are the focus of this frequency change analysis. Because of the difference in cloudiness reporting practice, the frequency of cloud type from Warren *et al.* (1986) and HW99 data *can and do* differ from the frequency in the national archive data of GBS00. For example, Sun and Groisman (2000) reported up to 70% countrywide average summer daytime frequency of convective clouds (*Cu* and *Cb*). Most probably this high value is due to frequent reports of *Cu* available in the comprehensive national archive (Razuvaev *et al.* 1995) but often omitted in the abridged synoptic reports used to compile the *Cu* climatology in Warren *et al.* (1986). (The typical *Cu* and *Cb* frequency in Warren *et al.* (1986) is about 25% and less than 15% respectively, thus the maximum frequency of *Cu and Cb* is less than 40%).

The temporal inconsistency in a cloud dataset could cause a serious bias in the trend analysis of cloud type frequency due to the diurnal variations of the occurrence of cloud type, especially the convective type of clouds. In 1966 the daily observational time schedule of the FUSSR meteorological network was switched from four times a day to eight times a day. This switch made the hours of observation incomparable over some time zones between the pre- and post- 1966 period: 1 PM of the local standard time was always available in all stations before 1966 but was available only at one third of total stations after 1966. *Over the FUSSR, the*

daytime cloud type frequency in this study is calculated from the observation at 1 PM. So, over those stations which did not have 1 PM measurement, two other measurements (noon and 3 PM, or 11 AM and 2 PM) are used to estimate the 1 PM value of cloud type and amount based on an interpolation procedure developed in Sun and Groisman (2000) (see Appendix A). In the U.S. station network, the meteorological data were saved every three hours per day from 1965 to 1981 (the 3-hourly daily schedule differs in different stations), but beyond this period the data are available with hourly resolution. Over the U.S., this temporal inhomogeneity is eliminated by the selection of the subset of daytime observations that have been conducted in the same daily time schedule throughout the entire period (1948-1994). For example, at station the Boston, the measurements at the local standard time of 7, 10, 13, and 16 were available throughout 1948-1994, and therefore were selected for analysis). Over the U.S, the hourly frequencies between 7 AM and 6 PM in each month are first calculated and then averaged to produce the daytime monthly cloud type frequency.

Practically, the entire station network was already in place over the U.S. in 1948 (Fig. 4.2A) and over the FUSSR in 1936 (Fig. 4.3A). The U.S. first order stations are well distributed over the contiguous land area with a higher density over the coasts. Currently 96% of the U.S. stations are at airports. A few of them (20) were transferred from downtown to airport sites after 1948. In order to keep station location homogeneity, the data from the downtown locations of these stations have been excluded from consideration in this analysis. Cloud type information from approximately 10 (in 1993) and 20 (in 1994) stations became unavailable because of the introduction of the ASOS at these stations. Over northern Siberia (north of 60°N) of the FUSSR, the station distribution is relatively sparse, so this region is not included in the cloud type analysis. In the European part of the FUSSR, a lot of missing values during World War II make it impossible to analyze cloudiness information, so this region during the period from summer of 1941 to autumn of 1944 is skipped in this study. Over the FUSSR south

A



B

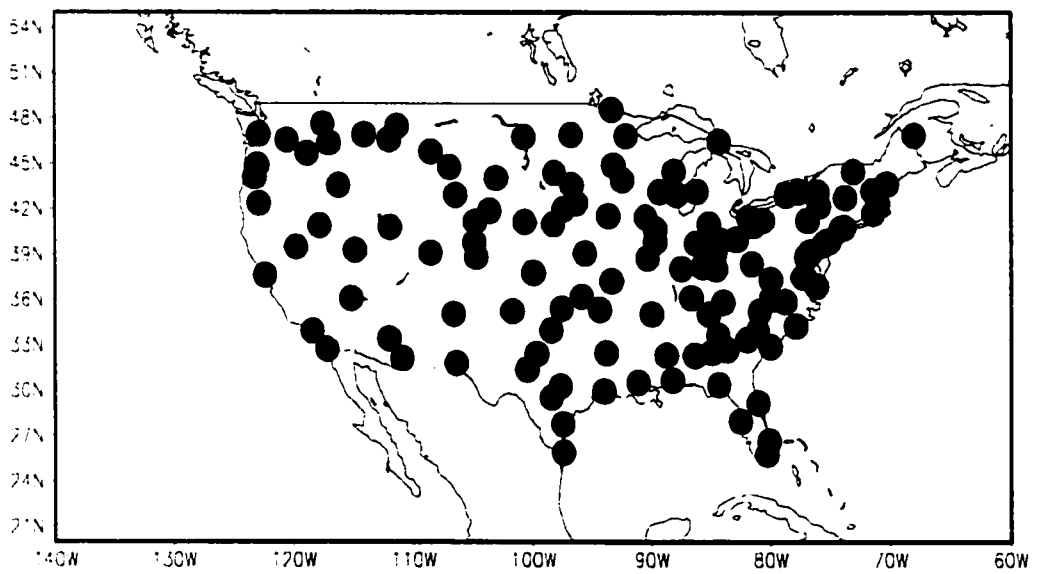
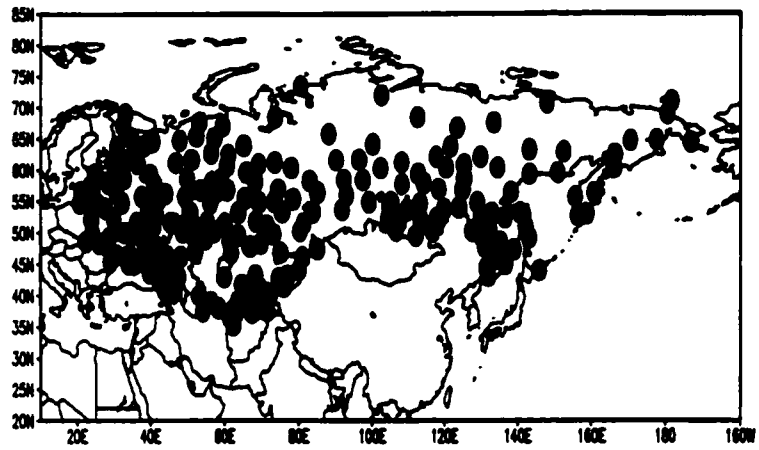


Figure 4.2 (A) 187 stations with at least 36-year records throughout 1949-1994 over the contiguous U.S. and (B) a subset of 127 stations with temporally homogeneous records throughout 1952-1992.

A



B

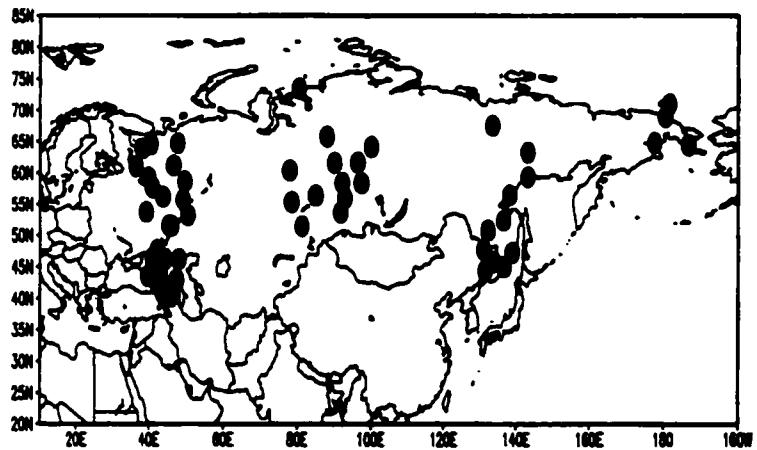


Figure 4.3 (A) 223 stations over the FUSSR over the period 1936-1990 and (B) a subset of 55 stations with temporally homogeneous records throughout 1945-1990.

of 60°N, the station network has the data availability of 78% over the period 1945-1990 (most of the missing values are in the nighttime). Also, in the period of the data overlap (1971-1990) this network has on average 20% more cloudiness information records for the same station than the recent release of the HW99 global cloudiness archive. So, the analysis of cloudiness change for the FUSSR is limited to the FUSSR south of 60°N.

The time series of cloudiness over the contiguous U.S. and the FUSSR (south of 60°N) shown below are calculated using the Thiessen polygon area-averaging method. To further avoid or reduce any spurious trends in area-averaged time series arising from any temporal and spatial inhomogeneity of the station network, the data are preprocessed in calculating the area-averaging (see Chapter 3). As an additional precaution against spurious trends, a comparison is made between the area-averaged cloudiness time series from the original station network (Fig. 4.2A and Fig. 4.3A) and the time series calculated from those and only those stations which have consistent and continuous measurements throughout the whole time period (Figs. 4.2B and 4.3B). It is noted that there are missing low cloud amount values particularly in summer months in the U.S. 127-station frozen network (see also Section 4.4.2). The following two subsections present recent changes in cloud type frequency over the FUSSR and the contiguous U.S. respectively. The comparison of our national archive cloud dataset (GBS00) with the HW99 dataset and the ISCCP D2 dataset is given in Section 4.4.3.

4.4 Recent Changes in Cloud Type Frequency

4.4.1 The Former USSR (South of 60°N)

The countrywide area-averaged time series of mean daily total and low cloud covers over the FUSSR south of 60°N for each season are shown in Fig. 4.4. The significance level of a linear trend in Fig. 4.4 is estimated using the Spearman Rank statistic test. This figure

Daily total and low cloud cover over the former USSR south of 60N

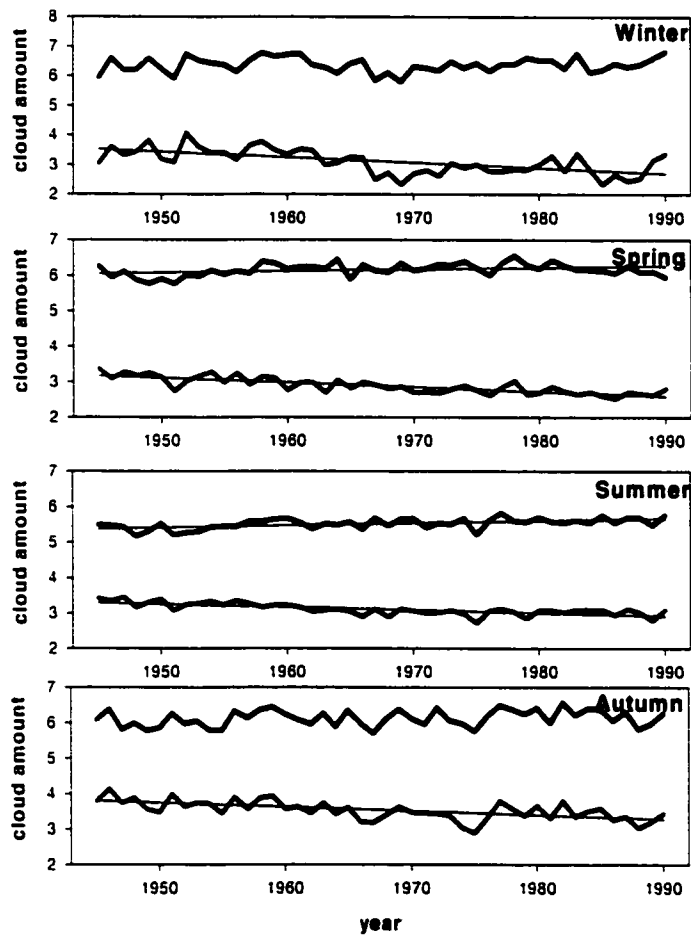


Figure 4.4 Seasonal variations of total and low cloud amounts over the F USSR south of 60°N. Linear trend at or above the 0.05 significance level is marked with a thin line.

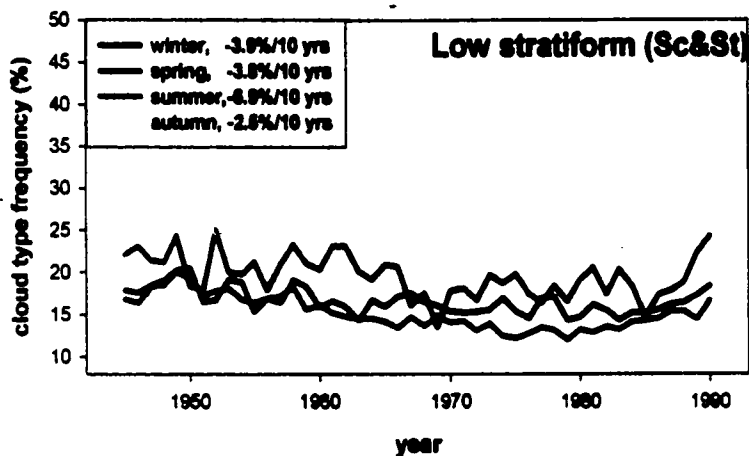
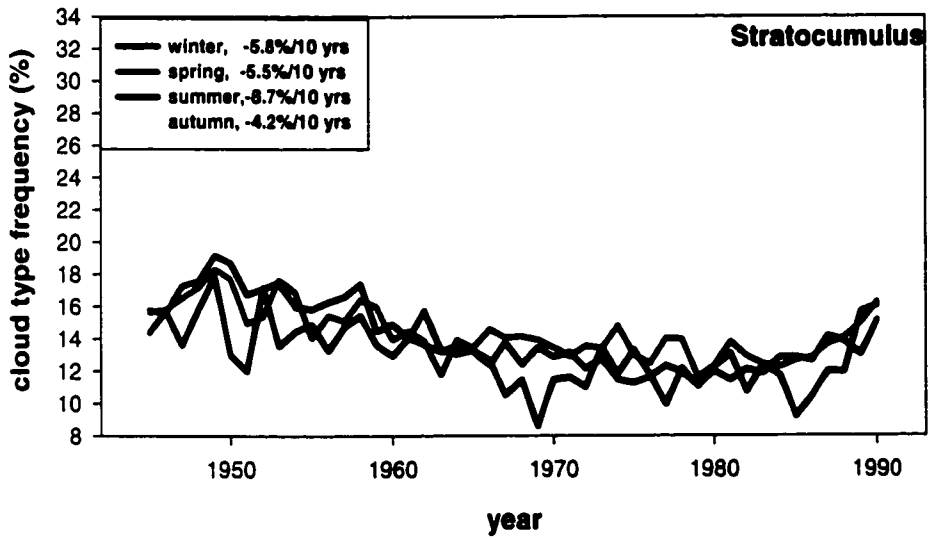


Figure 4.5 Seasonal frequency of stratiform clouds over the FUSSR south of 60°N. Any linear trend at or above the 0.05 significance level is denoted as a percentage change (relative to the mean over 1945-1990) per decade.

indicates that low cloud cover decreased over the period 1945-1990 in spite of increased (spring and summer) or stable (winter and autumn) total cloud amount. Sun and Groisman (2000) revealed that the decrease in low level cloud amount was much more pronounced in the European part of the country and West Siberia than the rest of the country.

Low cloudiness from surface observation is composed mainly of low stratiform clouds including *St* and *Sc*, and convective clouds including *Cu* and *Cb*. Fig. 4.5 presents the frequency change in stratiform clouds. Any linear trend of cloud type frequency in a season at or above the 0.05 significance level is denoted in the upper left corner of the figure as a percentage change (relative to the mean over the period 1945-1990) per decade. Despite a slight upward trend in the 1980s, the frequency of stratiform clouds exhibited a significant decrease in each season during 1945-1990. Sun and Groisman (2000) indicated that the frequency of the combination of *Ns*, *Fs*, and *Fc*, bad weather associated clouds, exhibited significant negative

A



B

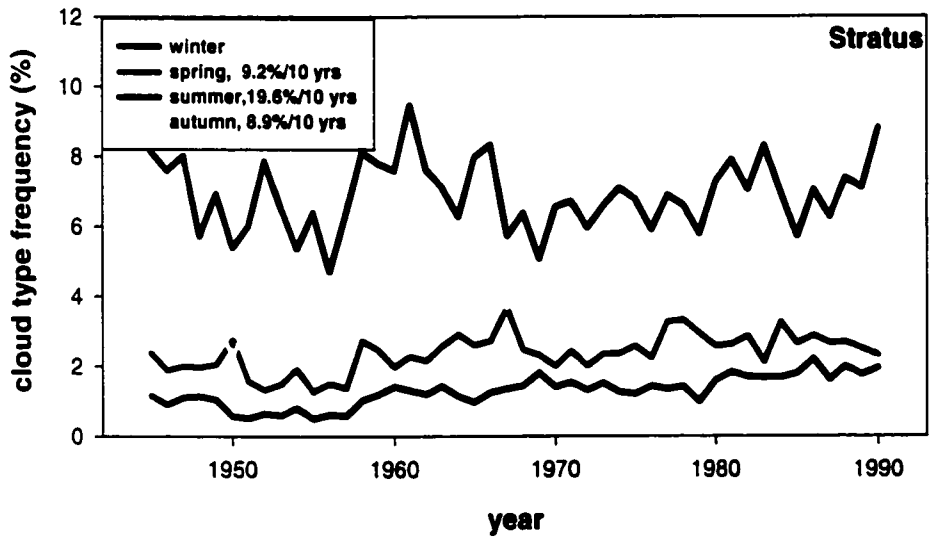


Figure 4.6 Same as Fig. 4.5 except for (A) *Stratocumulus* and (B) *Stratus*

Seasonal frequency of daytime Cu&Cb

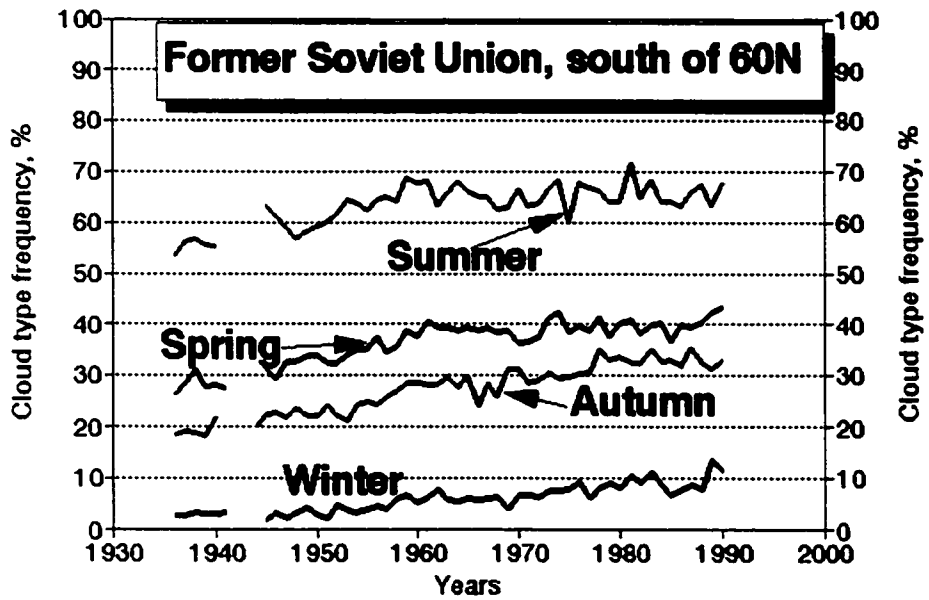


Figure 4.7 Same as Fig. 4.5 except for convective clouds (*Cu&Cb*).

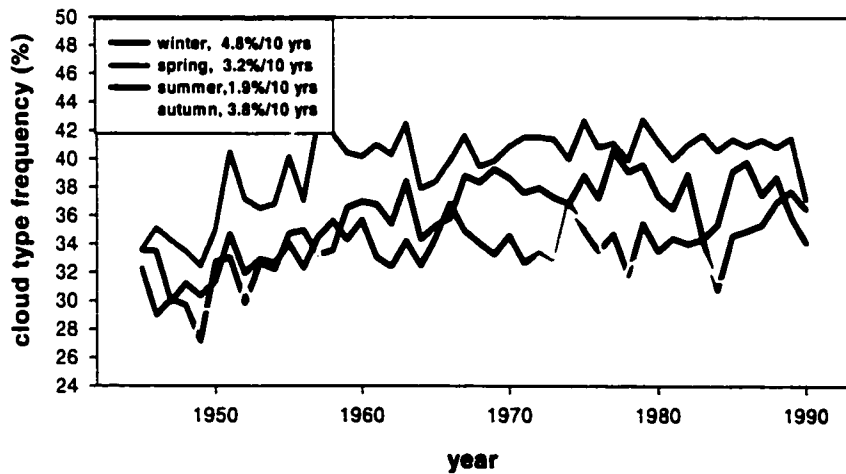


Figure 4.8 Same as Fig. 4.5 except for high level clouds.

trends in all seasons over the FUSSR over the period 1945-1990. But the frequency of the occurrence of $Ns+Fs+Fc$ (around 7.5% for annual mean) is much smaller than that of low stratiform clouds ($Sc&St$) (around 17.5% for annual mean).

The decrease in frequency of stratiform clouds shown in Fig. 4.5 was caused by the decrease in frequency of Sc (Fig. 4.6A) because the St frequency exhibited an increase in each season except winter over the period 1945-1990 (Fig. 4.6B).

Fig. 4.7 shows the changes in frequency of convective type of clouds, $Cb&Cu$. A significant increase in frequency of convective clouds in each season during the past several decades is impressive and implies a significant intensification of convective processes over the FUSSR. The Cu frequency (not shown) does not exhibit a significant trend over the period 1945-1990, and starting from the 1960s the Cu frequency decreased in all seasons. So, the increase in frequency of convective clouds shown in Fig. 4.7 results primarily from the increase in frequency of Cumulonimbus (Cb). Figure 4.7 also shows that the frequency of convective clouds is relatively stable (in summer) or trends slight upward after 1960. The rapid increase in the frequency before 1960, particularly in summer, thus largely contributes to the upward trend over the period 1945-1990.

Figure 4.8 shows that in addition to the increase in frequency of convective clouds, the frequencies of middle (Fig. 5 in Sun and Groisman 2000) and high level clouds also increased. Similar to the change in the frequency of convective clouds (Fig. 4.7), the frequency of high level clouds also shows an abrupt increase before the 1960s but remained practically stable afterwards. Over the contiguous U.S., a similar pattern of increase in frequency in both Cb and high clouds is found. Possible explanations for this increase are given in next section.

As mentioned before, area-averaged cloudiness time series can be biased by the instability of the station network, whether the instability is caused by a change in the number of stations with time and/or a discontinuity in the data record. In order to make sure that the time

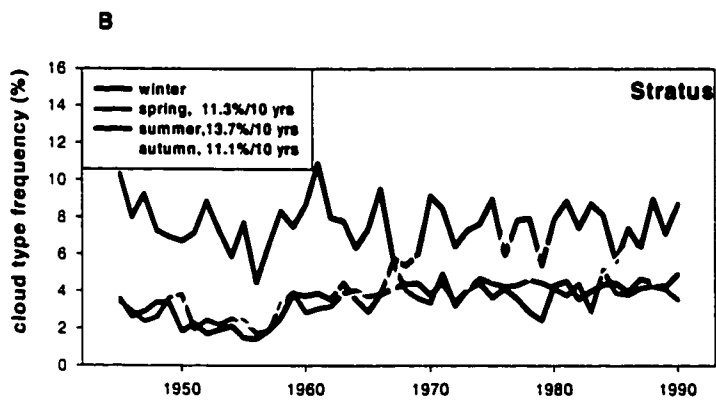
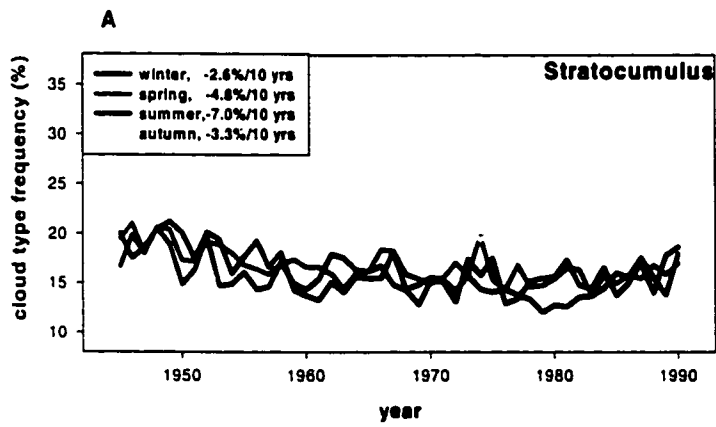


Figure 4.9 Same as Fig. 4.6 except from the frozen network (Fig. 4.3B).

series shown in Figs. 4.4-4.8 are reliable, I compare them with those calculated from the 55-station "frozen" network (Fig. 4.3B). All the station data from this network are temporally homogeneous throughout 1945-1990. Figs. 4.9A and 4.9B are examples of the arithmetically averaged time series of *Sc* and *St* based on the data from 38 stations (south of 60°N) of that network. The frequencies of *Sc* and *St* in all seasons except autumn (for *Sc*) show similar directions and percentage changes to those in Fig. 4.6. The results from the frozen network indicate that the area-averaging time series are not affected by the biases arising from any temporal and/or spatial inhomogeneity in the original FUSSR station network (Fig. 4.3A).

In summary, over the FUSSR south of 60°N over the period 1945-1990, low cloud amount decreased in spite of an increase in total cloud amount. The frequency of *Stratocumulus* clouds decreased while the frequency of *Stratus* increased. Low stratiform cloud (*Sc&St*) frequency still exhibited an upward trend. A rapid increase before the 1960s in the frequency of convective clouds (*Cu&Cb*) largely led to the upward trends in these cloud frequencies over the period 1945-1990, particularly in summer. However, in other seasons, the frequency of convective clouds still showed gradual increase after the 1960s. With the increase in convective cloud frequency, the occurrence of high level cloud increased.

4.4.2 The Contiguous United States

Over the contiguous U.S., a significant jump in 1984 occurred to the low cloud amount dataset: the values of low cloud amount after 1984 is systematically lower than those before 1984. We do not know the reason(s) for this data value discontinuity but the lower low cloud amount after 1984 may be related to the introduction of MAPSO to the U.S. station observing system in 1984. In this section, the low cloud amount data before 1984, combined with the low cloud type data, is thus used to infer the change in low cloud amount during the post WWII period.

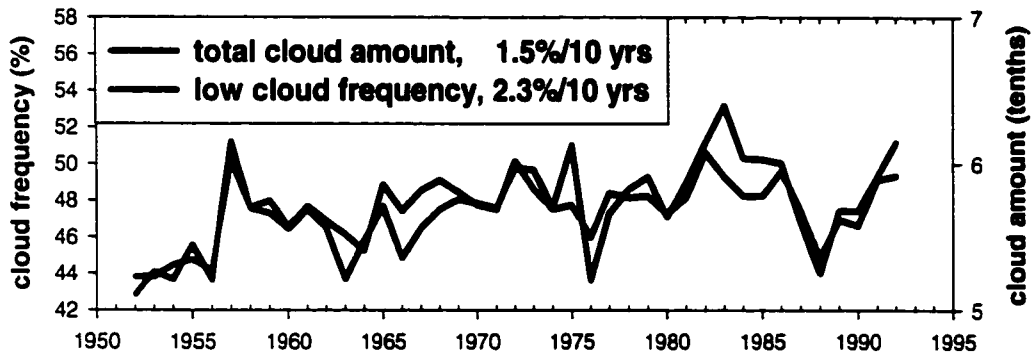


Figure 4.10 Changes in daytime annual mean total cloud amount (black line) and low cloud frequency (red line) over the contiguous U.S.. The correlation coefficient (after the removal of linear trends) is 0.80.

Figure 4.10 shows the changes in daytime annual mean total cloud amount and low cloud frequency over the contiguous U.S. The time series presented in Fig. 4.10 (and also in Fig. 4.11) are calculated from the 127-station network (Fig. 4.2B), and they are very similar to those calculated from the original 182-station network (Fig. 4.2A). Both elements shown in Fig. 4.10 exhibit significant upward trends. The cross correlation coefficient between them after the removal of their linear trends reaches 0.80. The upward trend in low cloud frequency is well supported by the increase in precipitation event (Fig. 4.21).

Changes in low cloud amount (black line) and low cloud frequency (red line) before 1984 are shown in Fig. 4.11. They match well with each other in terms of both interdecadal and annual time scales. The cross correlation between them after the removal of linear trend is significant in all seasons except summer. The low annual correlation in summer probably is

Contiguous United States. Daytime Low cloud amount Vs. Low cloud frequency

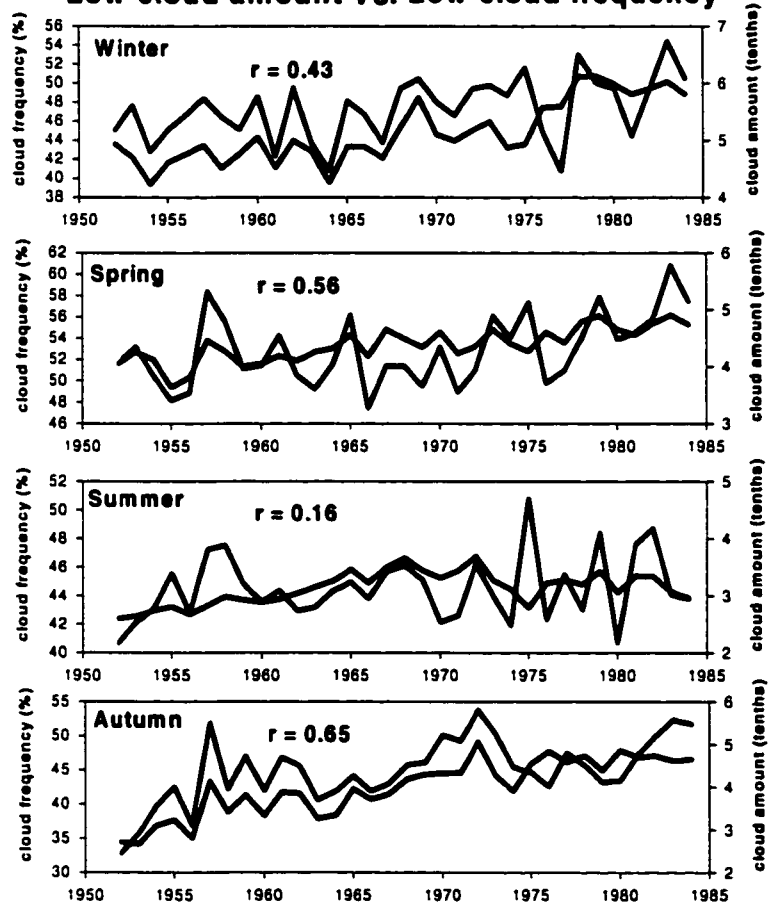


Figure 4.11 Changes in daytime seasonal low cloud amount and low cloud frequency. r is the correlation coefficient (after the removal of seasonal cycle).

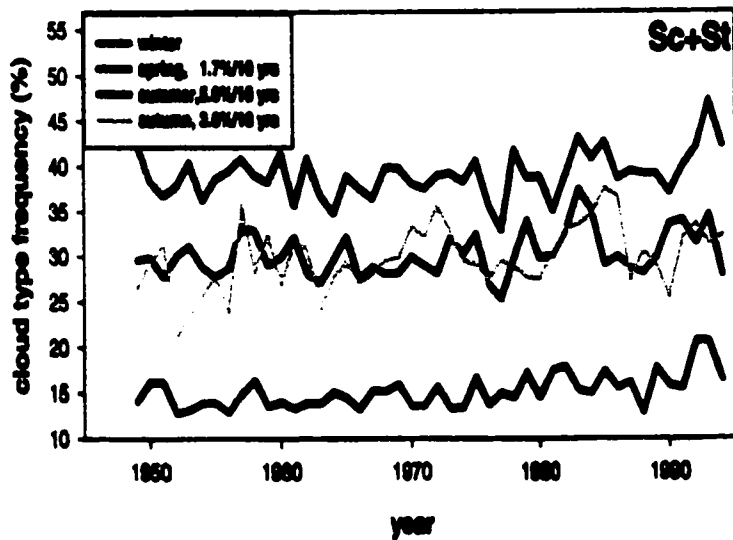


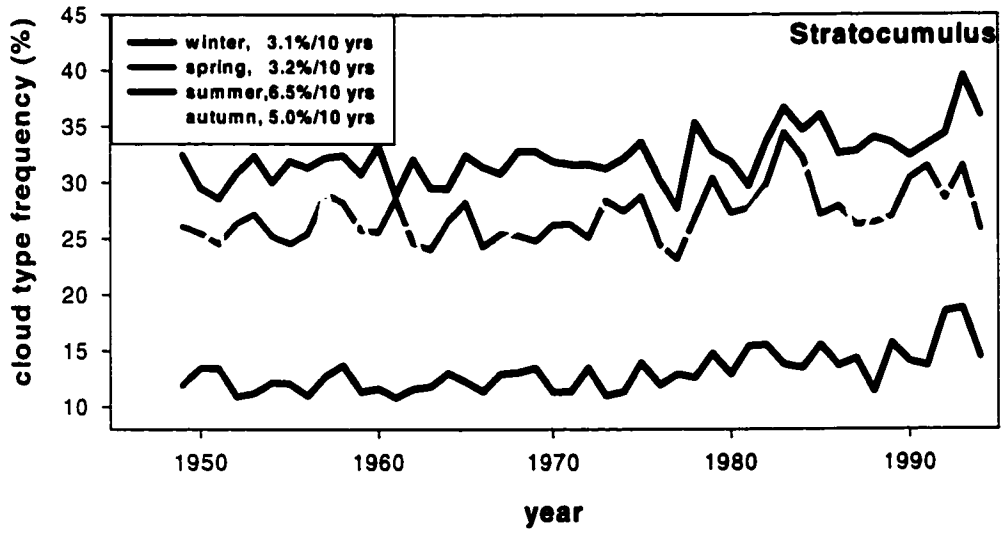
Figure 4.12 Seasonal frequency of the occurrence of stratiform clouds over the contiguous U.S.. Any linear trend at or above the 0.05 significance level is denoted as a percentage change (relative to the mean over the period 1949-1994) per decade. The threshold of 2 tenths of total cloud cover is used to select cloud type records.

due to too many missing values in the low cloud amount data. Anyhow, Figs. 4.10 and 4.11 indicate that over the contiguous U.S., with the increase in total cloud amount, low cloud amount is likely to increase as well during the post WWII period.

In contrast to the decrease in frequency of low stratiform clouds over the FUSSR (Fig. 4.5), the frequency of low stratiform clouds over the contiguous U.S. exhibits a significant upward trend over the period 1949-1994 in spring, summer and autumn (Fig. 4.12). The winter frequency of stratiform clouds has also increased but only since the late 1970s.

The upward frequency of stratiform clouds shown in Fig. 4.12 was caused by the frequency of *Sc* (Fig. 4.13A). The *St* frequency shows a downward trend (Fig. 4.13B).

A



B

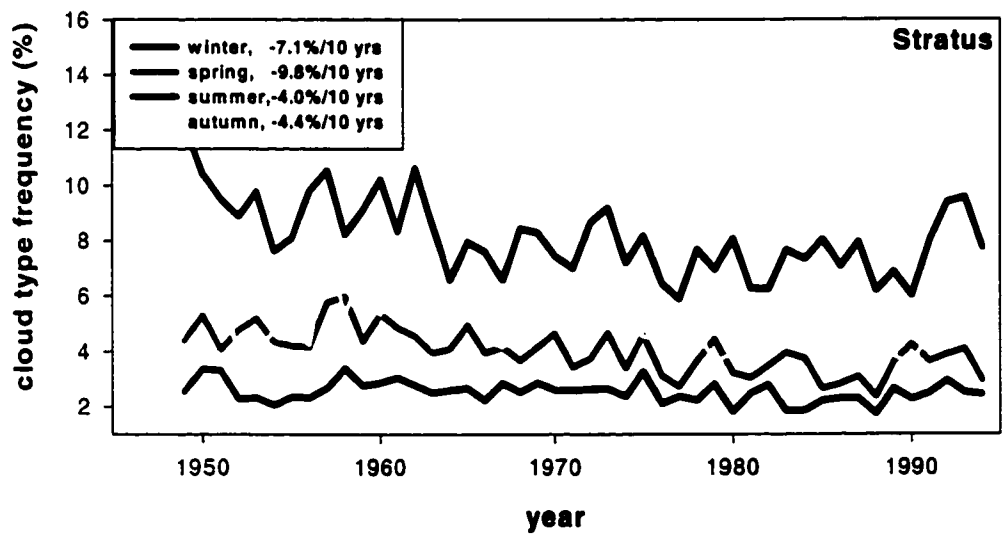
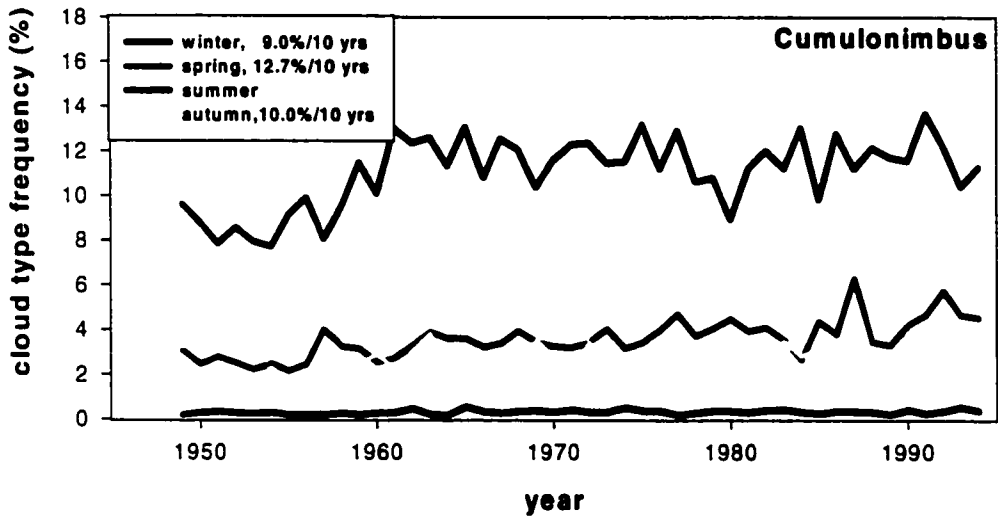


Figure 4.13 Same as Fig. 4.12 except for (A) *Stratocumulus* and (B) *Stratus*

A

Seasonal frequency of daytime *Cb* (%) with total cloudiness greater than 2 tenths



B

Seasonal frequency of daytime *Cb*, %

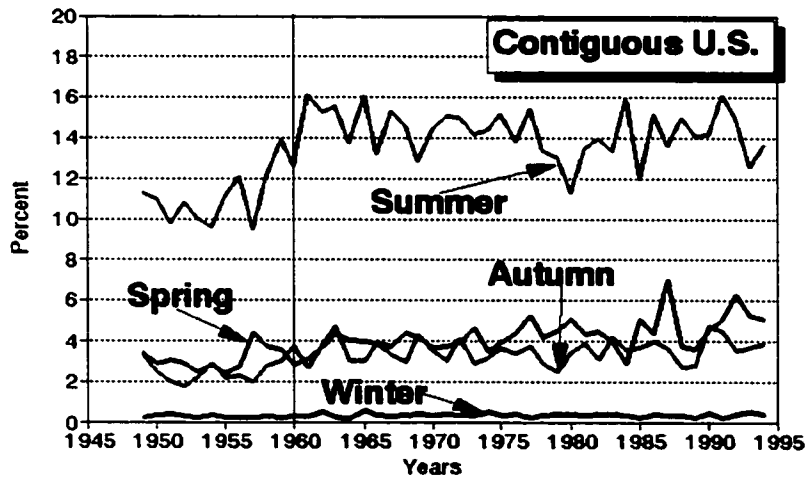


Figure 4.14 (A) seasonal frequency of occurrence of daytime *Cumulonimbus* area-averaged over the contiguous U.S. (B) same as A, except for the occurrence which was counted with total cloud cover greater than 2 tenths.

Over the contiguous U.S., the frequency of *Ns* and the combination of *Ns*, *Fs*, and *Fc*, increased, but the frequency of *Cu* decreased not shown. The decrease in *Cu* was caused mainly by the decrease in fair weather *Cu* (Sun et al. 2000). Fig. 4.14 shows the frequency change in *Cumulonimbus* clouds (*Cb*) for each season. Similar to the change in frequency of convective clouds over the FUSSR (south of 60°N), the U.S. *Cb* frequency exhibits an abrupt increase before the 1960s, leading to a significant upward linear trend in each season over the period 1949-1994. However, in autumn and spring, the *Cb* frequency still shows a (slow) upward trend after the late 1960s.

The upward jump in the *Cb* frequency around the year 1960, particularly in summer, needs careful assessment. A detailed analysis of the geographic distribution of the *Cb* frequency change indicated that the lower frequency of summer *Cb* frequency in the 1950s was confined only to the southern part of the contiguous U.S., while in Midwestern states the *Cb* frequency was the highest during the 1950s compared to the following decades. From the precipitation and stream flow data, Karl and Koscielny (1982) and Groisman et al. (2000) show that the southern regions indeed experienced drought in the 1950s (cf., Figs. 4.22 and 4.23). This independent evidence confirms that the low countrywide *Cb* frequencies in the 1950s are likely to be real.

Over the contiguous U.S., the frequency of high clouds (Fig. 4.15) shows a strong upward trend in each season throughout the period 1949-1994, particularly before the 1960s as seen over the FUSSR (Fig. 4.8), while the frequency of middle level clouds exhibits a negative trend over the period 1949-1994 (not shown).

The sky coverage and the occurrence of high clouds can be biased if the sky is obscured by low level clouds. One can argue that the decrease in the stratiform cloud activity over the FUSSR may make it easier for surface observers to see the clouds with high elevations that otherwise are obscured by low cloudiness. Although the increase in the frequency of

convective cloudiness can be considered as supporting information for the increase in the frequency of high clouds over the FUSSR, we refrain from such as an interpretation of the increase in high level cloudiness over this country. Over the contiguous U.S.. the increase in convective cloud frequency has been accompanied by an increase in high level and stratiform low cloudiness. In such a situation it should be more difficult for surface observers to see high clouds. But, this study reveals a continuous increase in high level cloud frequency in the past forty-five years. Therefore the observed increase in the frequency of high clouds, at least over the contiguous U.S. is likely to be real.

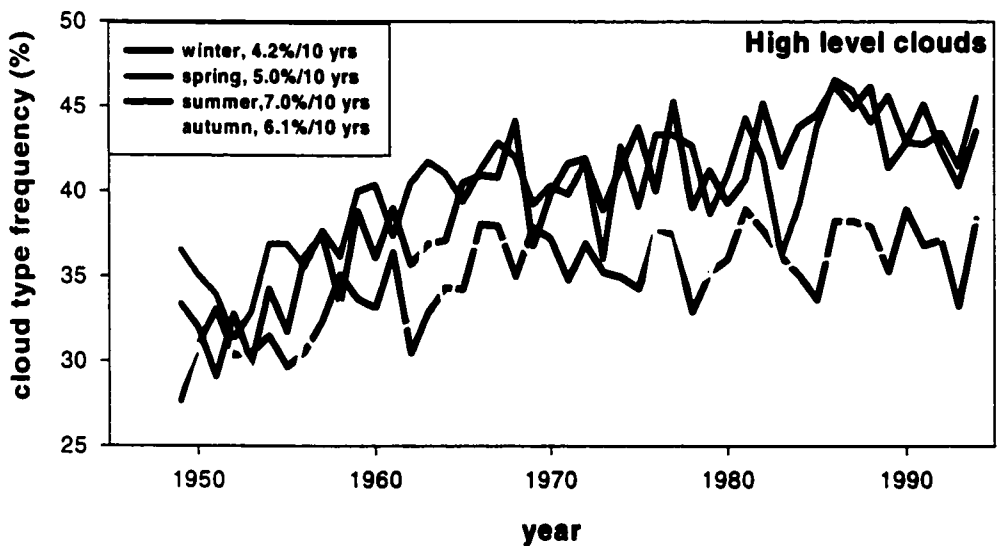


Figure 4.15 Same as Fig. 4.12 except for high level clouds.

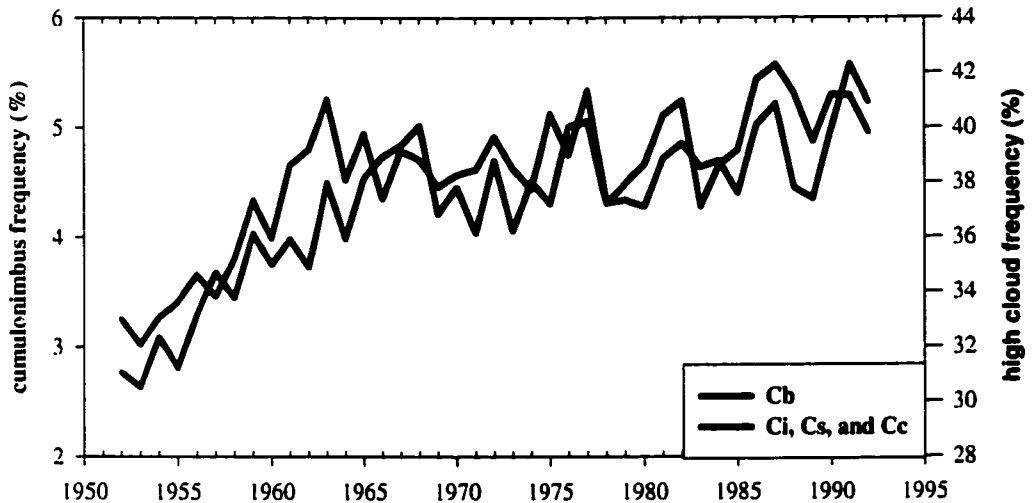


Figure 4.16 Annual mean daytime frequencies of *Cumulonimbus* and high level clouds over the contiguous U.S.. The correlation coefficient (after the removal of the linear trends), r , is equal to 0.64.

Figure 4.16 shows the variations of daytime *Cu* frequency and high level cloud frequency over the contiguous U.S.. The high consistency of variations between them indicates that the formation of high level clouds over middle latitude land areas may be related to strong convective activity, which transports low level moisture upward. The observed increase in the frequency of high clouds shown in Figs. 4.8 and 4.15 therefore may be (partly) caused by an increase in stronger convective processes as supported by the increase in the frequency of low level convective cloud types. Also, other factors can affect the formation of high level clouds. The increase in high-level cloud frequency, especially over the U.S. and the FUSSR, and especially between 1950 and the early 1970s, may be (partly) due to an increase in the

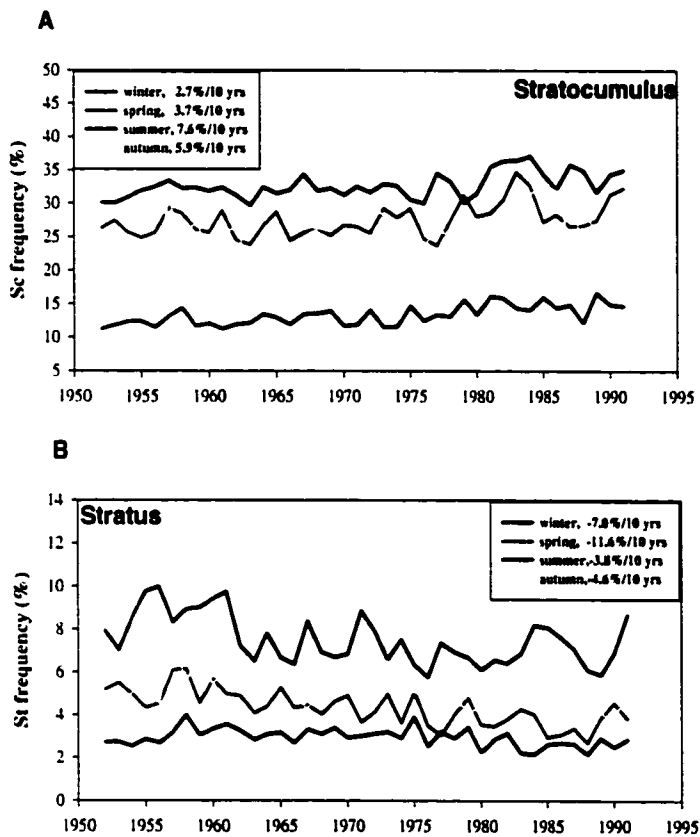
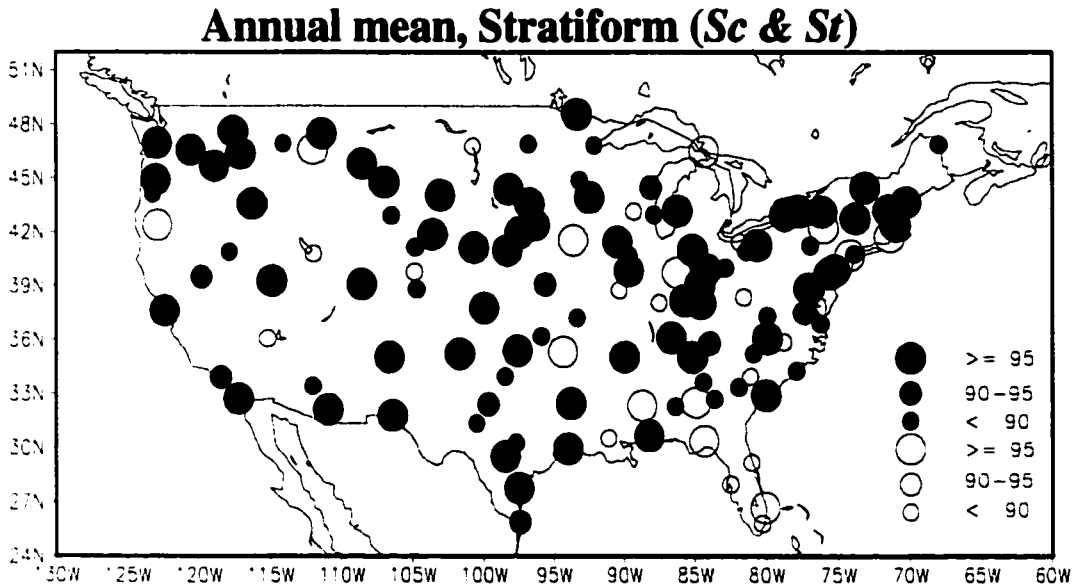


Figure 4.17 Same as Fig. 4.13 except from the frozen network (Fig. 4.2B).

A



B

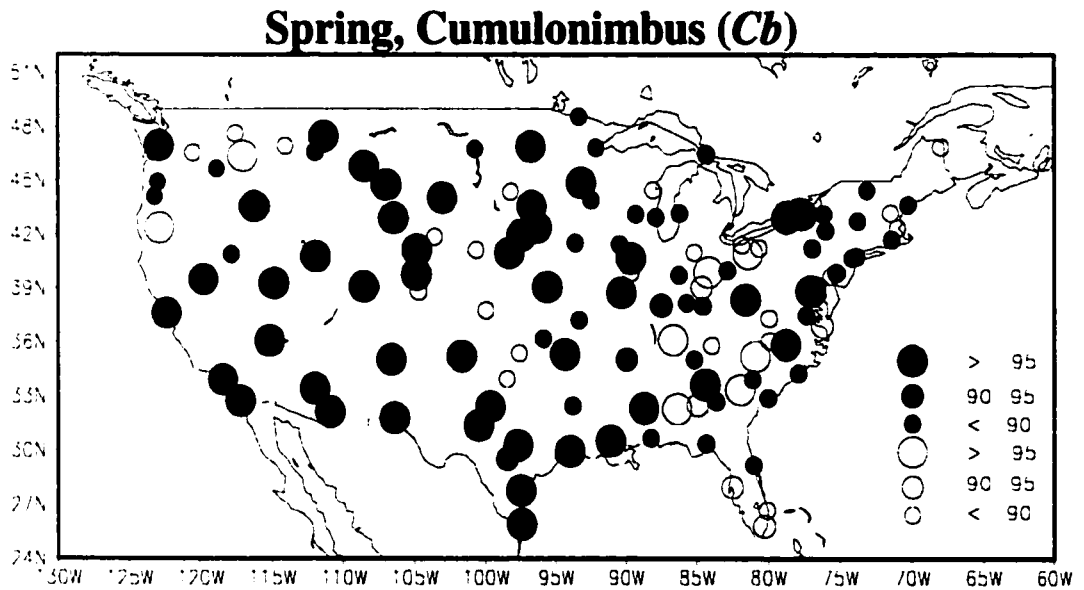


Figure 4.18 Spatial distribution of linear trend in cloud type frequency over the period 1952-1992. Black circle represents an upward trend while blank circle represents a downward trend. The value of the circle denotes the statistical confidence of the linear trend. For example, “>=95” indicates that the linear trend is at or above the 0.05 significance level. (A) stratiform and (B) *Cumulonimbus*.

formation of *Cirrus* and/or *Cirrostratus* from the spreading of jet contrails (Changnon 1981).

Cloud type frequency changes shown in Figs. 4.12-4.15 are based on the 182-station network (Fig. 4.2A). Of those stations 127 stations have continuous records throughout 1952 to 1992 (Fig. 4.2B). The area-averaged time series of cloud type frequencies calculated from this 127-station network are similar to those from the 182-station network (Fig. 4.2A). For example, the frequency of *Sc* (*St*) from the frozen network (Fig. 4.17) demonstrates a significant increase (decrease) trend in each season, which is similar to the corresponding frequency change shown in Fig. 4.13 in terms of both the direction and the magnitude of the linear trend.

Changes of cloud type frequency at each individual station are also checked in this study. In general, the upward (downward) trend found in the countrywide area-averaged cloudiness exists in most of the stations. For example, an upward trend in the frequency of stratiform clouds (Fig. 4.12) prevails over the whole area of the contiguous U.S. except over the southeast corner (Fig. 4.18A). An increase in the frequency of spring *Cb* (Fig. 4.14) exists in most of the areas of the contiguous U.S. (Fig. 4.18B).

In summary, over the contiguous U.S. over the period 1949-1994, with the increase in total cloud amount low cloud amount increased. The frequencies of *Nimbostratus* and stratiform clouds increased. The latter increase was due to an increase in *Stratocumulus* frequency because *Stratus* frequency decreased. An abrupt increase around 1960 in frequency of *Cumulonimbus* largely contributed to its upward trend over the period 1949-1994, particularly in summer. But, in spring and autumn, *Cb* frequency still showed a gradual increase after the 1960s. With the increase in *Cb* frequency, high cloud frequency also increased.

4.4.3 Cloud Cover Intercomparison

Comparing ground based, satellite determination of cloud type is different for two reasons. First, surface observers rely upon the cloud morphology to identify a cloud type while the satellite uses the visible and infrared radiance characteristics to identify a cloud type (Rossow and Garder 1993). Secondly, the range of satellite's downward view angle is different from that of surface observers' upward view angle. A large discrepancy of cloud type frequency therefore exists between surface and satellite based observations, making them incomparable. Also, as stated in Section 4.2.2, due to the difference in reporting policy, the frequency of cloud types, particularly of cloud type with small sky coverage, derived from GTS data, (such as HW99 data), generally is lower than that from conventional archive data, (such as GBS00 data). The cloudiness intercomparison in this section therefore focuses on total cloud cover among the datasets of GBS00, HW99, and ISCCP D2.

Fig. 4.19 shows the intercomparison of monthly cloud cover over the coincident time period (July 1983-December 1993) of GBS00, HW99, and D2 data. This comparison is made over the contiguous U.S., China east of 110°E, and the FUSSR south of 60°N, where surface weather stations are homogeneously and densely distributed. The number of stations with temporally complete records over 1983-1993 is 180 in GBS00 and 132 in HW99 over the contiguous U.S., 100 in GBS00 and 260 in HW99 over eastern China, and 155 in GBS00 and 810 in HW99 over the southern former USSR. The monthly cloud cover series are constructed from 3-hourly measurements except for the monthly series over China, where 4-hourly measurements are used. Fig. 4.19 indicates that the seasonal cycles of cloud cover match very well between the two surface based datasets over all three regions in consideration. Cloud cover series in each country and each dataset are calculated using the Thiessen polygon method, which accounts for the spatial inhomogeneity of station distribution (Kagan 1987; Sun et al. 2000).

Intercomparison of monthly total cloud cover with daily average

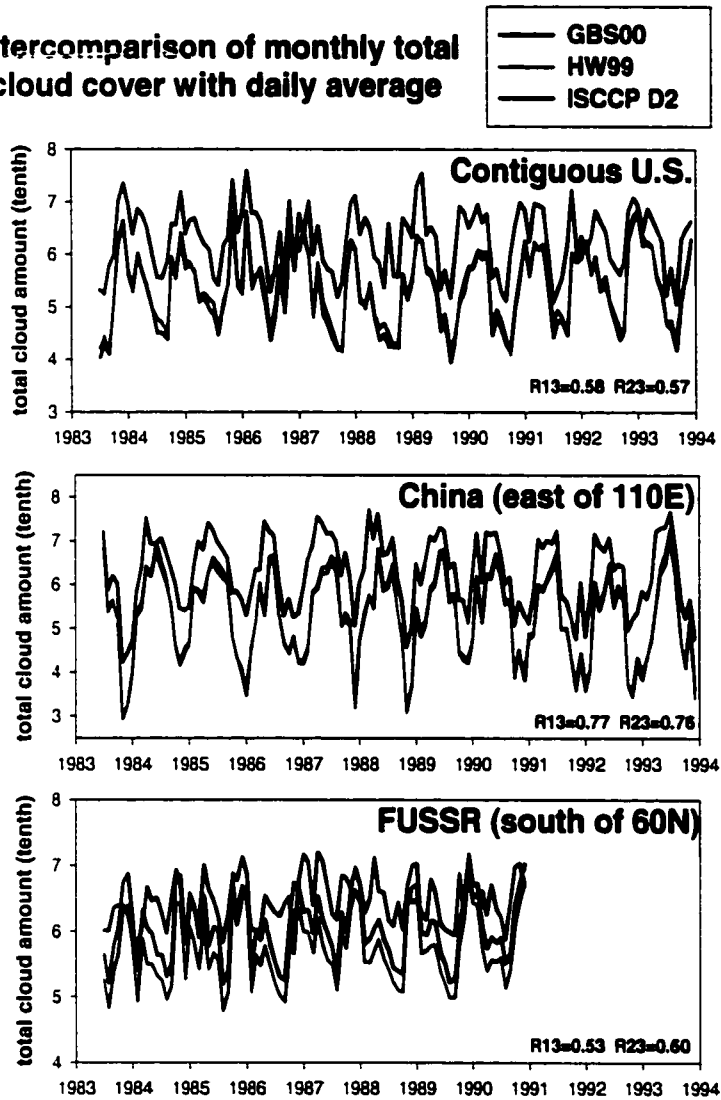


Figure 4.19 Intercomparison of monthly total cloud cover with daily average of three datasets: GBS00, HW99, and D2. R13 (R23) is the correlation coefficient between D2 and GBS00 (HW99) calculated after the removal of the seasonal cycle.

In spite of the difference in the number of stations, the value of area-averaged cloud cover is approximately the same in GBS00 and HW99 over the contiguous U.S. and eastern China. Over the southern FUSSR, cloud cover in GBS00 is larger than that in HW99 by 6%. This discrepancy is caused, perhaps, by a quality problem in HW99 data (only about 10% of the station data in HW99 were officially transferred by the USSR Hydrometeorological Service via GTS) and/or by the different number of stations in these two surface datasets

It is also clear from Fig. 4.19 that total cloud cover in D2 is systematically higher than that in the surface observations by approximately 17% for the period July 1983 to June 1991. For example, over the contiguous U.S., annual total cloud cover in D2 is 6.29 tenths, while it is 5.39 tenths in HW99. The lower value of total cloud cover in the surface data can be caused by nighttime cloud detection bias due to poor illumination (Hahn et al. 1995), our calculation (see also Fig. 4.20) indicates that the nighttime negative bias *lowers* surface based cloud cover by approximately 0.25 tenths for annual mean. So, over the contiguous U.S., the difference of total cloud cover between D2 and HW99 is still as large as 0.64 tenths, after the nighttime bias is taken into account. Despite the systematic difference in cloud cover value, the seasonal cycle of cloud cover in D2 is quite consistent with that in the two sets of surface data over the contiguous U.S. and eastern China. The different view angle between the satellite and the surface observer, and the inaccurate satellite detection of low cloud cover over snow covered surfaces (Rossow et al. 1993) may be responsible for the poor seasonal match over the FUSSR. After the removal of the seasonal cycle from the cloud datasets, the correlation coefficients between the satellite based and the surface based data over the contiguous U.S. and China, as well as over the southern FUSSR are all significant above the 0.05 level. So, the two sets of surface observed cloud cover match well with each other and also match well on seasonal cycles with the satellite D2 data over the land areas.

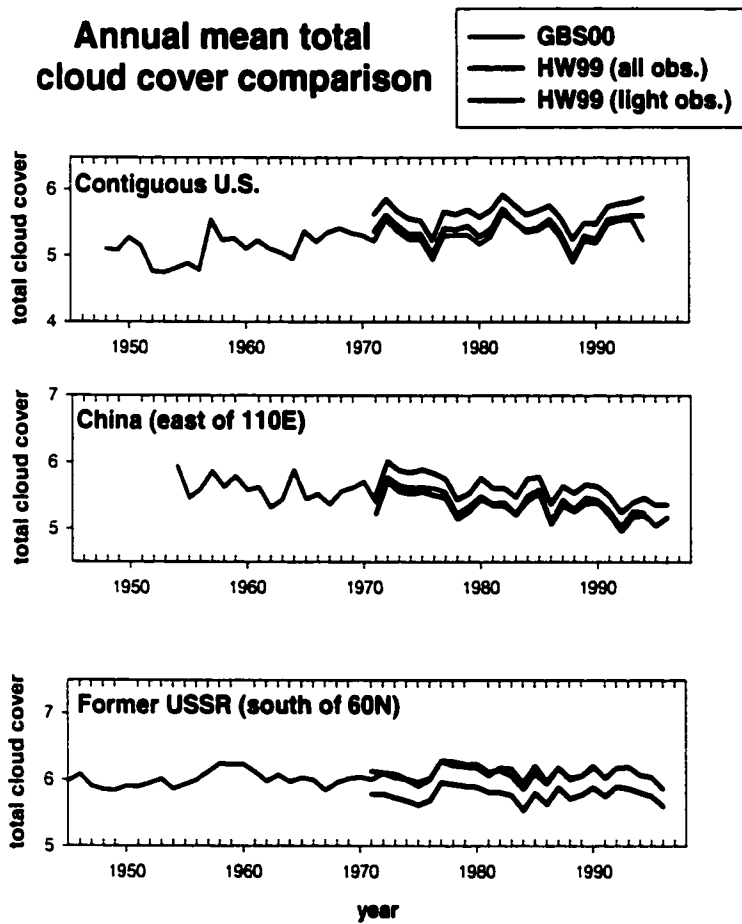


Figure 4.20 Comparison of annual total cloud amount between GBS00 and HW99, and between all observations and light observations in HW99. Light observations are selected based on the mooglight criterion suggested by Hahn et al. (1995).

The interdecadal change in the two set surface based cloud cover (GBS00 and HW99) over the contiguous U.S., eastern China, and the southern FUSSR are shown in Fig. 4.20. Annual mean cloud cover from GBS00 in all three regions is constructed from the same daily data as those used in Fig. 4.19. Annual cloud series created from all cloud observations (black line) and cloud observations with only light illumination (red line) from HW99 are also depicted in Fig. 4.20. Despite the difference of practice in recording cloud cover between GBS00 and HW99, the consistency of variations between these two datasets on both annual and decadal scales shown in Fig. 4.20 again indicates that surface based cloud data over land are likely to be reliable. It is also realized from Fig. 4.20 that nighttime cloud detection bias indeed lowers annual cloud cover by around 0.2-0.3 tenths but does not affect decadal variations of cloud cover.

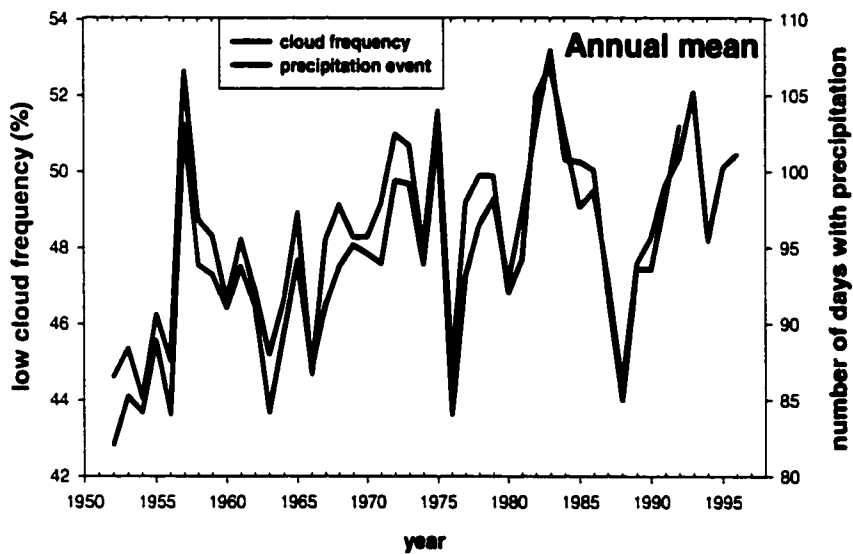
The intercomparison of cloud cover from different sources in Figs. 4.19 and 4.20 indicates that the conventional surface based cloudiness data over land used in this study are highly likely to be reliable. Next section will again corroborate the reliability of the GBS00 cloud data, using other cloud-related atmospheric variables.

4.5 Changes in Atmospheric Hydrological Cycle

Precipitation comes mainly from convective and stratiform cloud systems, or the mixture of the two. So, changes in cloudiness including cloud type frequency revealed in this study, if real, are expected to reflect changes in the atmospheric hydrological cycle.

Fig. 4.21 indicates that over the contiguous U.S. the significant increase in the annual frequency of all low cloud types over the period 1952-1992 matches extremely well with the increase in the number of days with all precipitation events (trace events not included) (Karl and Knight 1998). While over the FUSSR particularly over Siberia (Fig. 4.24), the decrease in the frequency of low clouds reflects a decrease in the number of days with all precipitation

Contiguous United States Precipitation event & low cloud frequency



Linear trend in low cloud frequency 2.3%/10 yrs (R²=0.27)
Linear trend in precipitation event 2.0%/10 yrs (R²=0.15)

Correlation coefficient R=0.94 (after detrend)

Figure 4.21 Changes in annual number of days with precipitation and in frequency of low cloud types area-averaged over the contiguous U.S.. R² is the variance ascribed to the linear trend.

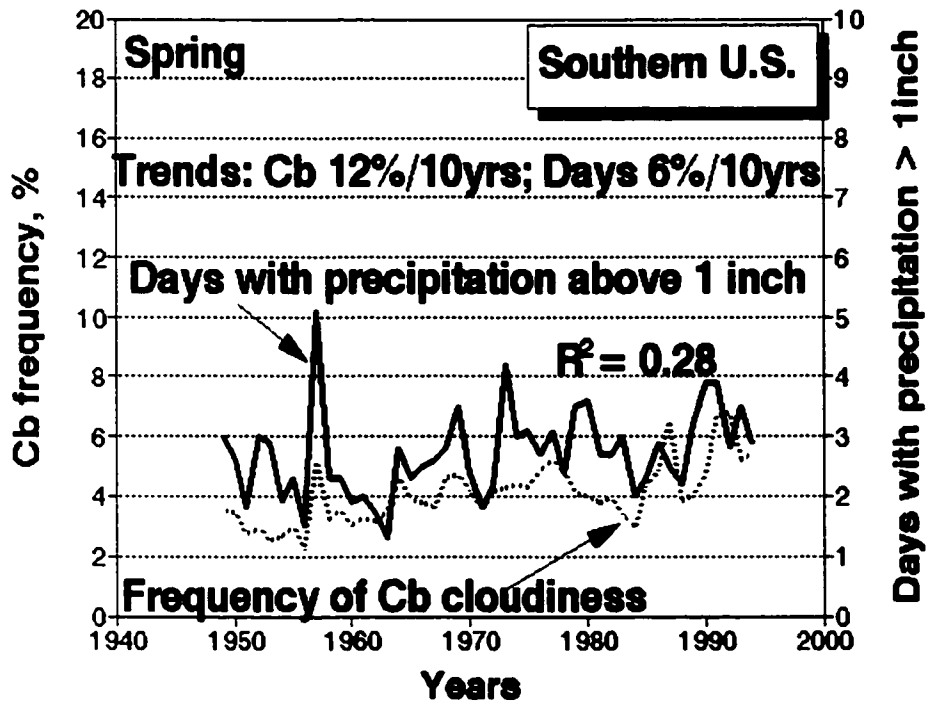


Figure 4.22 Changes in the number of spring days with heavy precipitation and *Cumulonimbus* frequency over the southern U.S. including Texas, Louisiana, Mississippi, Arkansas, Oklahoma, and Kansas.

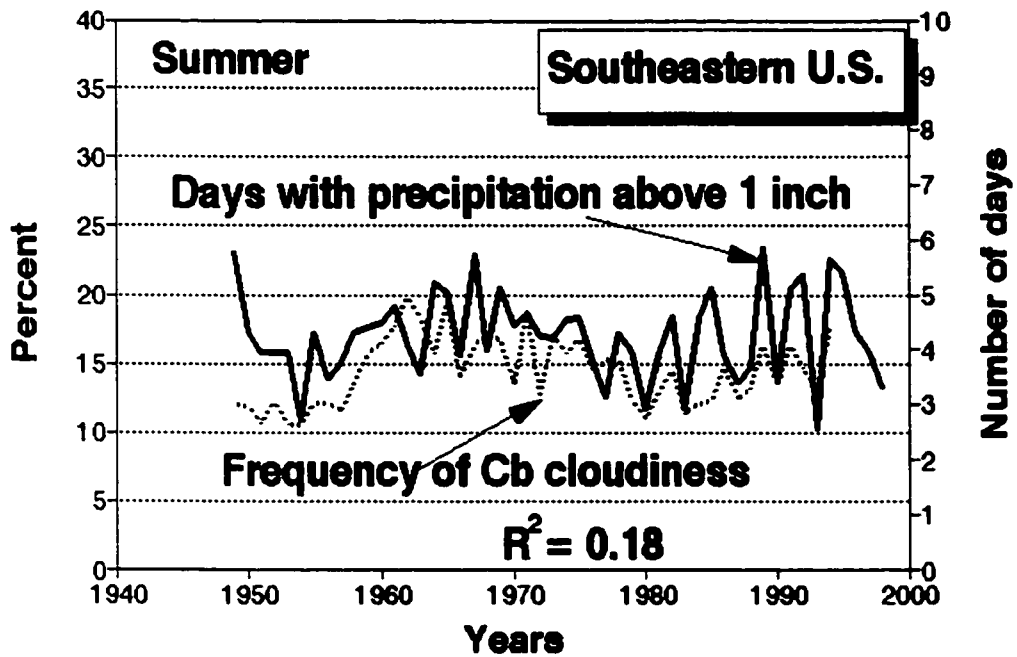
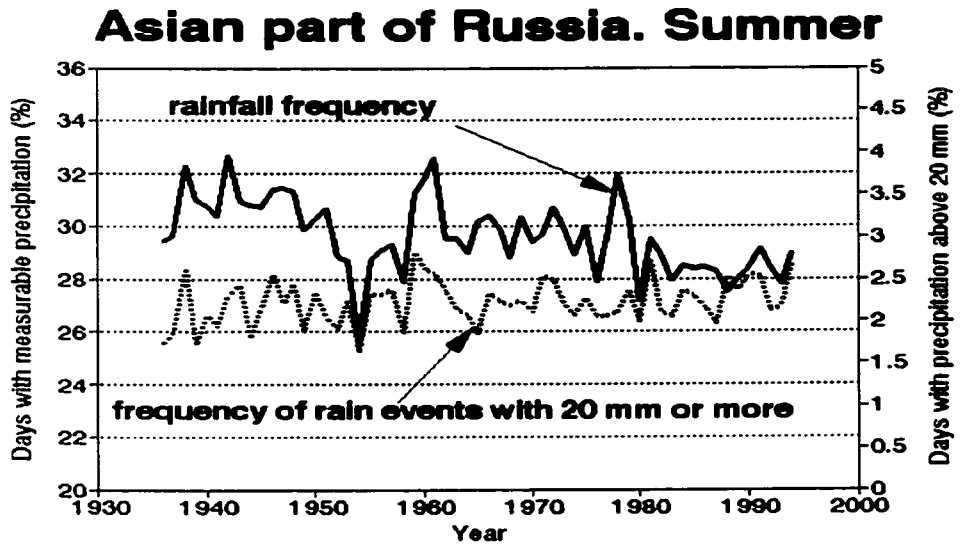


Figure 4.23 Same as Fig. 4.22 except for the southeastern U.S. and for summer season.

A



B

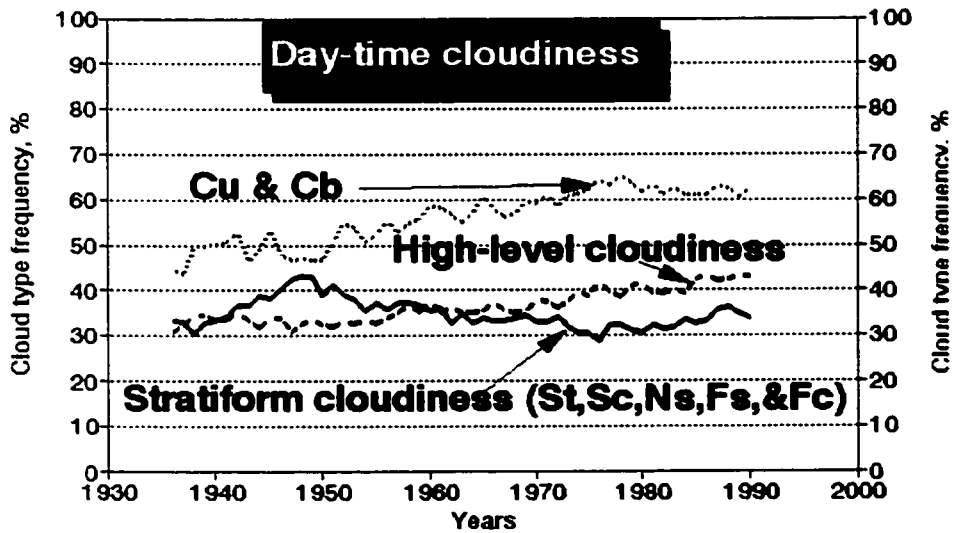


Figure 4.24 Changes in frequency of summer days with (heavy) precipitation and various cloud types over the Asian part of the FUSSR.

Asian part of Russia. Summer

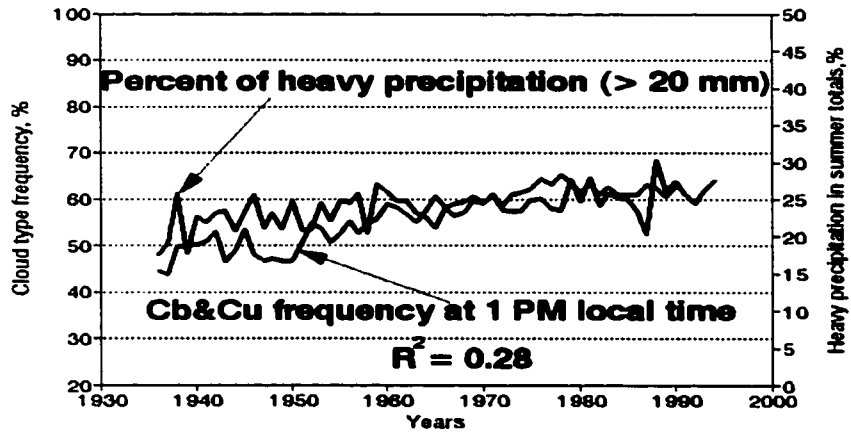


Figure.4.25 Changes in convective cloud frequency at 1 PM and percent of daily heavy precipitation over the Asian part of Russia. R is the correlation coefficient.

Table 4.1 Changes in components of the atmospheric hydrological cycle over the Asian part of Russia in summer during the period of 1936-1990. Statistically significant trends are marked with * (0.05 level) and ** (0.01) level) respectively.

Precipitation characteristic	Average	Linear trend, %/10yrs
Summer total, mm	213	-1.3**
Precipitation frequency (number of days with precipitation above 1 mm)	30	-1.5**
Number of days with precipitation above 20 mm	2.2	1.9*
Number of thunderstorm reports at the time of observation (four observations per day schedule)	2.5	6.4**
Frequency of stratiform cloudiness (St, Sc, Ns, Fc, and Fs), %	35	-2.8**
Frequency of convective cloudiness (Cu and Cb), %	56	6.0**
Frequency of high-level cloudiness (Ci, Cs, and Cc), %	37	5.4**

events (trace events not included) (Karl and Knight 1998). While over the FUSSR particularly over Siberia (Fig. 4.24), the decrease in the frequency of low clouds reflects a decrease in the number of days with all precipitation events (trace events not included). The presence of low stratiform clouds, including *Sc* and *St* or the combination of these two, generally is associated with a relatively stable lower troposphere. Figs. 4.21 and 4.24 (cf also Isaac and Stuart 1996) therefore also indicate that over northern middle latitude land areas most precipitation events occur around (before or after) the presence of low stratiform clouds.

Fig. 4.22 shows that over the southern U.S. during spring, the increase in *Cb* frequency is consistent with the increase in the number of days with heavy precipitation (i.e., in the top-

range percentiles, which are usually associated with thunderstorms). In summer over the southeastern U.S., the variations of *Cb* frequency are also basically consistent with those of heavy precipitation events but the relationship is not statistically significant (Fig. 4.23). Over Siberia, the increase in convective type of clouds may significantly contribute to the increase in the frequency of heavy precipitation (Fig. 4.24). Also, over Siberia, the annual variation of convective cloud frequency is consistent well with that of percent of heavy precipitation amount (Fig. 4.25). Table 4.1 also indicates that with the increase in the frequency of convective clouds over the Asian part of Russia, the number of thunderstorm reports also increased. All those examples indicate that the cloud type frequency changes observed in this study basically reflect changes in precipitation frequency and intensity.

4.6 Conclusions and Discussions

Significant changes and a general redistribution in cloud cover amount and cloud type frequency have been observed during the past forty to fifty years over the midlatitude land areas of the Northern Hemisphere. This is evident in the surface weather station based daytime synoptic data of the contiguous United States (1949-1994) and of the former USSR south of 60°N (1945-1990). The major conclusions are as follows.

- Over both countries, total cloud amount increased; the frequency of convective clouds increased. The abrupt increase in convective cloud frequency prior to the 1960s largely contributed to the upward trends over the post WWII period, particularly in summer. However, over both countries during the intermediate seasons and during the winter season over the FUSSR, convective cloud frequency still showed gradual increase after 1960s.
- Over the FUSSR (south of 60°N), low cloud amount decreased. This decrease is mainly related to the decrease in low stratiform (*Sc&Sr*) cloud frequency. The

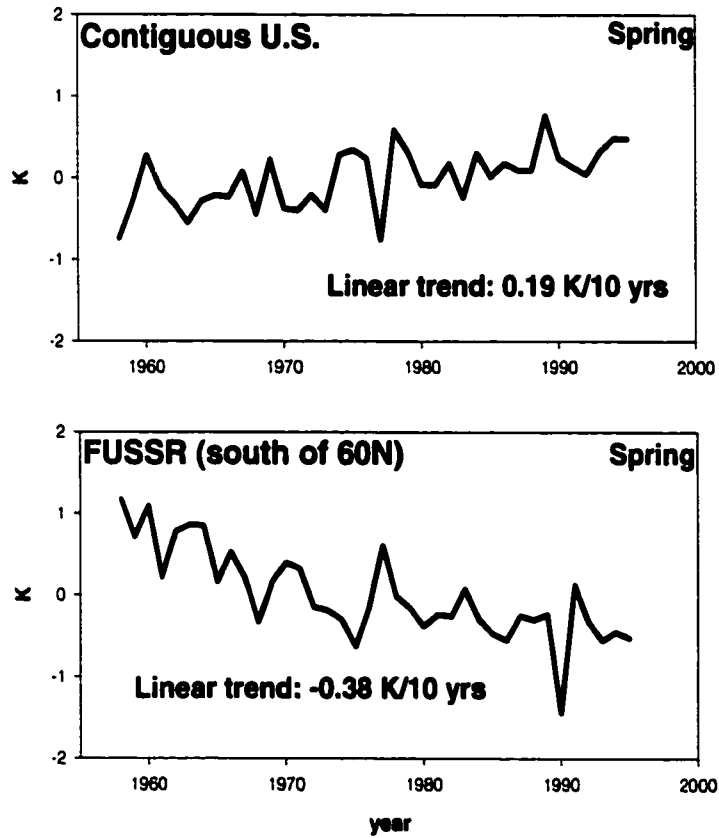
decrease in stratiform cloud frequency is caused by the decrease in low *Stratocumulus* frequency because low *Stratus* frequency increased.

- Over the contiguous U.S., low cloud amount increased. This increase is associated with the increase in frequencies of low *Stratocumulus* and *Nimbostratus*. Despite a decrease in low *Stratus* frequency, low stratiform (*Sc&St*) cloud frequency increased.
- Changes in cloud type frequency are consistent with changes in precipitation frequency and intensity.

The empirical data can provide a benchmark for verification of the reliability of cloud and related processes in contemporary global climate models. The redistribution of cloudiness revealed in this study such as (a) an increase in the frequencies of convective and high level clouds and (b) a decrease in low level clouds at higher latitudes (cf. the former USSR) and an increase in low level clouds in middle latitudes (cf., the contiguous U.S.) are seen as changes in most model-simulated warm climates compared to control runs (e.g., Mitchell 1989; Yao and Gel Genio 1999; Dai et al. 2000).

In addition to changes in the atmospheric hydrological cycle discussed in Section 4.5, the cloudiness redistribution revealed in this study also give us a hint of changes in the atmospheric thermal structure. The presence of low stratiform clouds generally is associated with a relatively stable atmosphere (Klein and Hartmann 1993; Norris 1998a). The observed decrease in the frequency of low stratiform clouds over the FUSSR may indicate that the lower tropospheric atmosphere has become unstable, meaning that the low tropospheric temperature shows less warming than the surface during the post WWII period. On the other hand, over the contiguous U.S., the increase in the frequency of low stratiform clouds may indicate that the low tropospheric temperature structure became more stable. This speculation indeed is supported by the NCEP reanalysis dataset (1958-1994).

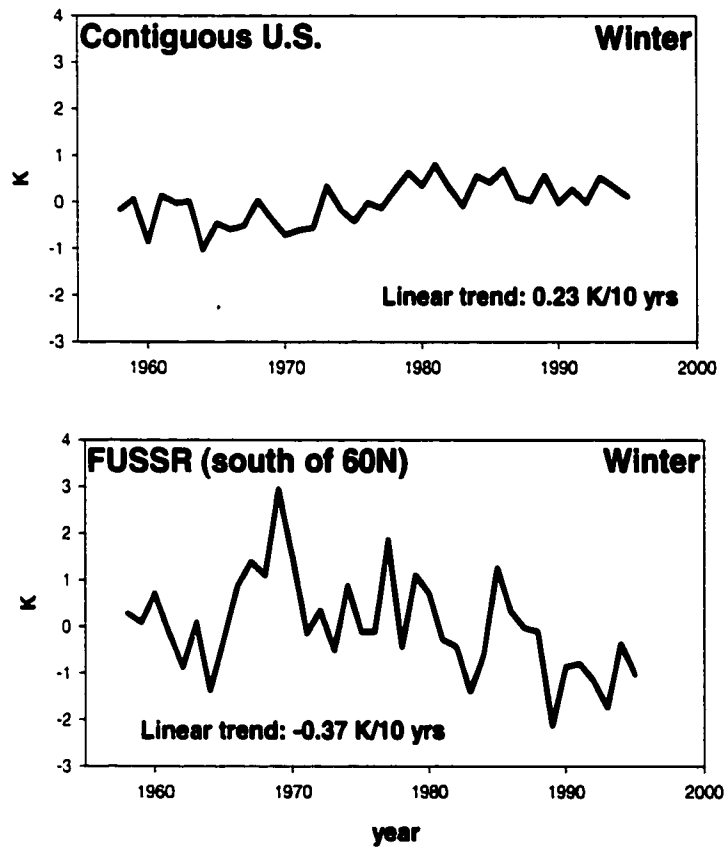
**Change in static stability of the low troposphere
(700 hPa - 1000 hPa) in NCEP reanalysis data**



**Y-axis: Anomaly of the potential temperature
difference between 700 hPa and 1000 hPa**

Figure 4.26 Changes in the lower tropospheric static stability over the FUSSR and the contiguous U.S. during spring.

**Change in static stability of the low troposphere
(700 hPa - 1000 hPa) in NCEP reanalysis data**



**Y-axis: anomaly of the potential temperature
difference between 700 hPa and 1000 hPa**

Figure 4.27 Same as Fig. 4.26 except for winter

Fig. 4.26 shows that changes in the lower tropospheric static stability over the FUSSR and the contiguous U.S. during spring. The potential temperature difference between 700 hPa and 1000 hPa is used as a measure of the low tropospheric static stability. During the data period (1958-1994), the static stability over the southern FUSSR shows a significant decrease, which is consistent with the requirement for a decrease in stratiform cloud frequency. Over the contiguous U.S. the static stability of the lower troposphere from the NCEP reanalysis dataset increased, which is somewhat consistent with the increase in the frequency of stratiform clouds (Fig. 4.12). Similar changes in the low tropospheric static stability over the FUSSR and the contiguous U.S. also exists in the winter NCEP reanalysis dataset (Fig. 4.27).

In Fig. 4.26, the lower tropospheric static stability index, calculated from the potential temperature, does not account for atmospheric moisture. Over the U.S., an increase in low tropospheric precipitable water (Ross and Elliott 1996) may contribute to an increase in convective available potential energy (Lucas et al. 1994a,b; Ye et al. 1997), which could cause the increase in frequency of *Cb*.

It has been noted that uncertainty exists in the NCEP reanalysis dataset regarding long-term change (Santer et al. 1999). Observational temperature and humidity profile data, such as radiosonde measurements (Eskridge et al. 1995) and satellite observations (Spency and Christy 1990; Christy et al. 1998), will therefore be needed to check the atmospheric thermal structure changes and their relationships with cloud type frequency changes.

The role of clouds in the climate system is recognized through their radiative forcing. The albedo cooling effect of low stratiform clouds is stronger than their infrared warming effect. Low stratiform clouds therefore generally have a net cooling effect on the surface. A decrease in the frequency of low stratiform clouds over the FUSSR suggests that the net cooling effect of stratiform clouds decreased over the period 1945-1990, thus probably leading to a stronger increase in near surface temperature (Fig. 4.28). However, the increase in the

Area averaged daily surface air temperature anomaly over the contiguous U.S. and the former USSR

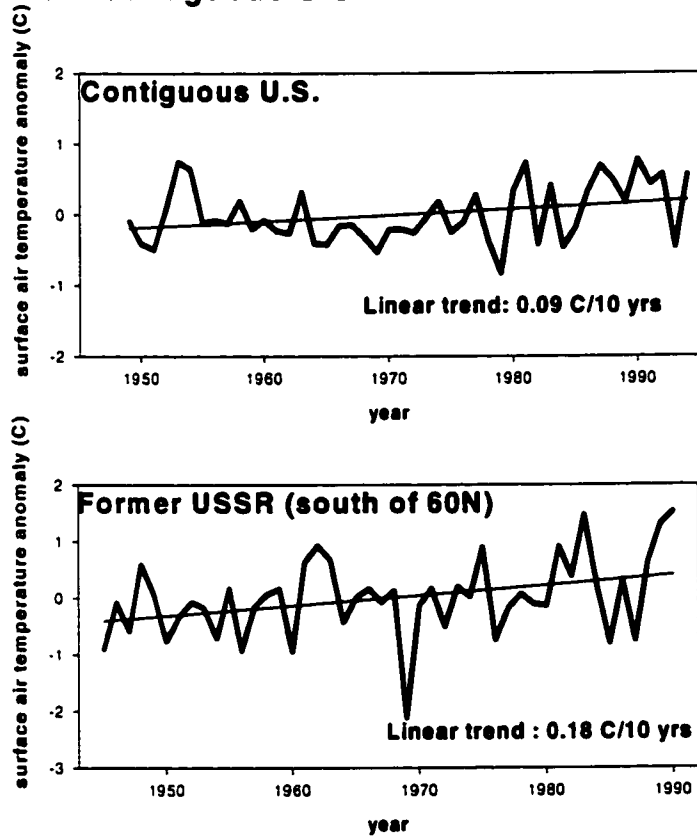


Figure 4.28 Changes in near surface temperature over the contiguous U.S. and the F USSR.

Changes in meteorological fields over Agana (13.48N, 144.80E)

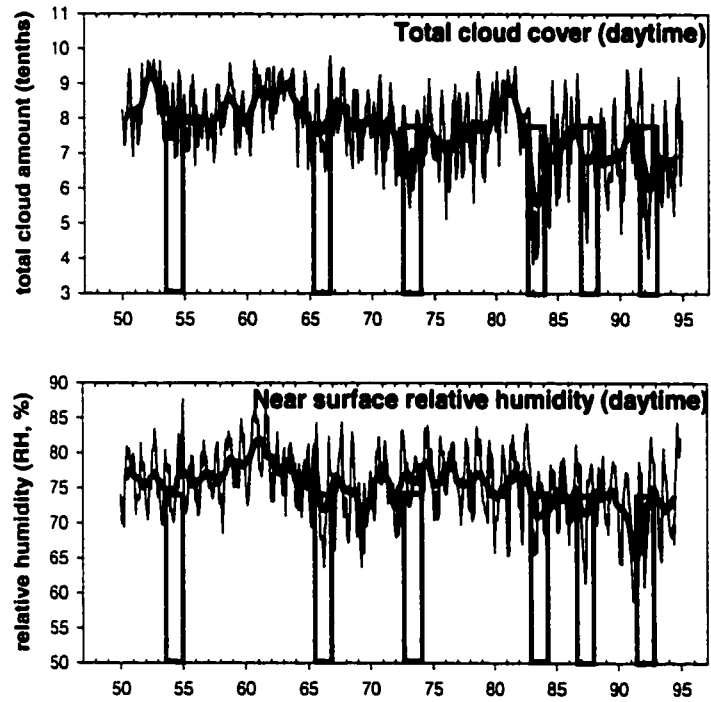


Figure 4.29 Changes in daytime total cloud amount and near surface humidity over Agana (13.48°N, 144.80°E). The red curve is 12-month running mean. The green band represents El Niño event.

frequency of low stratiform clouds over the contiguous U.S. indicates that the net cooling effect of low stratiform clouds should have increased over the period 1949-1994, thus probably contributing to less strong surface warming compared to the warming over the FUSSR (Fig. 4.28).

Over both the U.S. and the FUSSR, the increase in the frequency of *Cb*, combined with the increase in the frequency of high level clouds during the post WWII period, may indicate an enhanced upward moisture transport, and more water vapor might be transported to the upper troposphere by convection and large-scale circulation. Thus, the column greenhouse effect and the atmospheric profile of radiative heating may also change with time.

Overall, the cloudiness redistribution over the contiguous U.S. and the FUSSR during the post WWII period suggests that changes in the atmospheric hydrological cycle, the atmospheric thermal structure, and the cloud-climate feedback may all have occurred over middle latitude land areas of the Northern Hemisphere.

This chapter deals mainly with interdecadal cloudiness changes over middle latitude land areas. Actually, long-term changes in cloudiness were also found to have occurred over the tropics. Fig. 4.29 describes the changes in total cloud amount and near surface humidity from the station of Agana (13.48°N, 144.80°E) over the western tropical Pacific. In addition to pronounced interannual variations associated with the occurrence of El Niño (for example, during 82-83, 86-87, and 92-93, weaker convection associated with weaker low level moisture convergence as seen in lower near surface relative humidity led to less total cloud cover), total cloud cover exhibited a significant downward trend over the period 1952-1995. Unfortunately, most of the cloud type measurements over the tropical islands that we have, are inappropriate for long-term cloud type change analysis.

CHAPTER 5

CLIMATOLOGY OF THE CLOUD-RELATED NEAR SURFACE TEMPERATURE CHANGE: COMPARISON OF GCM SIMULATIONS WITH EMPIRICAL DATA

This chapter focuses on the climatology of the cloud-related near surface temperature change, OCET or OCET₁, over land areas of the Northern Hemisphere. OCET or OCET₁ is defined by Eq. 1.1 or 1.2 as the difference of near surface temperature between average and clear sky weather conditions or between overcast and average weather conditions. The long-term cloud-related near surface humidity change, defined as the difference of near surface water vapor pressure between average and clear sky weather conditions (OCEH) or between overcast and average weather conditions (OCEH₁), is also discussed in this chapter. The average or overcast conditions in this research represent overall sky conditions, including all cloud types present in the sky. The observed climatology of the cloud-related near surface temperature (humidity) change derived from the synoptic data set (GBS00 dataset) is then used to evaluate the performance of seven AMIP-1 climate models. The data-model comparison in this study is limited to only large scale spatial patterns due to (1) the difference between the method in calculating the observational daily OCET and the method in calculating the model simulated daily OCET (see Section 3.1) and (2) the spatial irregularity of the station distribution (Fig. 2.1).

Section 5.1 presents the observed climatology of the cloud-related temperature (humidity) and the data-model comparison over the northern extratropical land areas, where stations are reasonably well distributed (Fig. 2.1). The accumulation of synoptic data from the tropics (see Fig. 2.1) gives us an opportunity to make a pilot analysis of the cloud-related temperature change in the tropics, where the climate regime is different from those over the

extratropical areas. The results from the tropics are given in Section 5.2. Conclusions and discussions are presented in Section 5.3.

5.1 Extratropical Land Areas

5.1.1 Near Surface Temperature in the Presence of Clouds

Figs. 5.1-5.2 show the daily mean cloud-related near surface temperature in both observation data and seven models for January, April, July, and October respectively. All these figures are produced using the Spyglass Transform Graphic Software package with a spatial interpolation scheme inside. The unit of the values in these figures is Kelvin (K) in degree. The results over the extratropical land areas from the observational data should be reliable because stations there are relatively homogeneously and densely distributed.

The observational daily OCET (Figs. 5.1-5.2) demonstrates a pronounced seasonal variability. In January over the extratropical land areas, the observational daily OCET shows positive value with the maximum over the high latitudes (Fig. 5.1), suggesting that in cold seasons a surface warming is associated with cloud cover and this cloud-related surface warming is stronger over the high latitudes. In July the observational daily OCET is negative over the extratropical land areas (Fig. 5.2), indicating that a surface cooling is associated with the presence of clouds. In the transitional seasons (April and October) over the high latitudes, the daily mean near surface temperature difference between average and clear sky conditions (daily OCET) is positive, while it is negative over the subtropical regions.

Of the seven GCM runs tested, in January, UIUC, MPI, NMC, CCC and MGO are able to reproduce the sign and the pattern of the observed daily OCET. A negative daily OCET over east Siberia in the GISS model run as well as a negative OCET over the northeast Asia in the LMD model run, is not seen in the empirical data. In July, different models show different patterns of the daily OCET (Fig. 5.2). For example, the UIUC model properly reproduced the

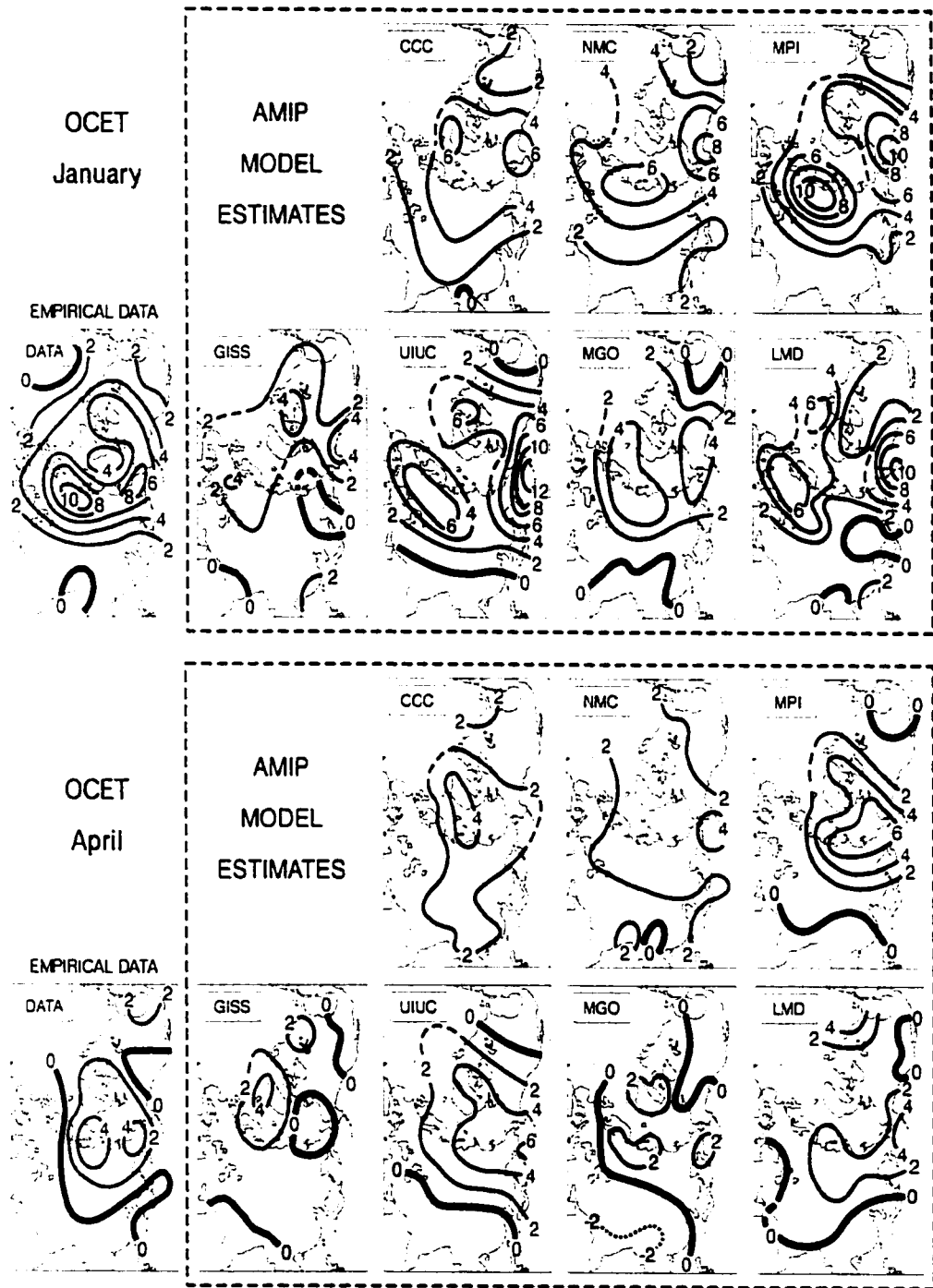


Figure 5.1 Daily mean OCET comparison between the observational data and the AMIP runs. Unit: K. January and July.

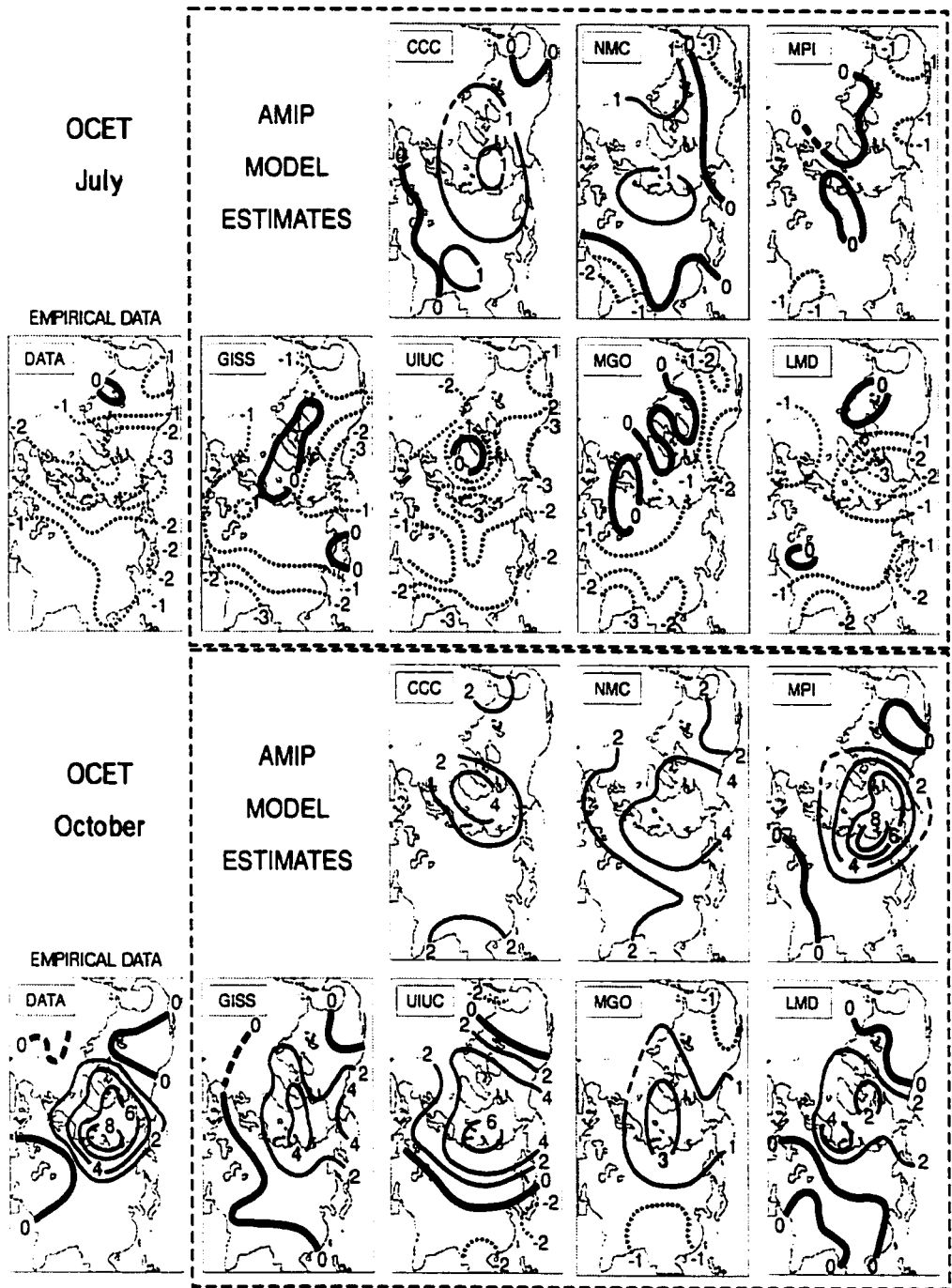


Figure 5.2 Same as Figure 5.1 except for July and October.

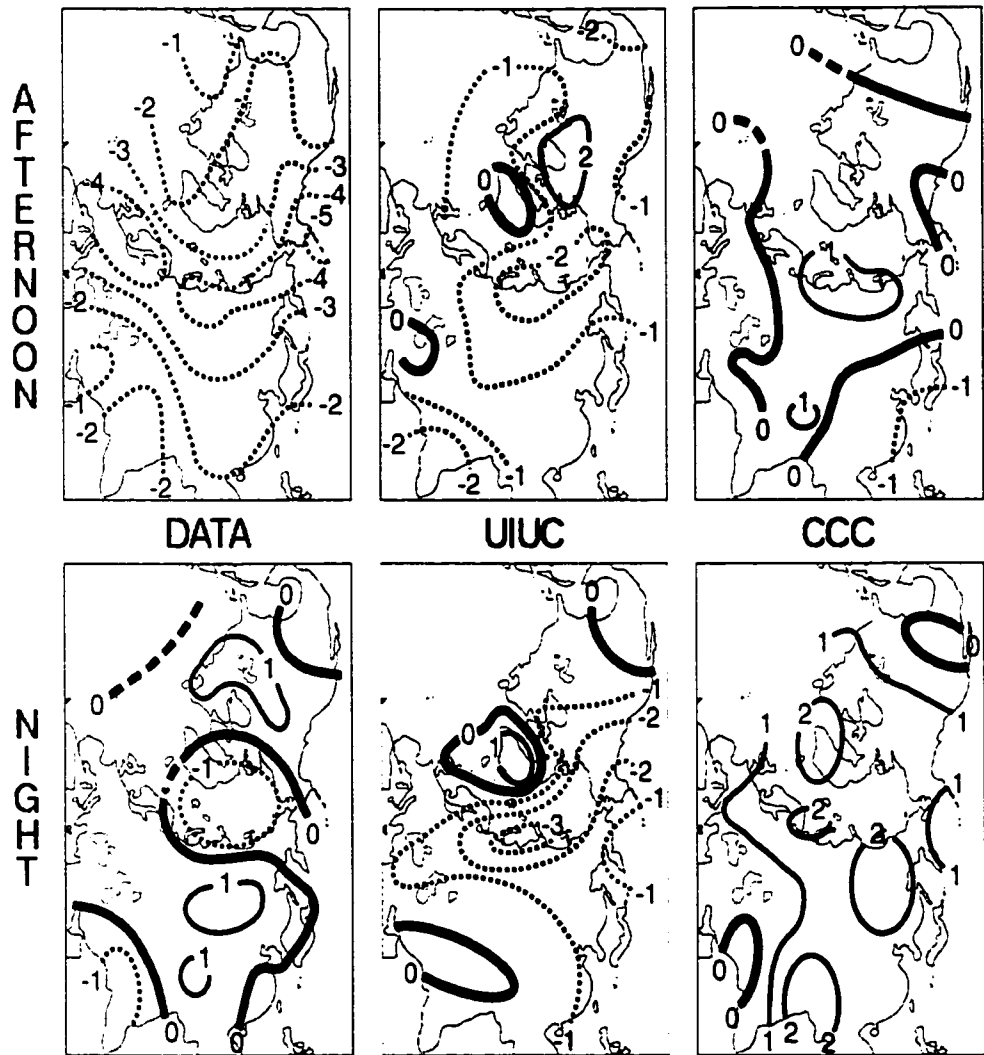


Figure 5.3 July OCET estimates over land areas from the CCC and the UIUC AMIP model runs and from the empirical data. Unit: K. Nighttime and daytime.

sign, the pattern, and the magnitude of the July daily OCET while an opposite daily OCET pattern was reproduced in the CCC and the NMC model runs. The model performance in the April and October simulations is between that in January and July.

Of the seven GCMs, the UTUC and the CCC runs provide both nighttime and daytime outputs for the month of July and thus can be evaluated on the diurnal cycle. Fig. 5.3 shows the July nighttime and daytime OCET for the empirical data and the model runs. The observational data indicates that on July afternoons, over the extratropical land areas a surface cooling is associated with the presence of cloud cover, while the opposite sign of OCET in July nighttime is observed over the extratropical land areas except the polar region (where the polar day phenomenon occurs). The UTUC model is able to properly reproduce the afternoon cooling while the nighttime warming associated with clouds over the middle latitudes is not shown in its run. Fig. 5.3 also indicates that the major problem revealed in Fig. 5.2 for the CCC model summer OCET simulation arises from the daytime simulation.

The detailed descriptions of the data-model comparisons of the seasonal and the diurnal variations of OCET over the extratropical land areas are given in Groisman et al. (2000). Here is a brief summary of the comparisons. The tested models generally agree in reproducing the cold season cloud-temperature relationship. The largest inter-model and model-data differences in the mean daily OCET occur in July. The mean daily OCET in the UTUC model is among the best in terms of its correspondence with the empirical data. However, this model still cannot correctly simulate the diurnal OCET variation.

5.1.2 Near Surface Humidity in the Presence of Clouds

There is a difference in characteristics that were selected by different modeling groups to represent the near surface humidity field in their AMIP runs. Four GCMs (GISS, NMC, LMD, and CCC) provide near surface specific humidity, the UTUC model output provides

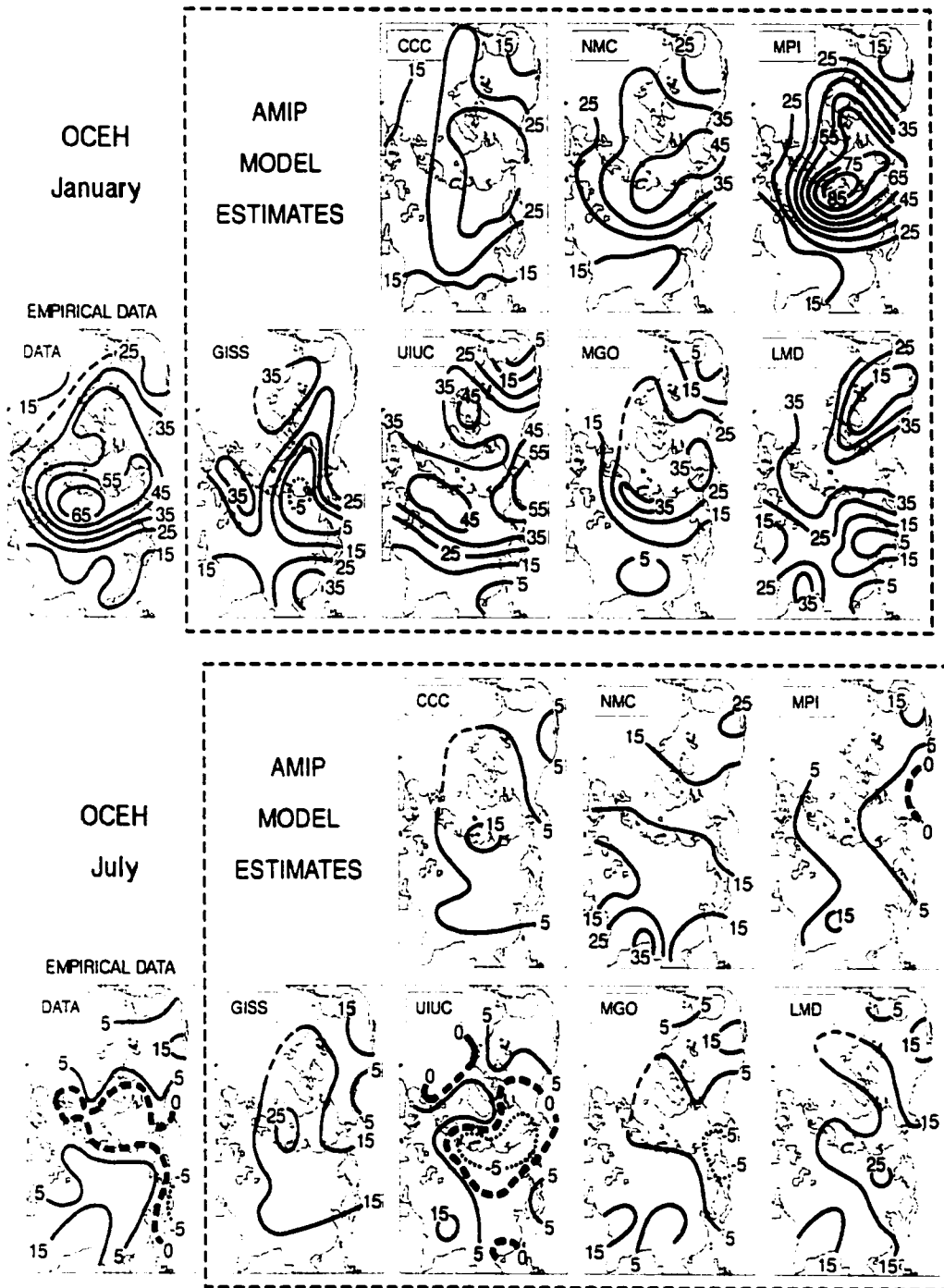


Figure 5.4 Same as Fig. 5.1 except for mean daily OCEH (in percentage of the mean daily water vapor pressure: $100\%(H_{ave} - H_{ctr})/H_{ave}$).

absolute humidity, and the MGO model output provides water vapor pressure, while the MPI model output contains near surface dew point temperature. The humidity characteristic selected for the intercomparison from the empirical data is water vapor pressure (H). For the purpose of comparability, the percentage of the variation of water vapor pressure between average (H_{ave}) and clear sky (H_{clr}) conditions, $(100\%(H_{ave} - H_{clr})/H_{ave})$, is used to present the OCEH estimate. Therefore, when the average water vapor pressure in the GCM differs from the observed value, that difference also contributes to the OCEH estimate.

Detailed descriptions are shown in Groisman et al. (2000) of the observed OCEH patterns in all four seasons and their comparisons with the model simulations. Fig. 5.4 shows examples of the data-model comparison for January and July. The empirical data indicate that OCEH is positive in both seasons (except for July over the Arctic and the North Pacific coastal areas), suggesting that clear sky conditions are usually associated with less than average surface water vapor. Compared to summer, the smaller near surface water vapor pressure in winter leads to a larger percentage value of the relative humidity change. Similar to the OCET case, the models simulated well the winter OCEH pattern but large discrepancies exist in summer among the models and between the models and the observational data.

5.2 Tropical Land Areas

The standard approach, OCET /OCEH, which has been used in the above sections to study the cloud-temperature/humidity relationships over the extratropical land areas, does not work well in the humid tropics because there are not enough clear sky meteorological events. So, the alternative statistics, $OCET_1/OCEH_1$, are used to describe the cloud-related near surface temperature/humidity change: the difference of the values between the meteorological element, T or H, under overcast and average weather conditions. In the tropical regions, the diurnal variations predominate over the wide range of time scales clouds exhibit and thus

influence the diurnal cycle of surface heat balance (Hartmann et al. 1991). Therefore this section focuses on the nighttime and daytime cloud-related near surface temperature/humidity change.

According to the characteristic of the station distribution over the tropics, seven regions are selected to study the cloud-temperature/humidity relationships: the central and western Pacific, south Asia, southeast Asia, central and south America, north Africa, the Hawaiian Islands, and high mountain stations. These seven regions (Fig. 5.5) are sorted in terms of the seasonal variation of near surface humidity into three groups: the all-year around wet region (the central and western Pacific), monsoon regions with a strong seasonal cycle of near surface humidity (south Asia, southeast Asia, north Africa, and central and south America), and the dry (semi-arid) region (the Hawaiian archipelago and ten high mountain stations). Table 5.1 shows the tropical $OCET_1$ for both nighttime and daytime over the selected seven regions based on observational data.

Table 5.1 indicates that daytime $OCET_1$ is negative over all tropical regions in each season. In nighttime, the sign of $OCET_1$ varies with season and geographic location. In the tropical dry zones (e.g., the Hawaiian Islands and mountainous plateaus) $OCET_1$ is positive in all seasons and decreases from January to July. Over the humid tropics (the central and western Pacific) negative nighttime $OCET_1$ is observed throughout the year. Over the tropical monsoon areas $OCET_1$ is positive over the dry seasons (i.e., January and October) and becomes negative over the wet seasons (i.e., April and July). Apparently, the nighttime cloud-related surface air temperature change is closely related to near surface specific humidity. This finding encourages us to explore further the impact of water vapor on the cloud-related temperature change over extratropical land areas (see Chapter 6).

$OCEH_1$ (not shown) does not vary dramatically over the tropics in the diurnal cycle. Near surface water vapor pressure in the tropics is much larger than in the tropical regions.

Therefore, the percent variation of near surface water vapor pressure associated with cloud cover is smaller than that over the extratropical land areas (varying by absolute value from 5 to 15%). Among features not observed in the extratropical land areas shown in Fig. 5.4, a negative $OCEH_1$ in July over southeast Asia is encountered. In general, the cloud cover / near surface specific humidity relation is the same over the tropical and the extratropical land areas.



Figure 5.5 Regions where cloud-related temperature change shown in Table 5.1 is assessed. Mountainous stations spreading over three continents are not shown.

Table 5.1 Specific humidity, q (g/kg) and cloud-related near surface temperature change, $OCET_1$ (K), in tropical regions based on observational data.

Afternoon.

		January		April		July		October	
		q	$OCET_1$	q	$OCET_1$	q	$OCET_1$	q	$OCET_1$
Central and Western Pacific	9	17	-0.5	18	-0.6	19	-0.6	19	-0.6
Southeast Asia	44	13	-1.4	17	-1.5	19	-1.0	17	-1.4
South Asia	23	13	-1.4	17	-1.5	19	-1.0	17	-1.4
Central and South America	72	15	-1.1	16	-0.9	17	-0.8	17	-1.0
Africa, Sahel	49	5	-1.3	8	-0.9	16	-1.4	12	-1.5
The Hawaiian Islands	4	13	-1.3	13	-0.9	14	-0.7	15	-0.9
Mountains	10	8	-2.2	9	-1.3	13	-1.0	9	-1.5

Nighttime

		January		April		July		October	
		q	$OCET_1$	q	$OCET_1$	q	$OCET_1$	q	$OCET_1$
Central and Western Pacific		17	-0.1	17	-0.1	18	-0.1	18	-0.1
Southeast Asia		11	0.3	15	-0.4	19	-0.3	16	-0.1
South Asia		14	0.6	16	-0.4	18	-0.3	16	0.4
Central and South America		14	0.2	15	0.2	17	-0.1	16	-0.0
Africa, Sahel		5	0.6	9	0.5	16	-0.5	14	0.2
The Hawaiian Islands		12	0.9	12	0.3	14	0.1	14	0.3
Mountains		8	0.9	10	0.3	13	0.1	N/A	

In summary, over tropical land areas, daytime surface cooling is associated with cloud cover in all seasons. The nighttime cloud-related near surface temperature change varies with geographic location and climate regime. In general, a nighttime surface cooling associated with cloudiness occurs in a moist atmosphere, while a nighttime cloud-related surface warming occurs in a dry atmosphere.

5.3 Conclusions

A physically based statistical approach, "overall cloud effect on near surface temperature", OCET, was used to characterize the cloud-related near surface temperature change. OCET was defined as the difference of near surface temperature between average and clear sky or between overcast and average weather conditions. These data were used to evaluate the AMIP-1 climate models. The major results are as follows.

- The climatological OCET exhibits strong seasonal and diurnal cycles, and varies with geographical location and climate regime. Over the northern extratropical land areas, from cold to warm season and from high to low latitudes, positive daily OCET decreases and becomes negative. Over the tropics, the daytime OCET remains negative in all seasons; the nighttime OCET is negative over humid areas (or seasons) and is positive over dry areas (or seasons). In all seasons a more humid near surface atmosphere generally is associated with the presence of cloud cover. The magnitude of the relative change in near surface humidity associated with the presence of cloudiness is larger in winter than in summer.
- The models generally successfully reproduce the daily mean OCET in cold seasons, but not for summer or for the diurnal scale.

In this chapter, OCET (defined by Eq. 1.1) was used to assess the near surface temperature change associated with the change in total cloud cover over the extratropical land

areas. It should be noted that at a specific location and in a month cloud-related near surface temperature change calculated from OCET can be different from that calculated from $OCET_1$ (see Appendix B). In other words, OCET is not anytime or anywhere comparable with $OCET_1$ in terms of magnitude and even of sign. As pointed out in Chapter 6 and Appendix B, nighttime OCET or $OCET_1$ is primarily a function of near surface humidity and cloud cover difference between average and clear sky condition (ΔCL) or between overcast and average condition (ΔCL_1); daytime OCET or $OCET_1$ is primarily a function of near surface humidity and other surface conditions, and ΔCL or ΔCL_1 . So, the difference in humidity between OCET and $OCET_1$ cases and/or the difference in ΔCL or ΔCL_1 can lead to the difference in value between OCET and $OCET_1$. However, the *major physics* which determines OCET is similar to that determining $OCET_1$. For example, at the station Springfield of Illinois, during the winter months with overcast days larger than clear sky days, the nighttime OCET is larger than $OCET_1$. The main reason for this difference is that ΔCL_1 is smaller than ΔCL in those months. In addition, the relative lower humidity in OCET case compared to $OCET_1$ case also contributes to the larger value of OCET. But, the positive values of both OCET and $OCET_1$ indicate that the nighttime surface warming in both cases is largely related to cloud downward longwave effect.

The cloud-related near surface temperature change, defined by OCET or $OCET_1$, is primarily the final result of cloud-climate feedback, which involves various dynamic and thermodynamic processes with a wide range of time and space scales. The large discrepancy between data and model and between the warm and cold season simulation (Figs. 5.1 and 5.3) indicate that it is still difficult for most climate models to correctly describe moist convective processes. The CCC model, for example, overpredicted the occurrence of convective clouds, as pointed out by Stuart and Isaac (1994).

CHAPTER 6

TEMPORAL VARIATIONS IN THE CLOUD-RELATED TEMPERATURE CHANGE

6.1 Introduction

Chapter 4, along with Angell (1990), Henderson-Sellers (1989, 1992), Kaiser (1998), Sun and Groisman (2000), and Sun et al. (2000a), reveal that significant changes in cloudiness, including total cloud cover and occurrence of different cloud type frequency, have occurred over the past several decades. Cloudiness changes have been accompanied by changes in surface air temperature (Vinnikov et al. 1990; Jones 1994; Nicholls et al. 1996; Serreze et al. 1999), tropospheric precipitable water (Ross and Elliott 1996, 1998; Zhai and Eskridge 1997), precipitation (Bradley et al. 1987; Groisman and Legates 1995; Dai et al. 1997), and land-surface meteorological processes (Peterson et al. 1995; Vinnikov and Robock 1996; Groisman et al. 1999). These climatic changes should be related to changes in the energy budget of the climate system including cloud-climate feedback. One of the purposes of this chapter is to investigate temporal (diurnal and decadal) characteristics of cloud-related temperature change in the march of contemporary climate change.

Clouds, as well as atmospheric water vapor and snow cover, are an internal component of the climate system. The radiative effects of cloudiness on the surface are closely related to atmospheric humidity (Fung et al. 1984; Sun and Groisman 1999; Table 5.1) and snow on the ground (Cess et al. 1991). The second purpose of this chapter is to quantify and parameterize the impact of water vapor and snow cover on the cloud-related surface air temperature change.

The daily mean surface warming or cooling associated with cloud cover shown in Figs. 5.1-5.4 largely depends upon the competition between the cloud albedo cooling effect and the cloud longwave warming effect. At a specific location and time, cloud cover is one of the important parameters that determine cloud radiative effects. This notion is also supported by

two examples shown in Appendix B: during daytime at the station Spring of Illinois negative $OCET_1$ becomes more negative with the increase in cloud cover difference between overcast and average condition (ΔCL_1); during nighttime at the station Miami of Florida positive $OCET$ increases with the increase in cloud cover difference between average and clear sky condition (ΔCL). In order to better understand the nature of the cloud-related temperature change defined by $OCET$, in this chapter, $OCET$ is normalized by the amount that cloud cover amount differs between average and clear sky conditions, or between overcast and average conditions, in a given month of a year:

$$NOCET = OCET/\Delta CL \quad (6.1.1)$$

$$NOCET_1 = OCET_1/\Delta CL_1 \quad (6.1.2)$$

Thus, these two equations represent the estimates of the full derivative of near surface temperature with respect to total cloud cover, dT/dCL . $NOCET$ ($NOCET_1$), "normalized cloud-temperature relationship", describes how much near surface temperature change is associated with a change in one tenth of total cloud cover. Interestingly, after the removal of cloud cover information from $OCET$ ($OCET_1$), there is no statistically significant relationship between $NOCET$ and ΔCL (between $NOCET_1$ and ΔCL_1) (see Appendix B). Thus, $OCET$ ($OCET_1$) here is decomposed into two relatively independent terms $NOCET$ and ΔCL ($NOCET_1$ and ΔCL_1).

The outline of this chapter is as follows. First, I describe the data processing. Next, the impact of water vapor and snow cover on the cloud-related surface air temperature change is assessed for nighttime and daytime respectively. A general $OCET$ model, represented by cloud cover, surface humidity, and snow cover, is also constructed in this section. Finally, in Section 4, interdecadal changes in $NOCET$ ($OCET$) in the past several decades in four regions of the Northern Hemisphere (the contiguous U.S., Canada south of $55^\circ N$, the FUSSR south of $60^\circ N$, and China east of $110^\circ E$) are analyzed.

6.2 Data Pre-processing

The national archives of synoptic data described in Chapter 2 from regions with a better station spatial coverage are used in this study: the contiguous U.S., southern Canada (south of 55°N), the southern area of the FUSSR (south of 60°N), and eastern China (east of 110°E). Data from nine stations over the humid western tropical Pacific islands are also used in this chapter to see if the cloud-temperature-water vapor relationship over the humid tropics is different from that over the extratropical land areas. Five measurements at local standard time (LST) 23, 24, 01, 02, and 03 (12, 13, 14, 15, and 16) in North America and the western tropical Pacific, one measurement at 02 (14) LST in China, and one at 01 (13) LST or two (after 1966) at around noon (midnight) and 03 (15) LST in the FUSSR, are selected to assess the cloud-related near surface temperature change for the nighttime (daytime) period.

OCET (see Eq. 2.1) is defined as the difference in near surface temperature between average and clear sky (total cloud amount ≤ 2 tenths) conditions. In each year for a given time of day, the mean monthly OCET is calculated by subtracting monthly mean T under clear sky conditions from mean temperature. These temperature differences are then averaged over the selected nighttime and daytime periods. Thus, time series of monthly OCET are constructed for both nighttime and daytime at each station. Time series of the normalized cloud-temperature relationship, NOCET, are then created by dividing OCET by the difference of monthly cloud amount between average and clear sky conditions at each station. In a humid atmosphere, the lack of a sufficient number of clear sky cases in a given month affects the estimate of OCET. To ensure that the OCET assessment over North America and Eurasia is robust, and to secure reliable OCET estimates in the tropics, where the clear sky observations are few, the same approach is used to construct the normalized OCET₁ and NOCET₁ time series at each station.

All OCET (OCET₁) estimates, as well as other climatic variables, such as monthly cloud amount (CL), near surface temperature (T) and specific humidity (q) under average, clear

sky, and overcast conditions are spatially averaged across the contiguous U.S., southern Canada, the southern FUSSR, and eastern China by using the Thiessen method (see Section 3.2). To estimate the averaged variables in the western tropical Pacific, arithmetic averaging is used. Finally, the countrywide averaged mean monthly (seasonal) time series of nighttime and daytime OCET, $OCET_1$, NOCET, $NOCET_1$, CL, T, T_{clear} , $T_{overcast}$, q, q_{clear} , and $q_{overcast}$ are created and used in various statistical analyses in next sections.

6.3 Parameterizations of the Cloud-Related Temperature Change

Daytime cloud-related near surface temperature change largely depends upon the competition between cloud shortwave cooling effect and cloud longwave warming effect. During nighttime, only cloud longwave effect works. So, understanding nighttime cloud-temperature relationship can help us separate the contribution of cloud shortwave effect to the daytime NOCET. In this section, the nighttime cloud-temperature relationship (represented by NOCET) is therefore first analyzed.

6.3.1 Nighttime

Figs. 6.1-6.5 shows the countrywide variations of the seasonal/annual NOCET and near surface specific humidity under clear sky conditions, q_{clear} . Please note that NOCET is multiplied by -1 on the y-axis of Figs. 6.1-6.5 in order to visually highlight the negative relationship between NOCET and surface humidity. The statistically significant anti-correlation between NOCET and q_{clear} in each season and region (except in autumn over eastern China, which will be discussed later in this section) indicates that changes in the nighttime NOCET are inversely associated with near surface humidity. This conclusion is also supported by the fact that over all regions of interest the winter NOCET is larger than the summer NOCET.

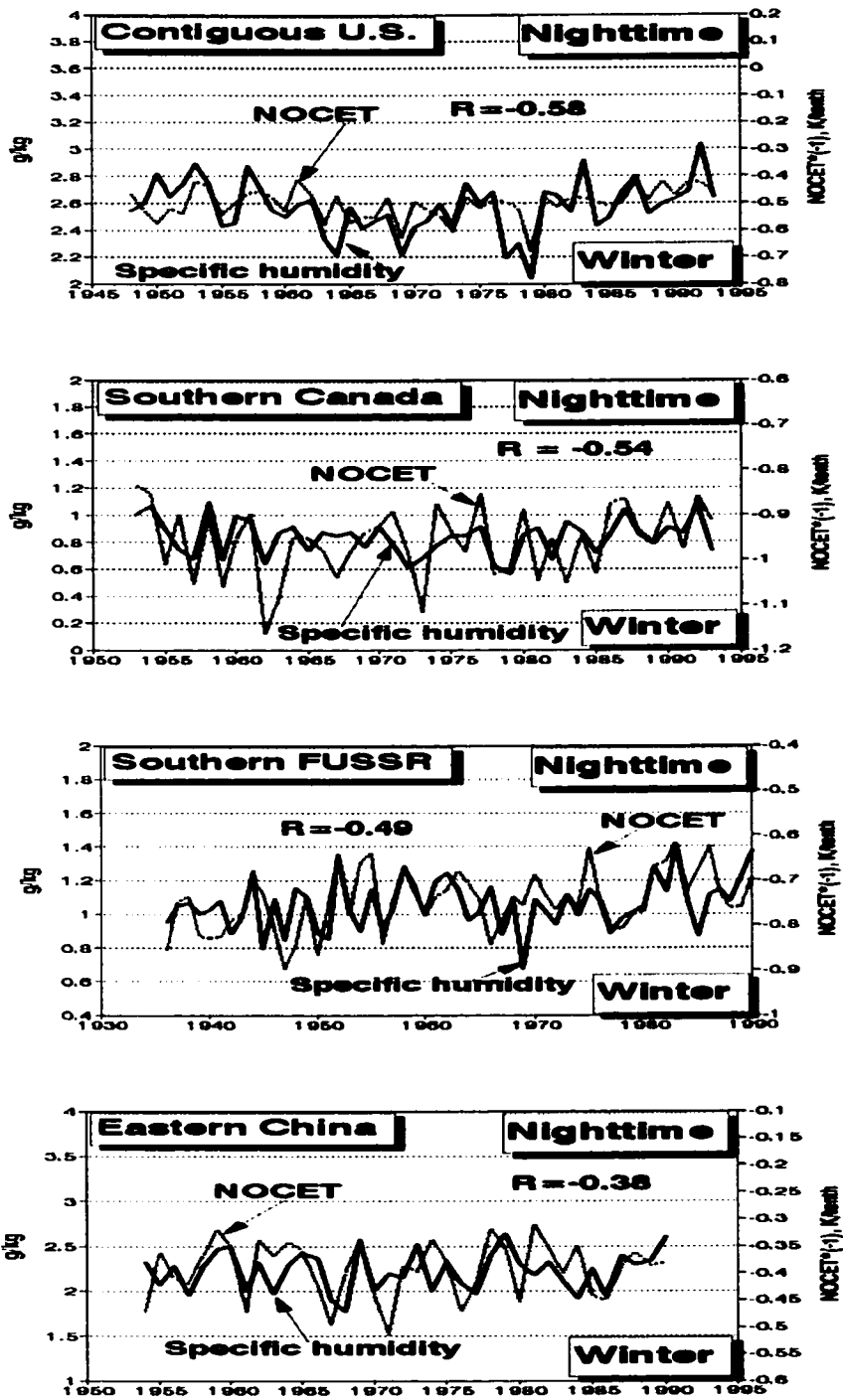


Figure 6.1 Variations of winter nighttime near surface specific humidity under clear skies and normalized cloud-related temperature change (NOCET) (multiplied by -1) area-averaged over the contiguous U.S., Canada (south of 50°N), the FUSSR (south of 60°N), and china (east of 110°E). Correlation coefficients, R, are statistically significant at the 0.05 level.

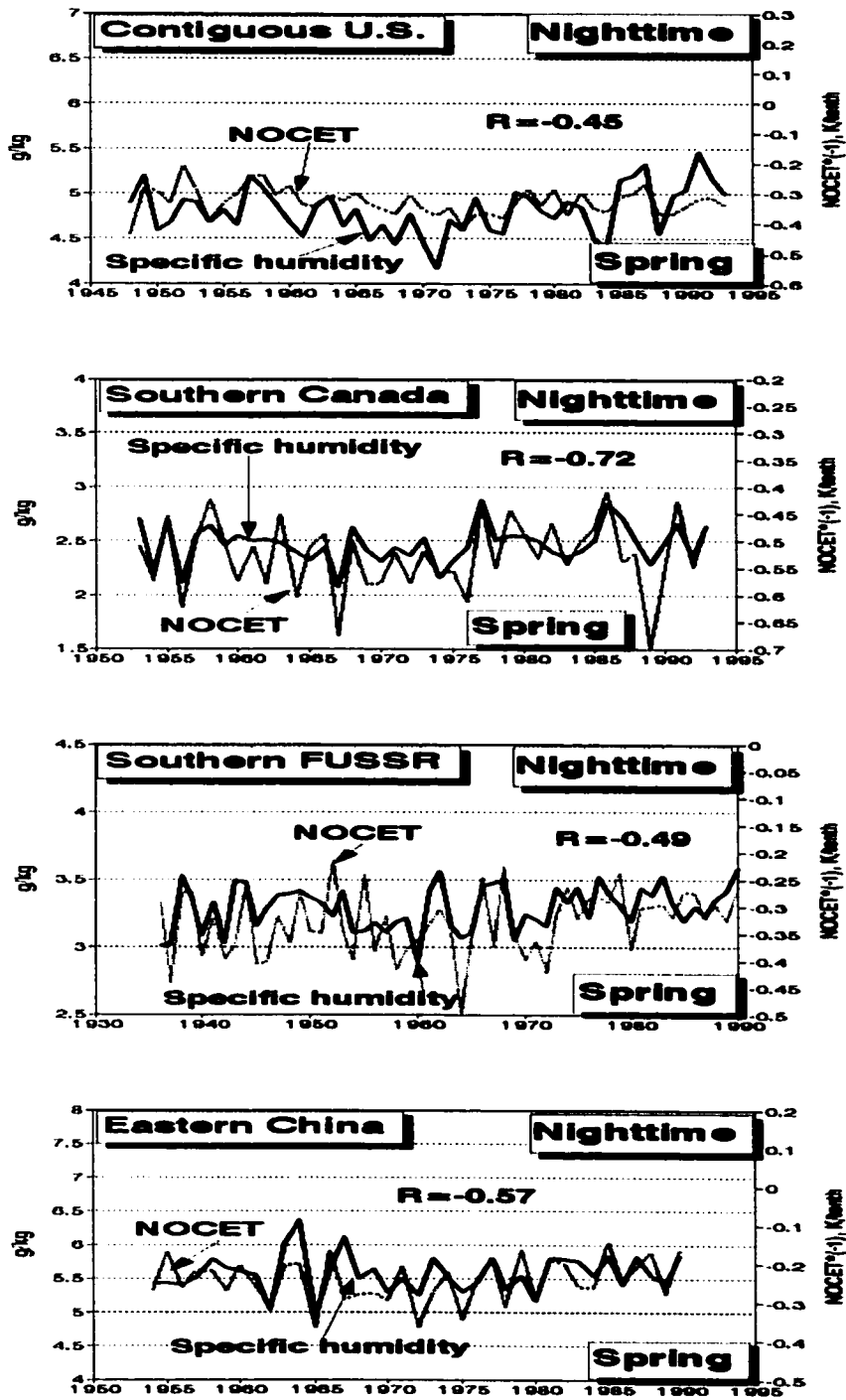


Figure 6.2 Same as Fig. 6.1 except for spring.

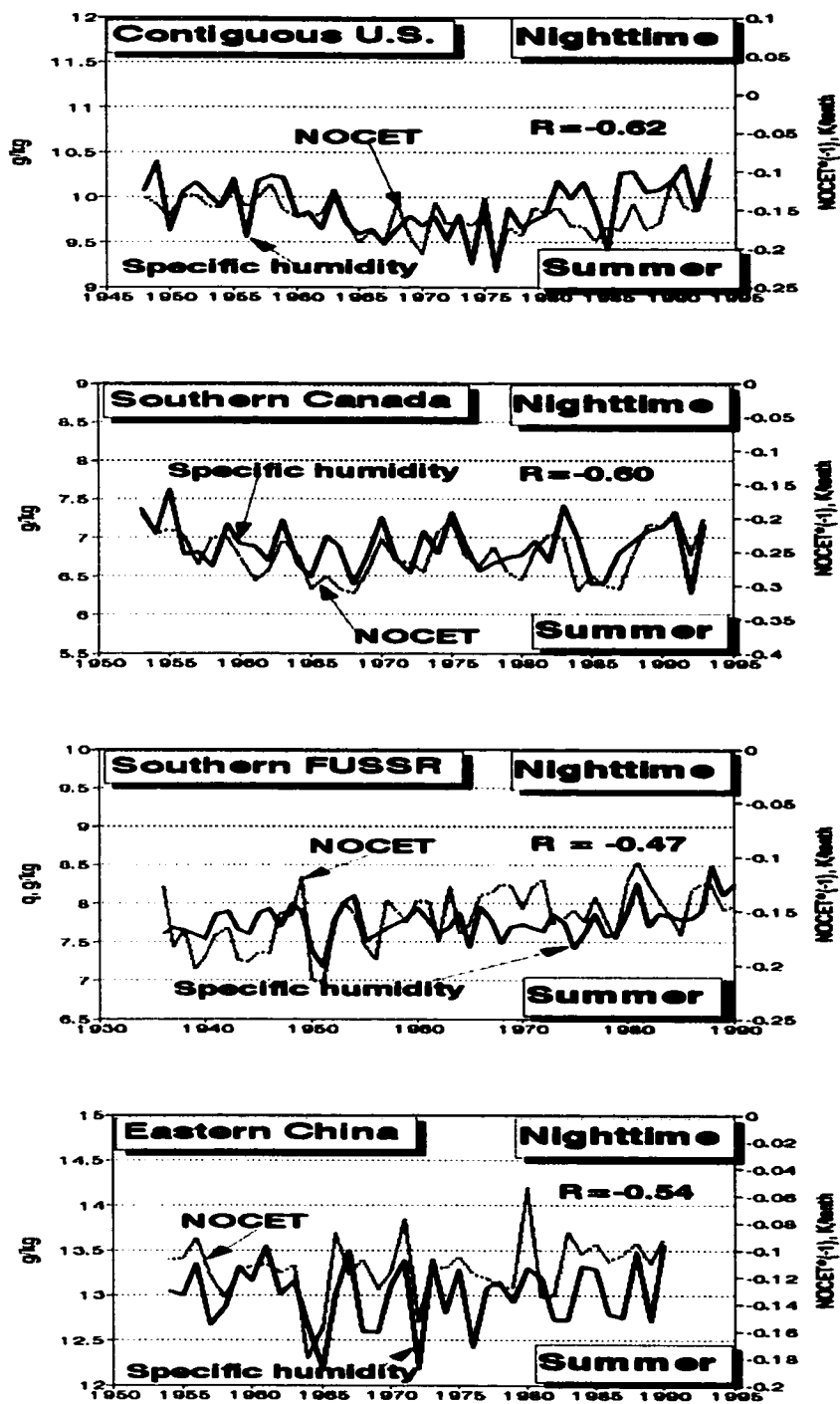


Figure 6.3 Same as Fig. 6.1 except for summer.

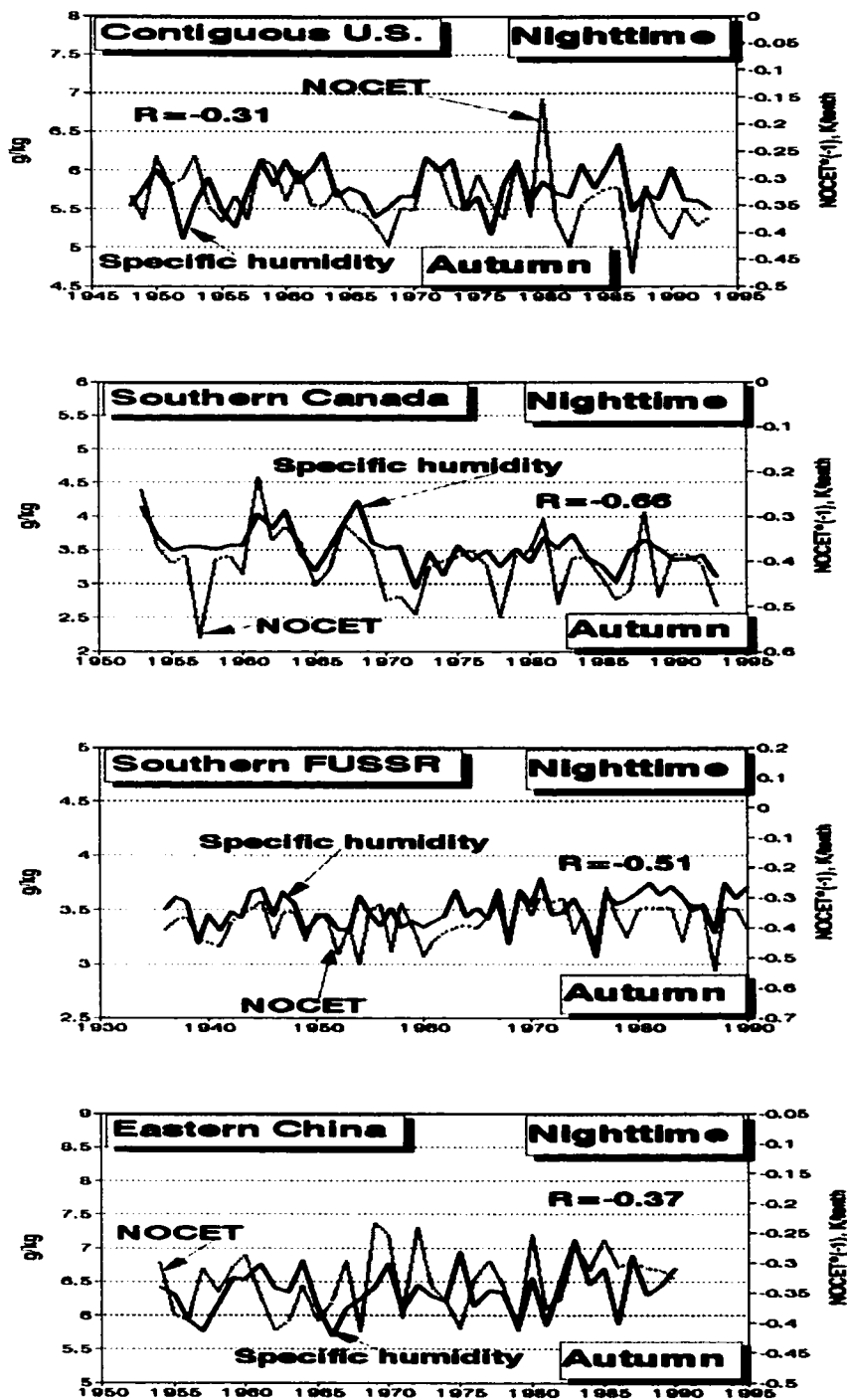


Figure 6.4 Same as Fig. 6.1 except for autumn.

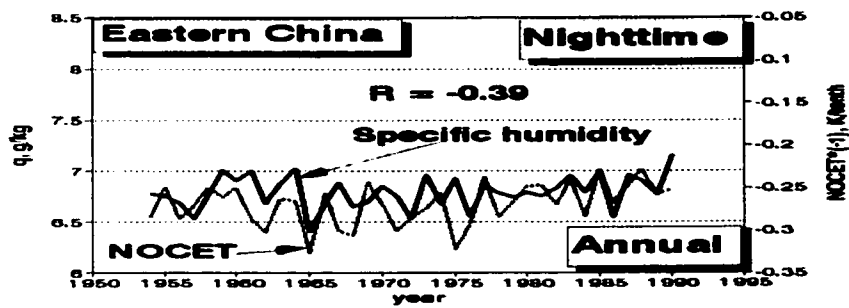
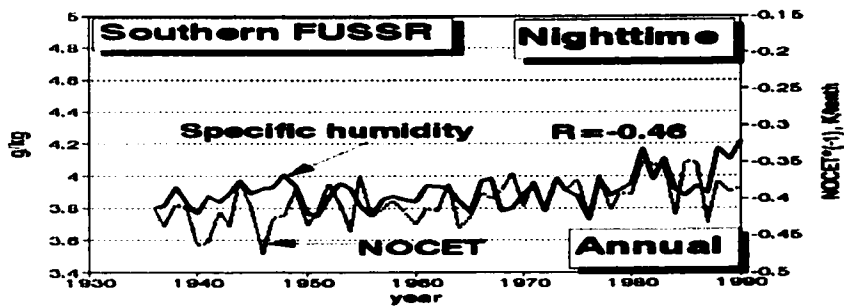
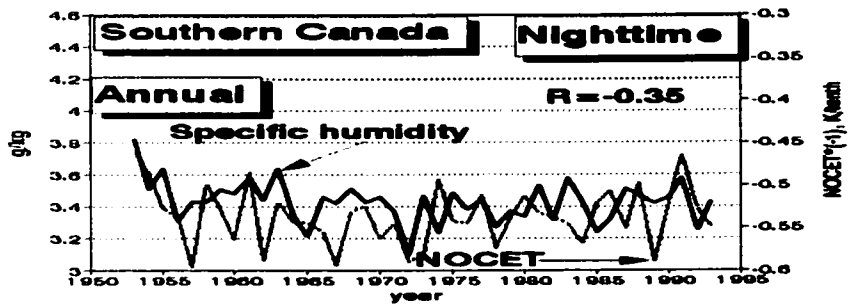
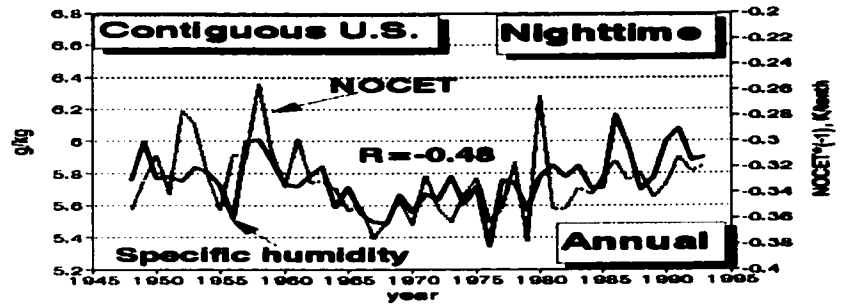


Figure 6.5 Same as Fig. 6.1 except for annual mean.

The statistical relationship between NOCET and near surface specific humidity under all sky conditions (q_{ave}) is similar to the one between NOCET and q_{clear} shown in Figs. 6.1 6.5., but the absolute value of the correlation coefficient between NOCET and q_{clear} is larger than the one between NOCET and q_{ave} . Also, the NOCET variance explained by q_{clear} (Fig. 6.6) is larger than the one explained by q_{ave} . Therefore, in this chapter, q_{clear} , instead of q_{ave} , is selected to estimate the impact of water vapor on the cloud-related surface air temperature change.

Fig. 6.6 shows the nighttime relationship between NOCET and near surface specific humidity under clear sky conditions. All the data points in this figure represent the monthly mean values area-averaged over the contiguous U.S., southern Canada, the southern FUSSR, and eastern China for the past several decades. So, the data points with lower q_{clear} come from higher latitudes and/or colder seasons while the data points with higher q_{clear} come from lower latitudes and/or warmer seasons. All values of the NOCET points in Fig. 6.6 are above zero, suggesting that at nighttime a surface warming should be associated with cloud cover. This cloud-related surface warming is much stronger in high latitudes and/or cold seasons than in low latitudes and/or warm seasons.

Fig. 6.6 clearly shows that the nighttime cloud-related surface warming is closely dependent upon near surface specific humidity: NOCET decreases with the increase in near surface humidity. Moreover, the NOCET- q_{clear} relationship in Fig. 6.6 is nonlinear: NOCET is more sensitive to humidity in a dry atmosphere than in a humid atmosphere. For example, an additional 10% increase in q_{clear} corresponds to a decrease in nighttime surface temperature of 1 K in a dry atmosphere with monthly $q_{clear} \sim 0.8$ g/kg, but only 0.1 K in a humid atmosphere with $q_{clear} \sim 14$ g/kg.

The negative correlation between near surface humidity and NOCET might be related to the fact that water vapor is a strong greenhouse gas (Brunt 1932; Raval and Ramanathan 1989) and it absorbs a portion of infrared radiation emitted from the cloud base. Therefore,

with an increase in atmospheric water vapor (Gandin et al. 1976), the cloud longwave warming effect on surface temperature is reduced (Stephens et al. 1994; Zhang et al. 1995; Dai et al. 1999).

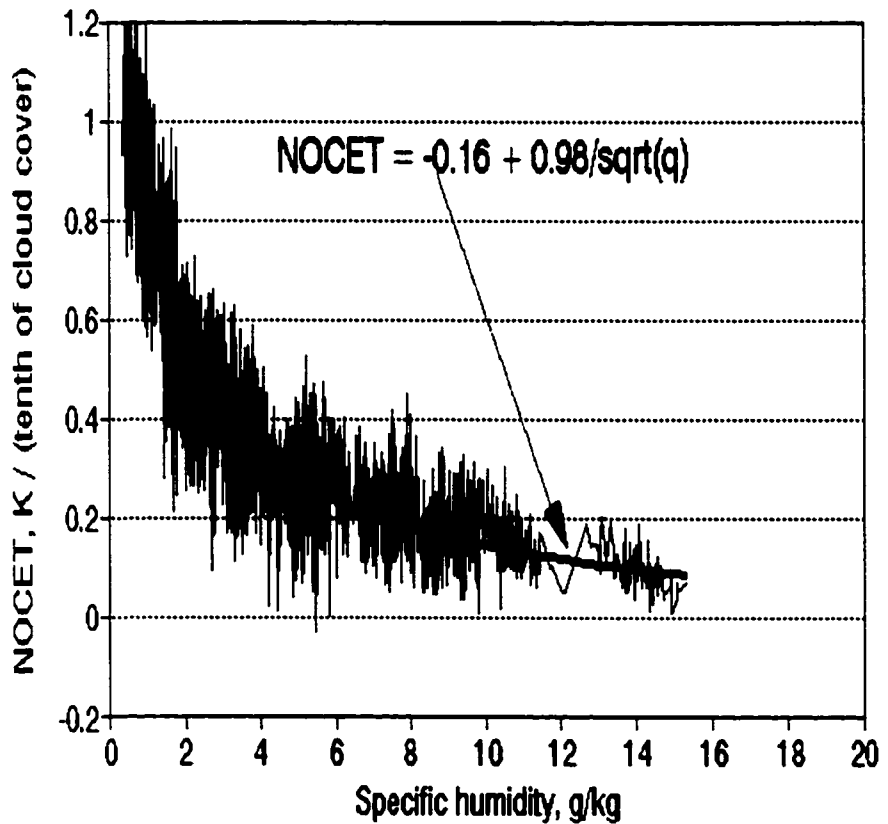


Figure 6.6 Normalized nighttime cloud-related temperature change (NOCET) as function of near surface specific humidity and its functional approximation. Estimates are based on 2148 individual monthly NOCET values area averaged over the four countries of interest.

Additionally, air advection may be the factor that leads to the larger sensitivity of NOCET to surface water vapor in a dry atmosphere than in a humid atmosphere shown in Fig. 6.6. According to Herman and Goody (1976) and Curry (1983), over high latitudes where the atmospheric water vapor content is small, the warm and moist air mass advected from the south contributes to the formation and development of low stratiform clouds. This cloud-related warm air advection therefore largely enhances surface warming caused by cloud downward longwave effect. Also, clear sky conditions over middle and high latitudes in winter are always associated with colder air advection or colder air masses, thus largely contributing to the cloud-related surface warming. For example, strong and frequent synoptic monsoonal advection over China during the cold season (Ding 1994) may affect surface air temperature associated with cloudiness, thus lowering the NOCET- q_{clear} correlation (see Fig. 6.1). In spring and summer, the cold air advection is less frequent, and, coincidentally, in these two seasons in each country under consideration, more than 23% (and up to 56% in spring in south Canada) of the interannual NOCET variance is ascribed to q_{clear} . The nonlinear nature of NOCET with near surface humidity shown in Fig. 6.6 indicates that cloud-related near surface temperature change, NOCET, is determined not only by cloud radiative flux but also is affected by the water vapor greenhouse effect and air advection.

The scattered nature of NOCET values at a given q_{clear} value in Fig. 6.6 can be caused by many factors. Firstly, although all NOCET points at a given q_{clear} are associated with one unit of cloud cover, the NOCET points from different time and/or location can have different cloud height, cloud thickness, and cloud microphysical characteristics, thus different radiative effects (see Appendix D). Secondly, the land surface with different characteristics, including vegetation, soil moisture, and snow cover extent, can have a different impact on surface-air heat exchange and surface air temperature (Groisman et al. 1997; Zeng and Dickinson 1998), thus on NOCET. Thirdly, the data points with the same value of near surface water vapor do not

certainly have the same amount of accumulated atmospheric water vapor between the surface and cloud base, which is the essential value determining the strength of the weakening of cloud downward longwave effect (Raval and Ramanathan 1989; Inamdar and Ramanathan 1994). For example, the amount of lower tropospheric precipitable water at the site (time) in the presence of a lower tropospheric inversion is larger than that at the same site (time) in the presence of a normal boundary layer structure; also the characteristic of lower tropospheric inversions change with time (Bradley et al. 1993). So, the degree to which cloud downward longwave effect reduced by atmospheric water vapor can differ. Lastly, the advection of air masses with different temperature can lead to the difference in NOCET.

The functional relationship of NOCET with q_{clear} shown in Fig. 6.6 is approximated by the formula:

$$\text{NOCET}=f(q_{\text{clear}})=-0.14 + 0.93 (q_{\text{clear}})^{-0.5} \quad (6.2.1)$$

Where q is measured in g/kg and the coefficients are estimated using the least squares method. The least squares method gives biased estimates of the parameters of the linear functional relationship, $Y=\alpha_0+\alpha_1X$, when the X -variable is measured with error. Usually the absolute values of the α_1 -estimates are reduced (Kendall and Stuart 1972). Therefore, after the form of $f(q_{\text{clear}})$ is selected, these parameters are debiased by applying the instrumental variable method (Geary 1949) (see Appendix E). The unbiased estimate of α_1 appears to be only 5% higher than that obtained by the least squares method. Eq. 6.2.1 is thus converted to

$$\text{NOCET}=f(q_{\text{clear}})=-0.16 + 0.98 (q_{\text{clear}})^{-0.5} \quad (6.2.2)$$

The red regression curve shown in Fig. 6.6 describes 83% of the monthly countrywide NOCET variance. So, the nighttime cloud longwave related near surface temperature change per one tenth change in total cloud cover can be well parameterized by near surface humidity term $0.98 (q_{\text{clear}})^{-0.5}$ and a constant -0.16.

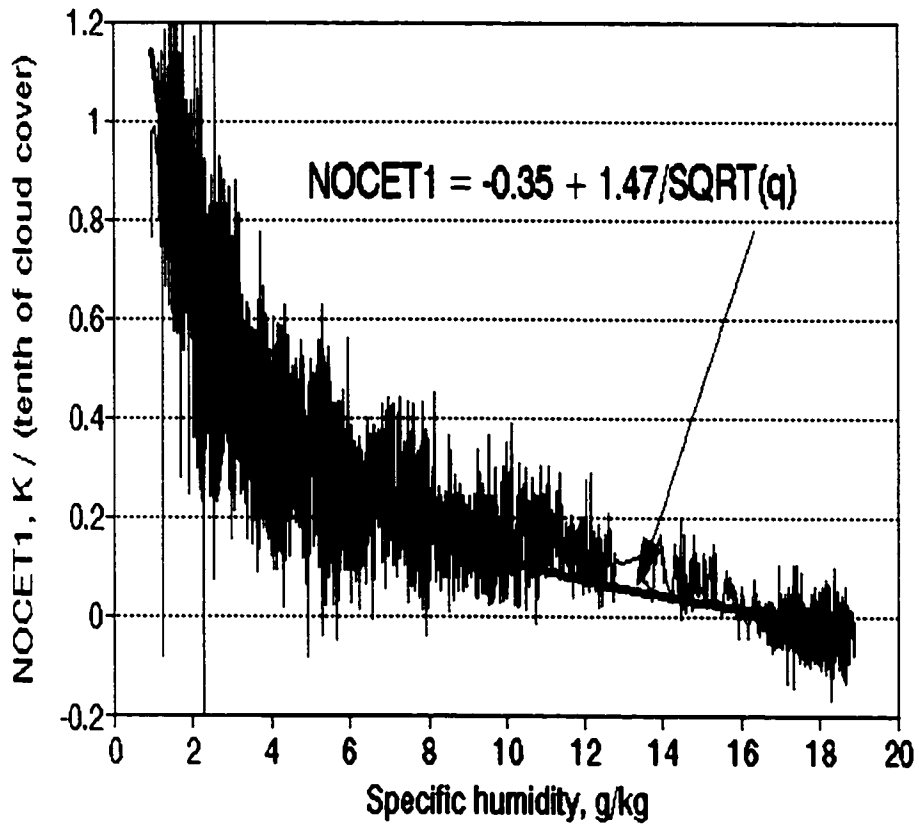


Figure 6.7 Same as Fig. 6.6 except for NOCET_1 on the y-axis and q_{overcast} on the x-axis. Estimates are based on 2688 individual monthly NOCET_1 values area averaged over the four countries in Fig. 6.6 and arithmetically averaged over the western tropical Pacific islands.

Fig. 6.7 is similar to Fig. 6.6 except for NOCET_1 on the y-axis and q_{overcast} on the x-axis. According to Eq. 6.1.2, NOCET_1 is defined as the near surface temperature difference between overcast and average weather conditions associated with one tenth of cloud cover. So Fig. 6.7 can include the data from the western tropical Pacific, where clear sky observations are few.

The data points with q values from -17 to 19 g/kg in Fig. 6.7 are from the western tropical Pacific islands.

Fig. 6.7 provides an important x-axis extension: for q_{overcast} above 16 g/kg the NOCET_1 estimates are close to zero or negative. So, in the atmosphere with a high level of moisture content, clouds may totally lose their downward longwave warming effect. In other words, the longwave radiation from the cloud base may be completely or largely absorbed in the lower troposphere and cannot reach the surface. Now the question is from where does the cloud-related surface cooling come? From our synoptic data set it was found that climatologically over the western tropical Pacific islands, the near surface wind speed under overcast conditions is larger than that under average conditions by more than 10%. So, the nighttime surface cooling over the western tropical Pacific islands associated with overcast conditions might be caused by stronger surface evaporative cooling related to a stronger lower level moisture convergence.

The cluster of data points from the western tropical Pacific islands in Fig. 6.7 therefore supports the notion that surface evaporative cooling plays an important role in maintaining the stability of the warm pool sea surface temperature (Fu et al. 1992; Hartmann and Michelson 1993) in addition to cloud albedo forcing (Ramanathan and Collins 1991). Though also operating over the extratropical land areas, the effect of surface evaporation on NOCET should be much weaker due to far less saturated surfaces. The regression equation of NOCET_1 is

$$\text{NOCET} = f(q_{\text{overcast}}) = -0.35 + 1.47 (q_{\text{overcast}})^{-0.5} \quad (6.2.3)$$

Where q is measured in g/kg. The de-biasing estimate technique increases $f(q_{\text{overcast}})$ by only 5% and this relationship again describe 83% of the monthly NOCET_1 variance. So, under NOCET_1 cases, the nighttime cloud longwave related near surface temperature change is simply parameterized by a constant term -0.35 and the near surface humidity term $1.47 (q_{\text{overcast}})^{-0.5}$.

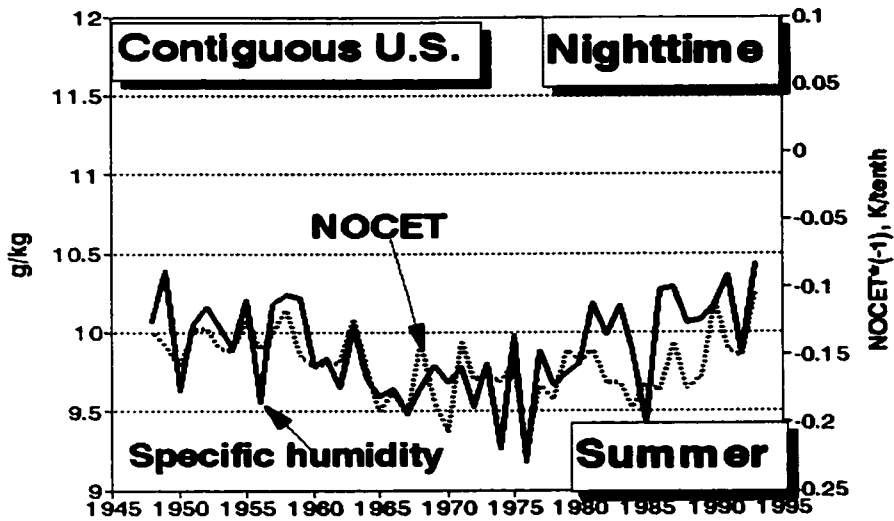
Surface based measurements of nighttime cloud amount are usually underestimated and clear sky occurrences are usually overestimated due to inadequate illuminations of the clouds (Hahn et al. 1995). This could affect the estimates of the nighttime cloud-related temperature change defined by OCET (NOCET). So, it is necessary to check the reliability of this cloud-temperature relationship by using the moonlight criterion suggested by Hahn et al. (1995). Appendix C indicates that the nighttime cloud detection bias is not critical in analyzing temporal changes in NOCET.

6.3.2 Daytime

The daytime NOCET is the daytime cloud-related surface air temperature change per one tenth change in total cloud cover, in which both longwave and shortwave effects of cloudiness are involved. Next, the nighttime cloud longwave related surface air temperature change, represented by $-0.16 + 0.98 (q_{\text{clear}})^{-0.5}$, will be used to account for the daytime cloud longwave related surface temperature change and thus to separate the cloud shortwave related temperature change from the daytime NOCET. But before doing this separation, we should make sure that it is reasonable to use the nighttime parameterization to account for the daytime cloud longwave related temperature change.

Fig. 6.8 shows an example of the similarity between the nighttime and daytime NOCET- q_{clear} relationship: over the contiguous U.S. during summer the correlation coefficient between nighttime NOCET and q_{clear} is -0.62, which is close to the daytime value of -0.45. However, a rigorous method of checking whether the nighttime NOCET- q_{clear} relationship can be used to account for the infrared radiation effect of cloudiness and its relationship with near surface temperature in the daytime NOCET, is to see whether the derivatives, $d\text{NOCET}/dq$, are the same (or statistically insignificantly different) between nighttime and daytime.

A



B

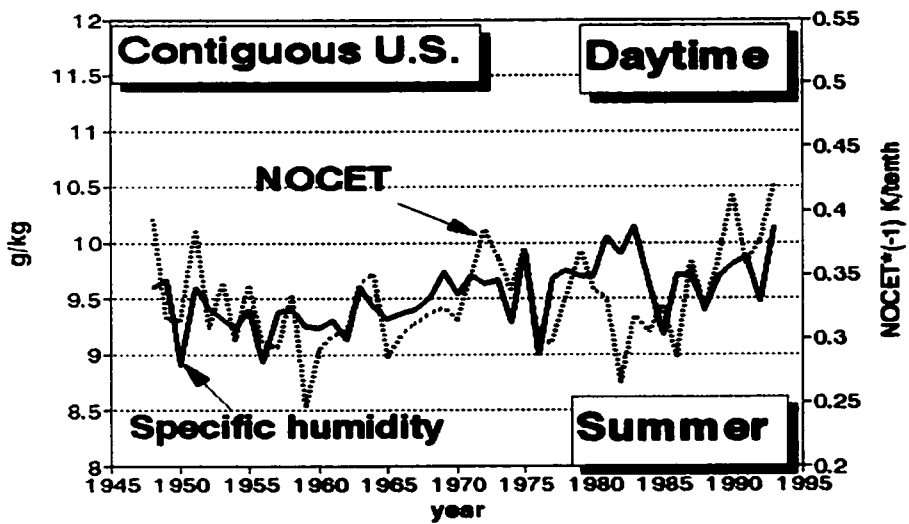


Figure 6.8 Relationship between NOCET (multiplied by -1) and near surface specific humidity under clear skies area-averaged over the contiguous U.S. during summer for (A) nighttime and (B) daytime.

Table 6.1 Estimates of derivative $d\text{NOCET}/dq_{\text{clear}}$ for night- and daytime over four different countries and seasons.

Country	Season	Nighttime estimates		Daytime estimates	
		$d\text{NOCET}/dq_{\text{clear}}$	its σ	$d\text{NOCET}/dq_{\text{clear}}$	its σ
Contiguous U.S.	winter	-0.163	0.035	-0.153	0.052
	spring	-0.077	0.022	-0.069	0.034
	summer	-0.051	0.010	-0.058	0.017
	autumn	-0.062	0.029	-0.077	0.032
Canada south of 55°N	winter	-0.317	0.079	-0.354	0.073
	spring	-0.266	0.041	-0.226	0.053
	summer	-0.068	0.015	-0.060	0.024
	autumn	-0.176	0.032	-0.235	0.039
FUSSR south of 60°N	winter	-0.220	0.054	-0.223	0.048
	spring	-0.180	0.044	-0.203	0.035
	summer	-0.054	0.014	-0.011*	0.021
	autumn	-0.203	0.048	-0.118*	0.044
China east of 110°E	winter	-0.091	0.038	-0.034*	0.027
	spring	-0.117	0.028	-0.005*	0.022
	summer	-0.034	0.009	-0.024	0.012
	autumn	-0.057	0.024	-0.029*	0.025

* This regression estimate is not statistically significantly different from zero.

Table 6.1 provides a proof that this is the case. Each line of this table gives two estimates of $d\text{NOCET}/dq_{\text{clear}}$ for nighttime and daytime respectively. Each of these derivatives is estimated using a simple linear regression equation that approximates the general relationship between NOCET and q_{clear} for a given season and country. In each case (except the regions where the daytime NOCET- q_{clear} relationship is not seen at all, for example, over eastern China) the hypothesis that these two derivatives are the same cannot be rejected at the 0.05 level of statistical significance. This exercise assures us that we can use the parameterization of the nighttime NOCET to account for the daytime cloud longwave related near surface temperature change and thus to separate the cloud shortwave related surface temperature change from the daytime NOCET (i.e., simply subtract the component responsible for the nighttime NOCET from the daytime NOCET).

However, it should be kept in mind that clouds, particularly the convective clouds, have a strong diurnal cycle, so the infrared radiative effect of clouds can differ between day and night even though the cloud amount stays the same. The method we use here is thus not very strict in terms of this aspect. Nevertheless, Table 6.1 suggests that the *climatological* dependence of cloud longwave related temperature change on near surface water vapor derived from nighttime case is approximately the same as that derived from daytime case.

During daytime, in addition to cloud albedo effects, changes in land surface characteristics, such as vegetation, soil moisture, and snow cover, can affect surface temperature, and therefore the daytime NOCET, through modifying surface-atmosphere heat fluxes and surface albedo. Of these factors, snow cover is the most effective in changing surface albedo, and therefore, surface temperature in the seasonal cycle: surface albedo increases quickly from ~ 0.2 for bare soil to ~ 0.8 for fresh snow on the ground (Henderson-Sellers and Robinson 1986). We do not have any large-scale representative soil moisture and vegetation data for the four countries under consideration and leave their effects to the further

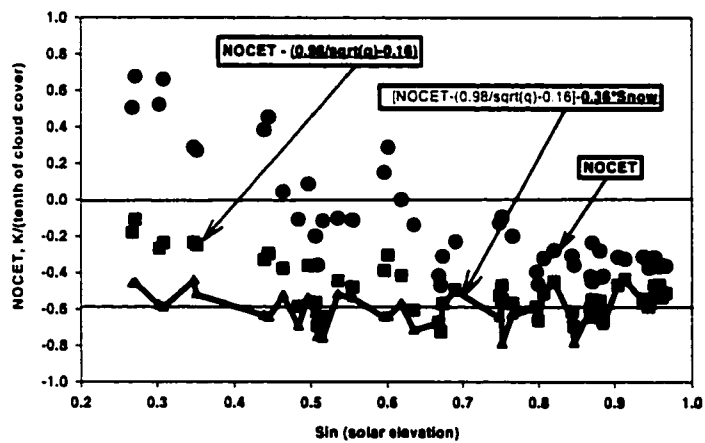


Figure 6.9 Daytime normalized cloud-related temperature change (NOCET) and its decompositions. The x-axis represents the sine function of monthly mean noontime solar elevation. All the data points in this figure represent long-term (1972-1990) monthly mean area-averaged values over the four countries of interest.

study. But snow on the ground is a first-order factor that should be taken into account when we try to analyze the daytime cloud-related temperature change.

Fig. 6.9 presents the daytime NOCET and its decomposition versus sine of mean monthly noontime solar elevation. All the data points in Fig. 6.9 represent long-term monthly mean (1972-1990) countrywide area-averaged values of NOCET and its decomposition over the contiguous U.S., southern Canada, the southern FUSSR, and eastern China. The solar elevation changes from 15° in December over the FUSSR south of 60°N to 75° in June over eastern China. The correlation graph in Fig. 6.9 illustrates how the daytime NOCET (represented by red plus symbol) changes with latitude and season: with lower solar elevation NOCET is positive, i.e., a daytime surface warming is associated with cloud cover; but with higher solar elevation NOCET is negative and so a daytime cooling associated with cloud cover prevails. After the cloud longwave related surface temperature change, represented by $-0.16+0.98 (q_{\text{clear}})^{-0.5}$, is removed from the daytime NOCET, Fig. 6.9 shows that the residual term (represented by the blue squares), RT_1 , is negative regardless of the value of the solar elevation. So, at this point, a surface cooling is associated with cloud cover anywhere and anytime. This cloud-related surface cooling, RT_1 , represented by blue squares, increases with the increase of monthly solar elevation (or incoming solar radiation), that is, it increases from cold to warm seasons and from high to low latitudes. RT_1 is found to be negatively correlated with snow cover extent (Fig. 6.10). The negative correlation between RT_1 and snow cover extent is accounted for by the following two reasons. Firstly, snow cover extent is inversely associated with solar elevation and thus negatively associated with the amount of solar radiation at the top of the atmosphere. Therefore, the surface with a larger snow cover extent tends to correspond to a weaker cloud shortwave cooling effect and thus a weaker cloud-related surface cooling. Secondly, due to high albedo, snow on the ground reduces the difference in the amount of solar radiation which the surface receives between average and clear sky conditions.

thus reducing the near surface temperature difference between average and clear sky conditions. The impact of snow cover albedo on cloud shortwave related temperature change (RT_1) is also seen in Fig. 6.11. In Canada and the FUSSR, the December snow cover extent is close to that in February, but, on average, the upper layer of snow on the ground during the accumulation period is "fresher" than that at the end of the winter. As a result, snow aging affects RT_1 by reducing the snow cover albedo, increasing the difference in shortwave radiation which the surface absorbs between average and clear sky conditions, therefore enhancing the near surface temperature difference between these two cases compared to the situation with new snow on the ground. The February RT_1 over both the FUSSR and Canada is therefore much less (more negative) than in December.

The year-round correlation coefficient between RT_1 and snow cover extent, S , for all four countries together is 0.60, and for three countries (except eastern China) is 0.70. Only a small portion of eastern China has permanent snow cover during the winter, thus making the relationship between snow cover and RT_1 insignificant over this country.

The linear regression of monthly RT_1 on S yields

$$RT_1 = 0.31S - 0.74 \quad (R^2 = 0.36, \text{ with sample size, } N = 912) \quad (6.3.1)$$

The use of the instrumental variable method increases the dRT_1/dS parameter to 0.36:

$$RT_1 = 0.36S - 0.75 \quad (6.3.2)$$

After the S -effect on surface temperature represented by $0.36S$ in Eq. 6.5 is further removed from RT_1 , the residual term of the daytime NOCET, RT_2 , represented by the red curve (Fig. 6.9), is negative and no longer correlated with the solar elevation and thus the amount of incoming solar radiation (Fig. 6.9). Its mean value is ~ -0.59 and its standard deviation is less than 0.1. The random nature of RT_2 with solar elevation is better seen in Fig. 6.12, where each dash represents a countrywide area-averaged monthly value over the period 1972-1990.

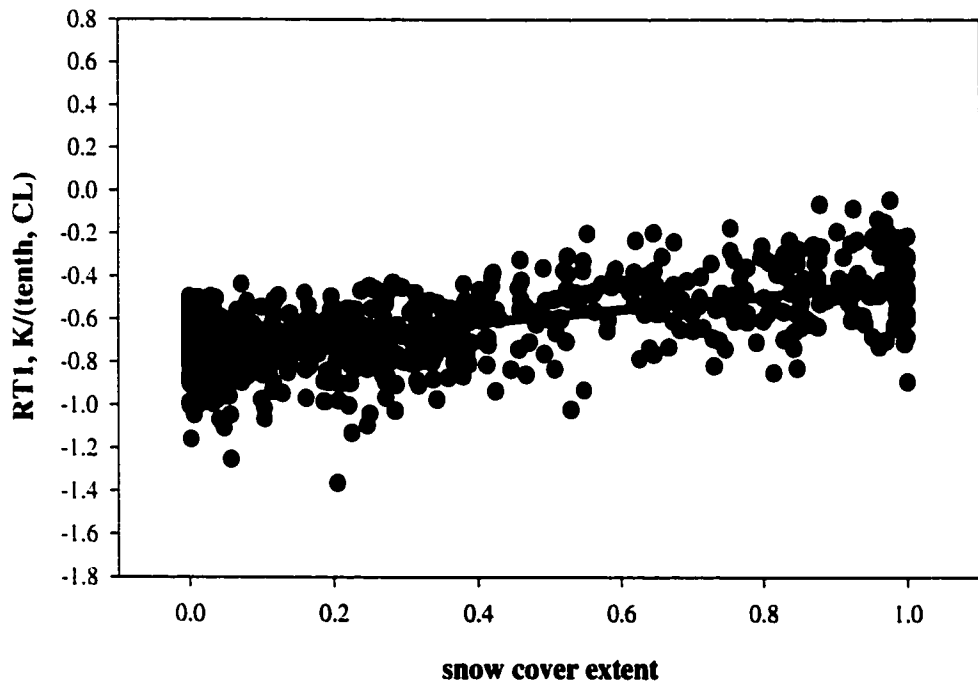


Figure 6.10 Relationship between snow cover extent and RT_1 ($= \text{daytime NOCET} - (0.16 + 0.98 (q_{\text{clear}})^{-0.5})$). All the data points represent monthly mean area-averaged values over the four countries in consideration over the period 1972-1990.

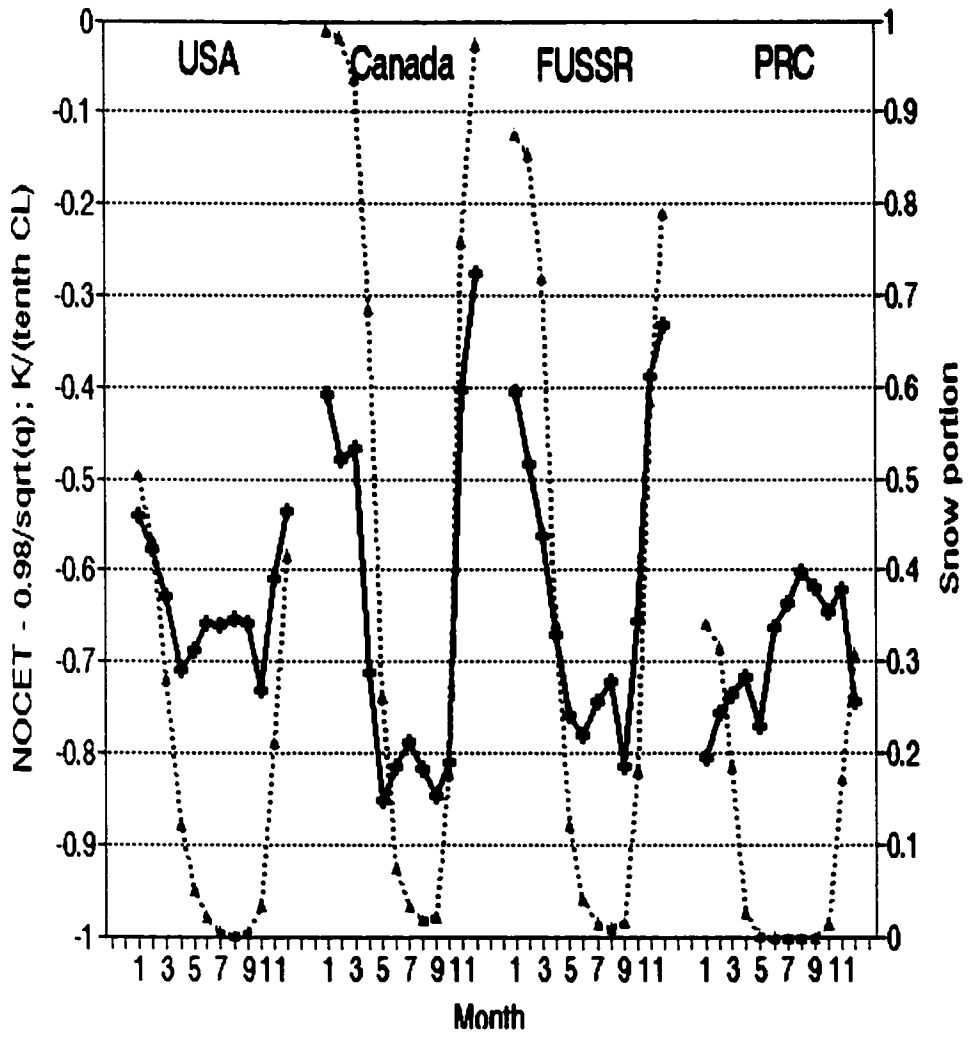


Figure 6.11 Relationship between snow cover extent and residual term RT_1 . The black solid line represents RT_1 (the left y-axis) and the red dotted line represents snow cover extent (the right y-axis).

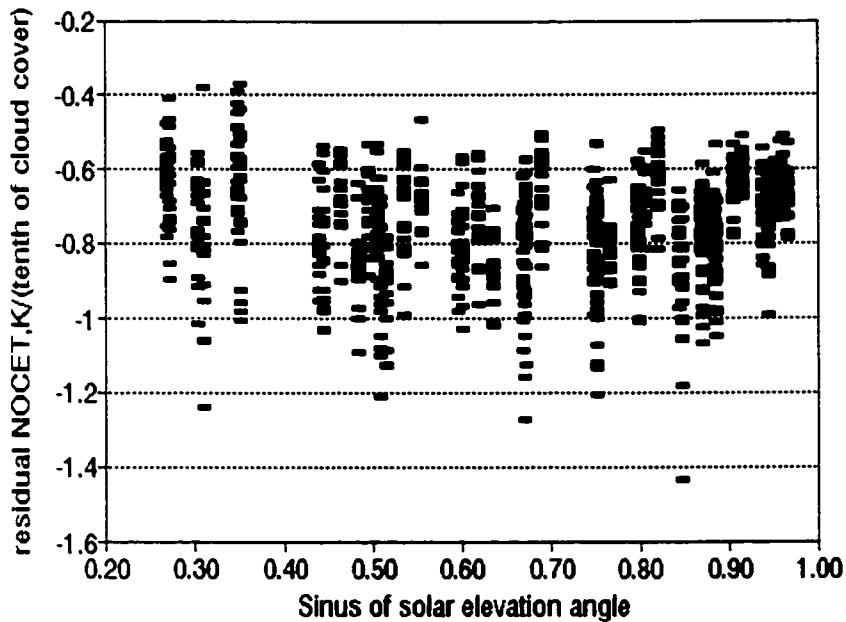


Figure 6.12 Residual term, RT_2 , for individual months of 1972-1990 area-averaged over the four countries of interest. Here $RT_2 = \text{NOCET} - (0.98/\sqrt{q_{clr}}) - 0.16) - 0.36*\text{snow}$.

Fig. 6.9 indicates that daytime surface temperature change associated with a change in one unit of cloud cover can be well represented by a snow cover term ($0.36S$, S is snow cover extent) and a constant of -0.59 (K/tenth of cloud cover) after cloud longwave related temperature change is removed.

6.3.3 General Model of the Cloud-Related Temperature Change

In the above two sections, based on hourly data from several regions of the Northern Hemisphere extending from mid-high latitudes to the tropics, the near surface temperature

change associated with cloud cover has been consequently decomposed into the product of cloud cover, CL, and NOCET.

$$\text{OCET} = \text{NOCET} * \Delta\text{CL} \quad (6.4)$$

The latter then was parameterized using two other internal climatic variables, surface specific humidity under clear skies, q_{clear} , and snow on the ground, S:

$$\text{NOCET (nighttime)} - 0.98 (q_{\text{clear}})^{-0.5} + 0 + 0.16 = \epsilon_1 \quad (6.5.1)$$

$$\text{NOCET (daytime)} - 0.98 (q_{\text{clear}})^{-0.5} - 0.36S + 0.75 = \epsilon_2 \quad (6.5.2)$$

Eqs. 6.5.1 and 6.5.2 can be interpreted as empirical estimates of the derivative dT/dCL . A unit of cloud cover, after the removal of cloud longwave related temperature change and snow information, is noticeably associated with a daytime surface cooling of 0.59 K. The same cooling occurs in winter in high latitudes and in summers in the tropics.

Table 6.2 NOCET variance, D, and the variance of residual terms in equations (6.5.1) and (6.5.2) ($K/\text{tenth of cloud cover}$)². ϵ are the residual terms of the monthly countrywide averaged NOCET estimates over the four countries under consideration; $\bar{\epsilon}$ are long-term time averaged values of ϵ .

Period	D(NOCET)	D ϵ	D $\bar{\epsilon}$
Nighttime	0.06	0.01	0.004
Daytime	0.11	0.02	0.01

The residual terms, ϵ_1 and ϵ_2 in Eqs. 6.5.1 and 6.5.2, are rather small compared to NOCET variations (Table 6.2). There is no systematic change or trend in these terms. Moreover, in each season over each region the mean values of ϵ in Eqs. 6.5.1 and 6.5.2 are close to zero.

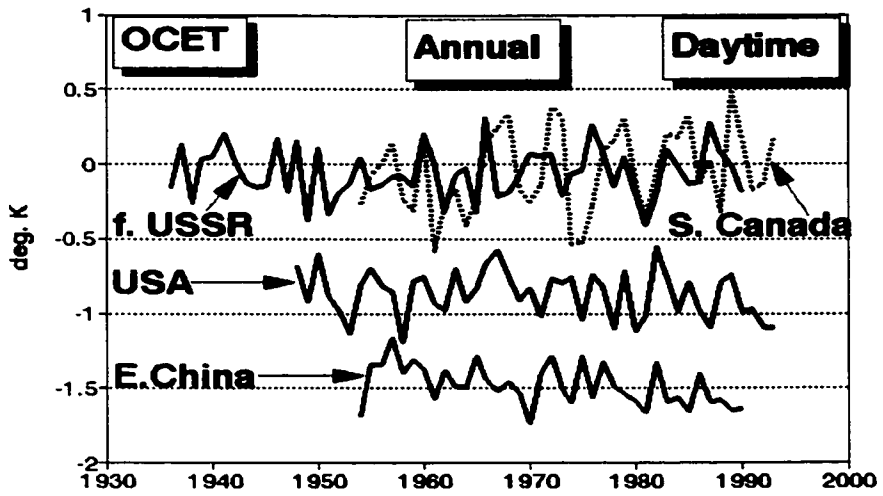
The constant -0.59 K/tenth was obtained after the cloud longwave related temperature change $(-0.16 + 0.98 (q_{\text{clear}})^{-0.5})$ and snow information (0.36S) were removed from daytime NOCET. As suggested in section 6.3.1, the term $(-0.16 + 0.98 (q_{\text{clear}})^{-0.5})$ is determined mainly by cloud downward longwave radiative flux; but other processes or factors including synoptic advection and surface heat flux also can affect it. Also, meteorological processes generally experience diurnal variations. For example, surface evaporation is stronger during daytime than during nighttime. It is difficult to attribute the universal constant -0.59 K/tenth to any specific forcing without physical modeling. It is speculated that the daytime cooling 0.59 K is primarily a direct result of cloud shortwave cooling effect. Surface heat flux loss and precipitation cooling can also contribute to this cloud-related surface cooling. Whatever the nature of these factors, they may represent the empirical estimates of the global overall cloud effect on near surface temperature, dT/dCL .

6.4 Trends of Temporal Variations in the Cloud-Related Temperature Change

Figs. 6.13-6.14 presents the annual countrywide area-averaged time series of daytime OCET, NOCET, CL, and q_{clear} for the period of records available to us.

A statistically significant increase in total cloud cover over the contiguous U.S. and the southern FUSSR, and a significant decrease over eastern China are observed during the post WWII period. Over southern Canada (south of 55°N) no significant trend in annual total cloud cover CL is exhibited during 1953-1993. A significant increase in near surface clear sky humidity over three of these regions is found, except southern Canada where q_{clear} decreased. These changes in CL and q_{clear} largely define interdecadal changes in the daytime OCET and NOCET especially when CL and q_{clear} effects act in the same direction (e.g., over the contiguous U.S.).

A



B

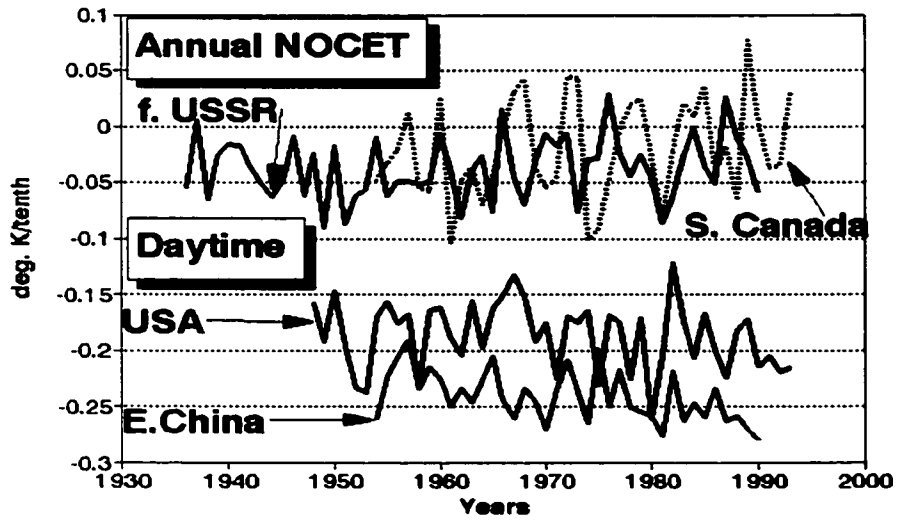
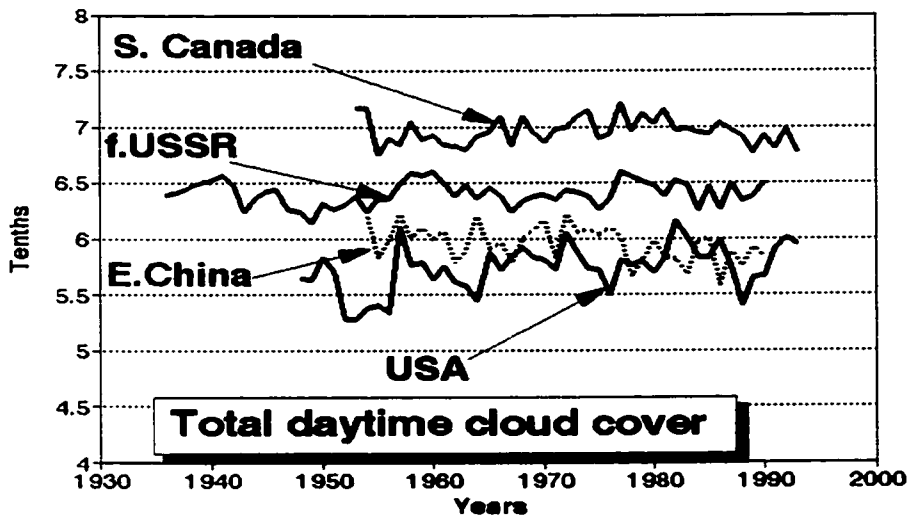


Figure 6.13 Annual mean area-averaged time series of daytime (A) OCET and (B) NOCET over the four countries in consideration.

A



B

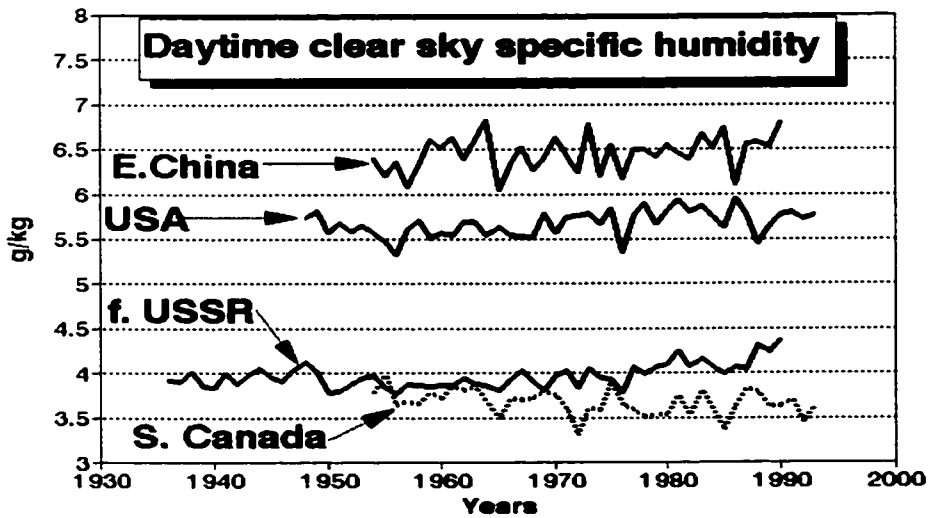


Figure 6.14 Same as Fig. 6.13 except for (A) daytime total cloud amount and (B) daytime near surface specific humidity under clear sky condition.

The daytime OCET tends to become more strongly negative over eastern China (at the 0.05 significance level) and the contiguous U.S. (at the 0.1 significance level), and to increase over the southern FUSSR and southern Canada (at the 0.05 significance level) during the post WWII period. This suggests that daytime surface cooling associated with cloud cover has become stronger in the subtropical land areas (approximately from 25°N to 45°N), and somewhat weaker in the middle latitude land areas (approximately from 45°N to 60°N). The factors causing the observed changes of OCET (Fig. 6.13) in different countries can be different. Over the middle latitude land areas, a significant retreat of snow cover has been documented for the post WWII period (Groisman 1994; Brown 1997). According to Eq. 6.5.2 this should "exaggerate" the cloud interaction with surface temperature by making daytime NOCET more negative, when it is negative. But, in Canada, this retreat was accompanied by a decrease in humidity that opposed the cooling associated with snow cover retreat and thus reversed trends in OCET and NOCET.

Generally speaking, not many significant changes in the nighttime NOCET and OCET are found over these four countries during the post WWII period (see Table 6 in Sun et al. 2000b). However, Figs. 6.1-6.5 indicate that since the 1970s all four countries in almost all seasons, particularly in winter, had a downward trend in nighttime NOCET, suggesting that the nighttime surface warming associated with one unit of cloud cover has decreased.

Finally, I focus on the following three regions where the temporal variations of the cloud-related temperature change for the past several decades deserve special attention/discussion.

Summer over the contiguous U.S.. A significant increase in the U.S. cloud cover (especially in summer and autumn) has already been reported by Plantico and Karl (1990) and Karl et al. (1993). These trends should be the major forcing behind the increase of the absolute OCET values: at night more warming and in daytime more cooling should be exhibited, both

associated with the increase in cloud cover. However, Fig. 6.8A shows a non-linearity in nighttime temporal NOCET changes and shows why the trends in nighttime OCET can differ from those in cloud amount (Fig. 6.15).

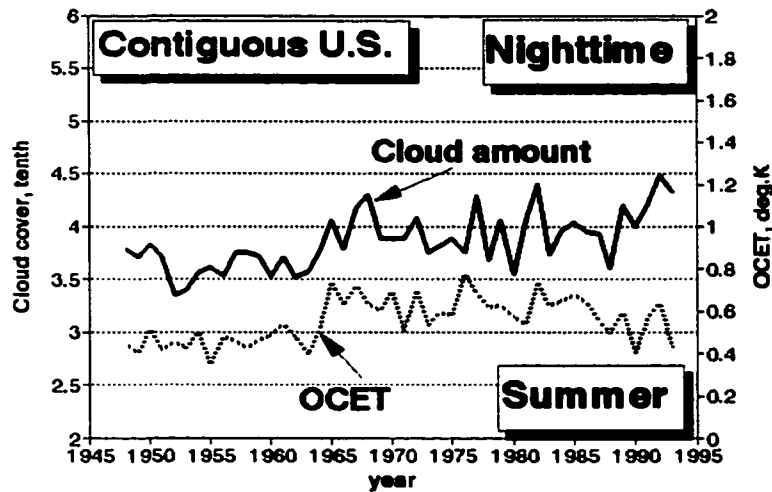


Figure 6.15 Variations of nighttime total cloud amount and OCET over the contiguous U.S. during summer.

Fig. 6.15 indicates that over the contiguous U.S., CL has been increasing from the 1950s to the 1990s while OCET increased only from the mid-1950s to the early 1970s (and the increase in OCET is obviously more rapid than the increase in cloud amount), but afterward decreased somewhat. Our present analysis indicates that these differences in the interdecadal changes have been modulated by the decrease in q_{clear} from the mid-1950s to the late 1970s and the increase in q afterwards (Fig. 6.8).

Summer over the former USSR south of 60N. In this region the most prominent feature of systematic changes during the period from 1950 to 1990 is a significant increase (by 1-3%/10yrs) in mean monthly near surface air humidity, which should lead to a decrease in nighttime NOCET. As a result, there is no upward trend in nighttime surface warming

associated with cloud cover (that is, an increase in nighttime OCET) during the past forty years (Fig. 6.1) in spite of a pronounced increasing trend in cloud amount.

Diurnal temperature range changes over China. An increase in total cloud cover has been suggested as one of the most important factors responsible for the observed decrease in the diurnal temperature range DTR (Karl et al. 1993; Hansen et al. 1995; Dai et al. 1999). In China, the DTR decreased in the past several decades, as in many other regions of the world, but total cloud cover has also decreased during the same period (Kaiser 1998). Figs. 6.1 and 6.9 clarify this. First of all, due to the higher level of atmospheric water vapor, the long-term mean nighttime OCET over China is smaller and daytime OCET is larger compared to the other three countries. Secondly, an increase in near surface specific humidity (and also an increase in atmospheric precipitable water, cf., Zhai and Eskridge 1997) led to a decrease in the nighttime NOCET, but the decrease in the daytime NOCET became even stronger due to an increase in q during the same period and perhaps also due to an increase in atmospheric aerosol loading (Hahn et al. 1995; Karl et al. 1995) since the late 1970s (see next paragraph). So, the daytime changes in surface air temperature associated with cloud cover have thus been stronger than those at night and nullified (or even reversed) the contribution of the cloud cover changes to the change in the DTR over eastern China.

Sulfate aerosols impact the radiation budget of the climate system in two ways: a) directly through scattering solar radiation back to space and b) indirectly through modifying cloud microphysics and thus cloud albedo (Albrecht 1989; Charlson et al. 1992; Chuang et al. 1997). Starting from the late 1970s eastern China experienced fast economic growth, leading to more emissions of industrial sulfur compounds into the air. The increase in sulfate aerosol concentration may lead to an increase in cloud reflectance through increasing the number density of cloud condensation nuclei and reducing the cloud droplet effective radius. So, it is speculated that cloud albedo cooling effect may be enhanced, thus leading to a stronger daytime

surface cooling associated with one tenth of cloud cover (NOCET, see Fig. 6.13) after the late 1970s.

6.5 Conclusions

Based on synoptic observational data the full derivatives of near surface temperature (T) with respect to total cloud cover (CL), dT/dCL , were estimated over five regions of the Northern Hemisphere land areas: the contiguous U.S., Canada, the former USSR, China, and the western tropical Pacific islands. These derivatives reflect how much the near surface temperature change is associated with a change in one unit of cloud cover and show that the area averaged monthly values (nighttime and daytime separately) can be well parameterized as a function of two other internal variables: near surface specific humidity and (in daytime only) snow cover fraction. Thus, the daytime cloud-related near surface temperature change is reduced to a product of CL and a known function of two better known variables: near surface humidity and snow cover. The most important among these cloud-related near surface temperature changes during the post WWII period are:

- A general increase in daytime surface cooling associated with cloud cover over subtropical land areas (the contiguous U.S. and China) and a slight decrease of this cooling in higher latitudes;
- Since the 1970s, a prominent increase in atmospheric humidity has significantly weakened the effectiveness of the surface warming associated with cloud cover (best seen at nighttime) over all four extratropical regions under consideration.

After cloud longwave related temperature change and snow information are removed from the daytime cloud-related near surface temperature change, one tenth of cloud cover is empirically associated with a daytime surface cooling of 0.59 K. This value appears to be invariant-it does not change geographically, seasonally, interannually, and during the past

several decades, and may therefore represent the empirical estimate of global overall cloud effect on near surface temperature.

CHAPTER 7

SUMMARY AND CONCLUSIONS

The cloud-related near surface temperature change over land areas of the Northern Hemisphere is assessed using the synoptic meteorological weather station data as well as the NOAA satellite snow cover data and the NCEP reanalysis data. The cloud characteristics used in this study are visual observations from surface including total and low cloud amounts, and low, middle, and high cloud types. This study discusses temporal (diurnal, seasonal, and interdecadal) variations and spatial characteristics of the cloud-related near surface temperature change and the impact of water vapor and snow cover on that temperature change. The cloud-related temperature change is defined as the near surface temperature difference between average (all) and clear sky weather conditions or between overcast and average (all) sky weather conditions. The cloud-temperature relationship derived from the observational data set is used to evaluate the performance of seven AMIP-I climate models. Continental scale changes in cloudiness, particularly the occurrence of cloud types, and their climatic implications are also investigated in this work. The main conclusions are as follows.

- The surface temperature change associated with a change in one tenth of cloud cover, varies from -0.05 K over the wet tropics to 1.0 K over middle latitudes in winter during nighttime, and varies from -0.4 K in the tropics to 0.7 K over middle latitudes in winter during daytime.
- The nighttime cloud-related surface warming decreases with the increase in near surface specific humidity. Over the humid tropics, surface evaporation may largely dominate nighttime cloud-related surface temperature change.
- The near surface temperature change associated with a change in one unit of cloud cover can be simply parameterized by near surface specific humidity and snow

cover on the ground. After cloud longwave related temperature change and snow cover information are removed, one tenth of cloud cover is empirically associated with a surface cooling of 0.59 K, which may represent the empirical estimate of overall cloud effect on near surface temperature.

- The data-model intercomparison indicates that the Atmospheric Model Intercomparison Project (AMIP-1) models generally are able to reproduce the cold season cloud-temperature relationship, but not for the warm season and for the diurnal cycle.
- The daytime surface cooling associated with cloud cover over China and the contiguous U.S. generally strengthened, but slightly weakened over Canada and the former USSR during the post WWII period. Since the 1970s a prominent increase in atmospheric humidity has weakened the effectiveness of the surface warming associated with cloud cover (best seen at nighttime) over the extratropical land areas.
- Significant changes and a general redistribution of surface observed daytime cloudiness are found over the contiguous U.S. and the former USSR (south of 60°N) during the post WWII period: (a) over the former USSR (south of 60°N) total cloud amount increased while low cloud amount decreased, and this decrease was primarily related to a decrease in frequency of low stratiform clouds; (b) over the contiguous United States, with the increase in total cloud amount low cloud amount increased, and the increase in frequency of low stratiform and *Nimbostratus* clouds largely contributed to the increase in low cloudiness; (c) An abrupt increase prior to the 1960s largely contributed to the upward trend in the frequency of convective clouds over both regions, particularly over the warm season. However, over both regions during the intermediate seasons and during the winter season over the

FUSSR, the frequencies of convective clouds still showed gradual increase after the 1960s;(d) the increase in the frequency of convective clouds over both regions has been accompanied by an increase in the frequency of high clouds (at elevations above 6 km); (e) changes in occurrence of different cloud types are consistent with changes in precipitation frequency and intensity.

The following two suggestions may deserve further study.

1.To understand the radiative effect of cloud type/cloud distribution. Different cloud types have different radiative effect because of the difference in their microphysical and optical characteristics (Hartmann et al. 1992; Wang and Rossow 1998; Chen et al. 2000). In general, low level clouds with extensive sky coverage have net cooling effect on climate while high level clouds have a net warming effect on climate. Quantitative estimates of radiative fluxes of individual cloud types and of the impact of changes in cloud vertical distribution on radiation budget at the top of the atmosphere and at the surface are required in order to understand the role of cloudiness changes (as revealed in Chapter 4) in contemporary climate changes.

2.To understand the physical conditions responsible for the presence and variations of cloudiness over land areas. Clouds have important effects on the radiation budget of the Earth's climate, but their formation, maintenance, and dissipation are closely related to large-scale dynamic and thermal conditions, such as surface heat and moisture fluxes, vertical motion, and atmospheric stability. Much of previous observational and modeling work has focused on marine clouds (e.g., Klein and Hartmann 1993; Norris and Leovy 1994; Bretherton and Wyant 1997; Weaver and Ramanathan 1997; Norris 1998a,b), but continental clouds are also key elements of the climate system. Also, the radiative characteristics of continental clouds can be different from those of marine clouds due to the differences in surface condition, moisture, boundary layer structure, and aerosol loading. Understanding the relationships of land clouds

with surrounding meteorological conditions thus help us (1) understand cloud processes and (2) improve cloud parameterizations in climate models.

APPENDIX A
AN INTERPOLATION SCHEME FOR DIURNAL VARIATION
OF CLOUD TYPE FREQUENCY

In January 1966 the daily observational schedule in the FUSSR primary meteorological network was switched from four times per day to eight times per day. This switch changed the hours of observations from local standard time to UTC. The FUSSR spans 11 time zones. This switch made the hours of measurements at 75% of total stations incomparable with those previously used. Our major concern is that this temporal inhomogeneity may bias the trend analysis of convective clouds particularly in the warm season, which has a distinctive diurnal cycle (Warren et al. 1996).

One remedy to this inhomogeneity (Sun and Groisman 2000) was selection of the nearest observational hour (i.e., 12 PM or 2PM) to the old 1 PM (before 1966) to describe the 1 PM cloudiness at the stations after January 1966. This method left us a possible observation time discrepancy of no more than one hour between the old and the new times of observation. The robustness of the results from this method were tested and proved to be statistically significant (see Sun and Groisman 2000).

This study (see also Sun and Groisman 2000) creates another method to reduce the inhomogeneity of cloudiness time series. The post-1966 3-hourly measurements are used to simulate the diurnal cycle of cloudiness including cloud type and cloud cover. The time with a maximum value of cloudiness, T_{max} , in each season, is from the seasonal maps describing the diurnal cycle of each cloudiness characteristics provided by Warren et al. (1986). This diurnal evolution of cloudiness allows us to interpolate the cloudiness value at anytime including 1 PM. Fig. A1 shows the adjusted time series of summer low cloud cover at 1PM local time (solid line) compared with the time series calculated from original data including the

measurements at noon, 1PM, or 2PM (dashed line). This comparison indicates that the two time series are almost indistinguishable.

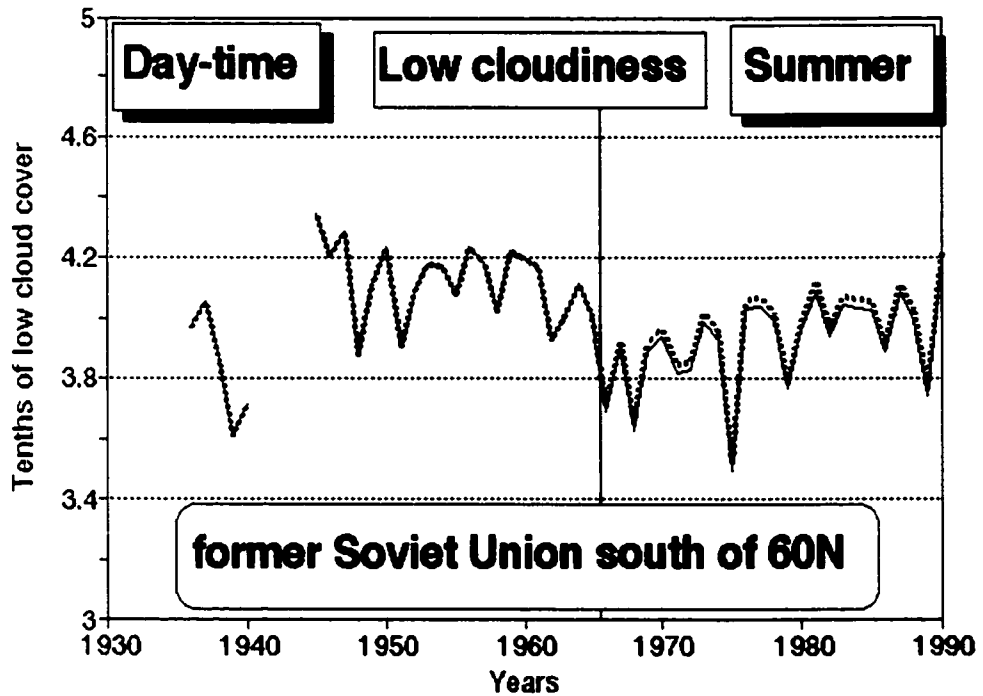


Figure A1 A sensitivity test of summer 1 PM cloud cover time series to the change in observational time in 1966. Cloud amount was area-averaged over the former USSR south of 60N. The cloud amount measurements for the period of 1966-1990 were interpolated to the 1 PM observation times (used before 1966) using additional climatological diurnal cloud information. The result of this interpolation (thin solid line) and the original time series (dotted line) from Figure 2 of Sun and Groisman (2000) are shown. The trend in the interpolated time series is $-1.4\%/10$ yrs compared to $-1.1\%/10$ yrs in the original time series. The difference in trends is not statistically significant.

APPENDIX B

RELATIONSHIP BETWEEN THE TWO DEFINITIONS OF THE CLOUD-RELATED TEMPERATURE CHANGE

In this research, OCET is defined as the difference in near surface temperature between average and clear sky conditions, and $OCET_1$ is defined as the difference in near surface temperature between overcast and average conditions. Eqs. 3.1 and 3.2 of Chapter 3 are their respective mathematical expressions. In this study, both OCET and $OCET_1$ are used to assess the near surface temperature change associated with a change in total cloud cover. Now the question is if they are comparable? This appendix tries to answer it.

In Chapter 6, OCET ($OCET_1$) is decomposed into two terms: NOCET ($NOCET_1$) and ΔCL (ΔCL_1). The physical principle for this decomposition is that cloud cover is one of the important properties that determine cloud radiative effects on surface air temperature. Three examples shown in Figs. B1.A, B2.A, and B3.A indicate that OCET ($OCET_1$) is indeed the linear function of ΔCL (ΔCL_1). After the removal of cloud cover amount information, changes in cloud cover amount (ΔCL or ΔCL_1) no longer have significant affect on the normalized cloud-related near surface temperature change ($NOCET$ or $NOCET_1$) (Figs. B1.B, B2.B, and B3.B). So, OCET ($OCET_1$) can be well determined by two independent items: NOCET ($NOCET_1$) and ΔCL (ΔCL_1).

During nighttime, over the northern extratropical land areas, largely due to the cloud downward longwave warming effect, both NOCET and $NOCET_1$ are positive. Chapter 6, along with Figs. B1.D, B2.D, and B3.D, indicates that NOCET ($NOCET_1$) is inversely related to atmospheric humidity. In general, atmospheric humidity in the NOCET case is smaller than that in the $NOCET_1$ case. Thus, the value of NOCET generally is larger than that of $NOCET_1$. Table A1 of Sun et al. (2000) indicates that in all seasons NOCET is larger than $NOCET_1$ (by 5%-

20%) over the contiguous United States, southern Canada, the southern former USSR, and eastern China. Figs. B1.C and B2.C also show that over the station Miami of Florida and the station Springfield of Illinois, NOCET_1 is linearly correlated to NOCET , but smaller than NOCET . The relation of NOCET_1 to NOCET can be expressed as:

$$\text{NOCET}_1 = a * \text{NOCET} \quad (a < 1)$$

Also, the relation of ΔCL_1 to ΔCL can be expressed:

$$\Delta\text{CL}_1 = b * \Delta\text{CL}$$

Where b is an unknown parameter, depending on the distribution of cloud cover amount frequency.

At a location and in a month, the comparability of NOCET with NOCET_1 is thus related to both a and b .

If overcast frequency is larger than or equal to clear sky frequency, then, $b \leq 1$ and $\text{OCET}_1 < \text{OCET}$. Fig. B4 shows this case.

If overcast frequency is smaller than clear sky frequency (overcast < clear sky), then, $b > 1$ and OCET_1 can be larger or smaller than or equal to OCET depending on the ratio of overcast frequency to clear sky frequency.

During daytime, NOCET (NOCET_1) is related to both cloud longwave and shortwave effects. So the sign of NOCET (NOCET_1) can be positive, negative, or zero, depending on the competition of cloud cooling and warming effects. In general, over the northern extratropical land areas, during warm season and/or low latitudes, both NOCET and NOCET_1 are negative (Fig. B5.A); during cold seasons and/or high latitudes, both NOCET and NOCET_1 are positive (Fig. B5.B); during transition seasons and/or transition latitudes, NOCET can be positive while NOCET_1 can be negative (Fig. B5.C). The answers to the comparability of OCET to OCET_1 are given in the left part of Fig. 5.

Nighttime, winter monthly data

Miami, FL

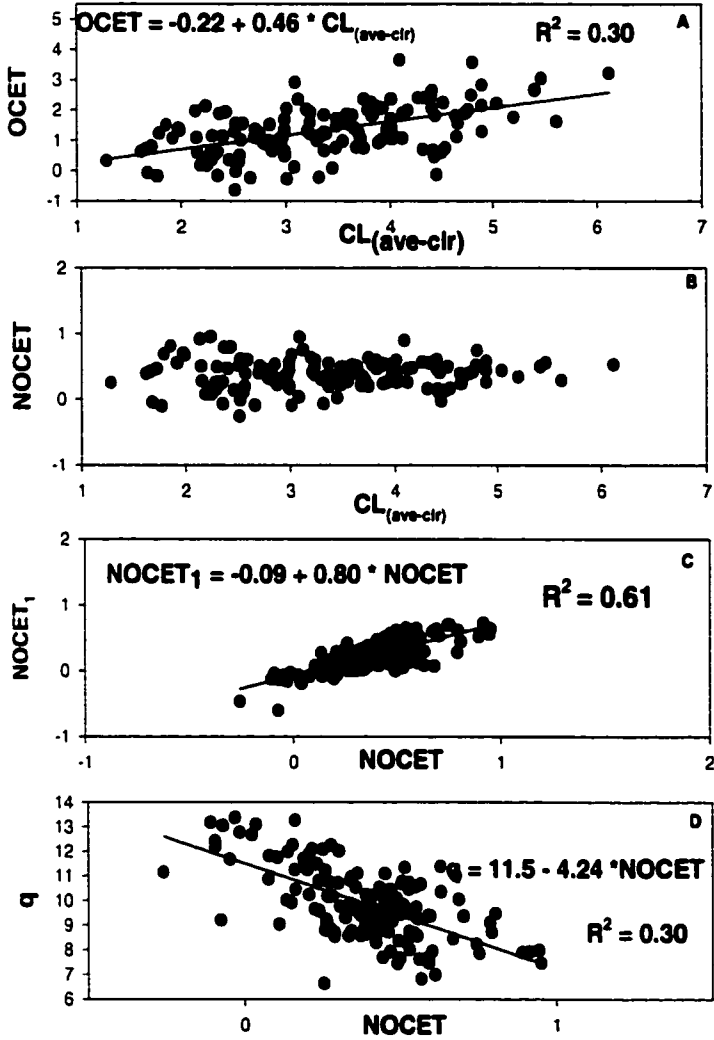


Figure B1 Relationship between various relevant elements of the nighttime cloud-related near surface temperature change in winters at the station Miami of Florida.

**Nighttime, winter monthly data
Springfield, IL**

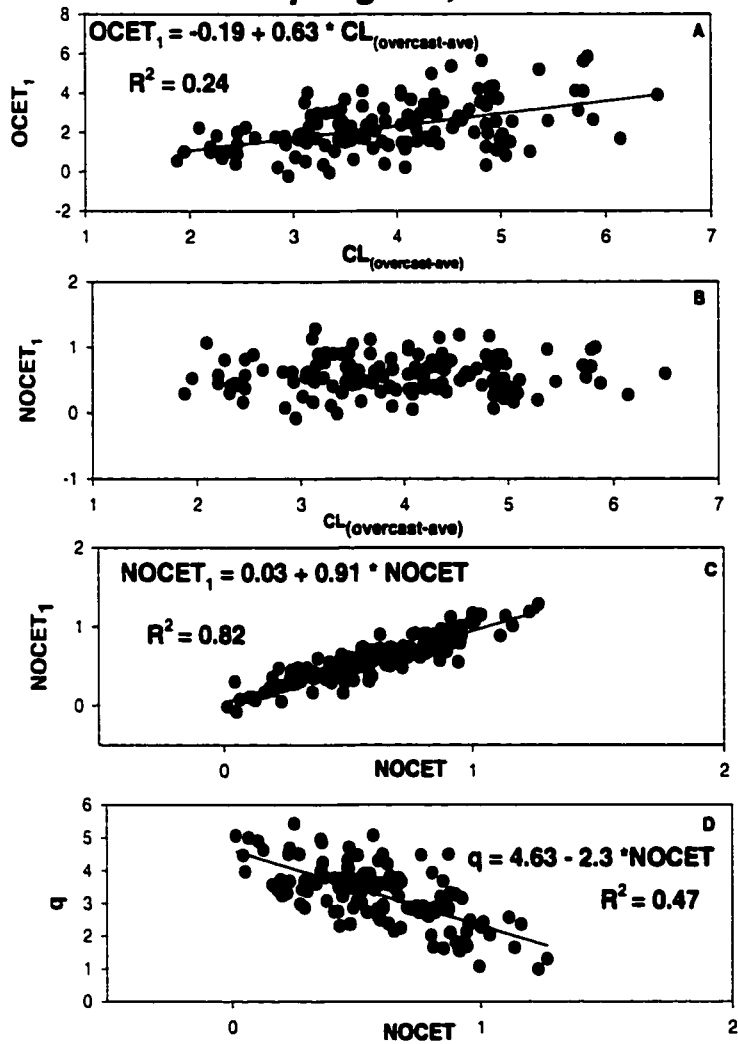


Figure B2 Same as Fig. B1 except for the station Springfield of Illinois.

**Daytime, summer monthly data
Springfield, IL**

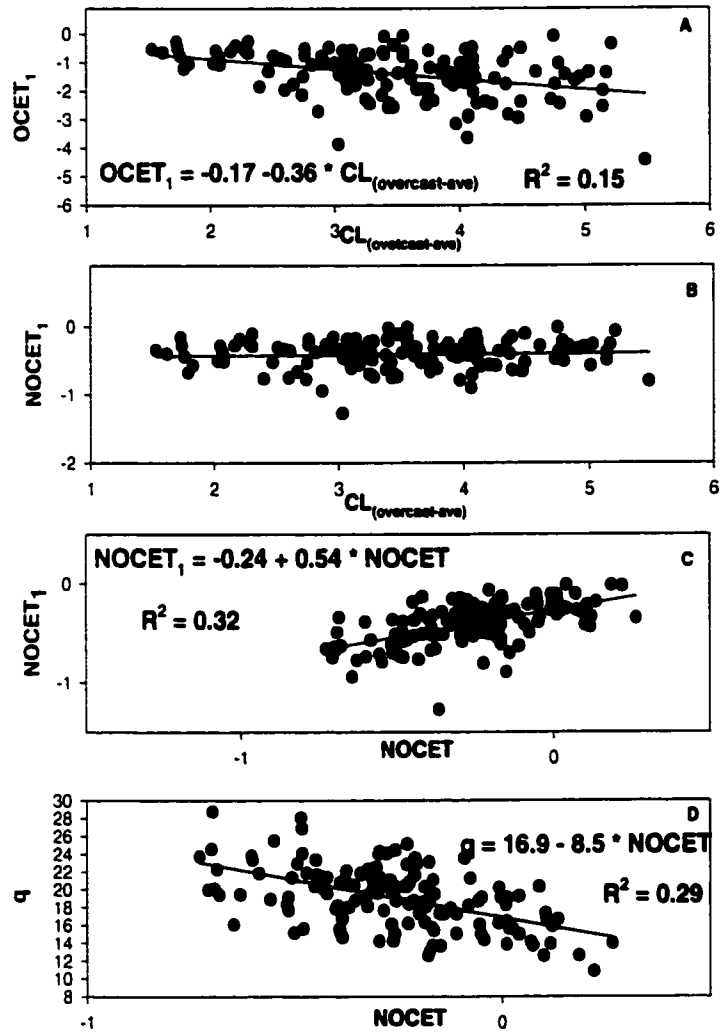
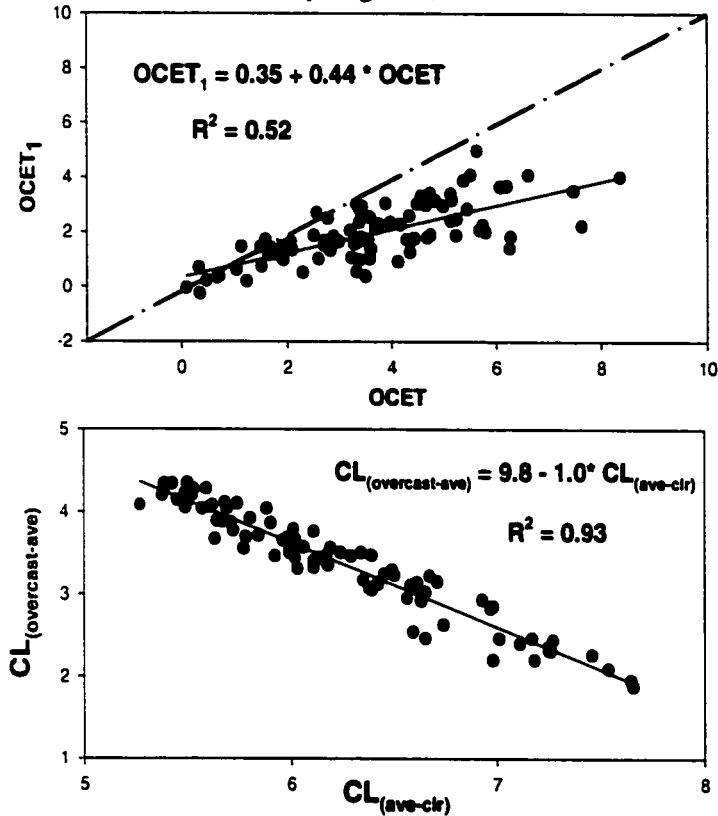


Figure B3 Same as Fig. B2 except for daytime.

**Nighttime, winter monthly data
overcast frequency larger than clear sky frequency by 10%**

Springfield, IL



NIGHTTIME CASE: NOCET₁ < NOCET

If overcast case >= clear sky case, CL_(overcast-ave) =< CL_(ave-clr), OCET₁ < OCET

If overcast case < clear sky case, CL_(overcast-ave) > CL_(ave-clr), OCET₁ ? OCET

Figure B4 Example of the relationship between nighttime OCET and OCET₁. The formulas below the black solid line are the general conclusions on the relationship between nighttime OCET and OCET₁.

DAYTIME OCET & OCET₁

monthly daytime data from the U.S. stations

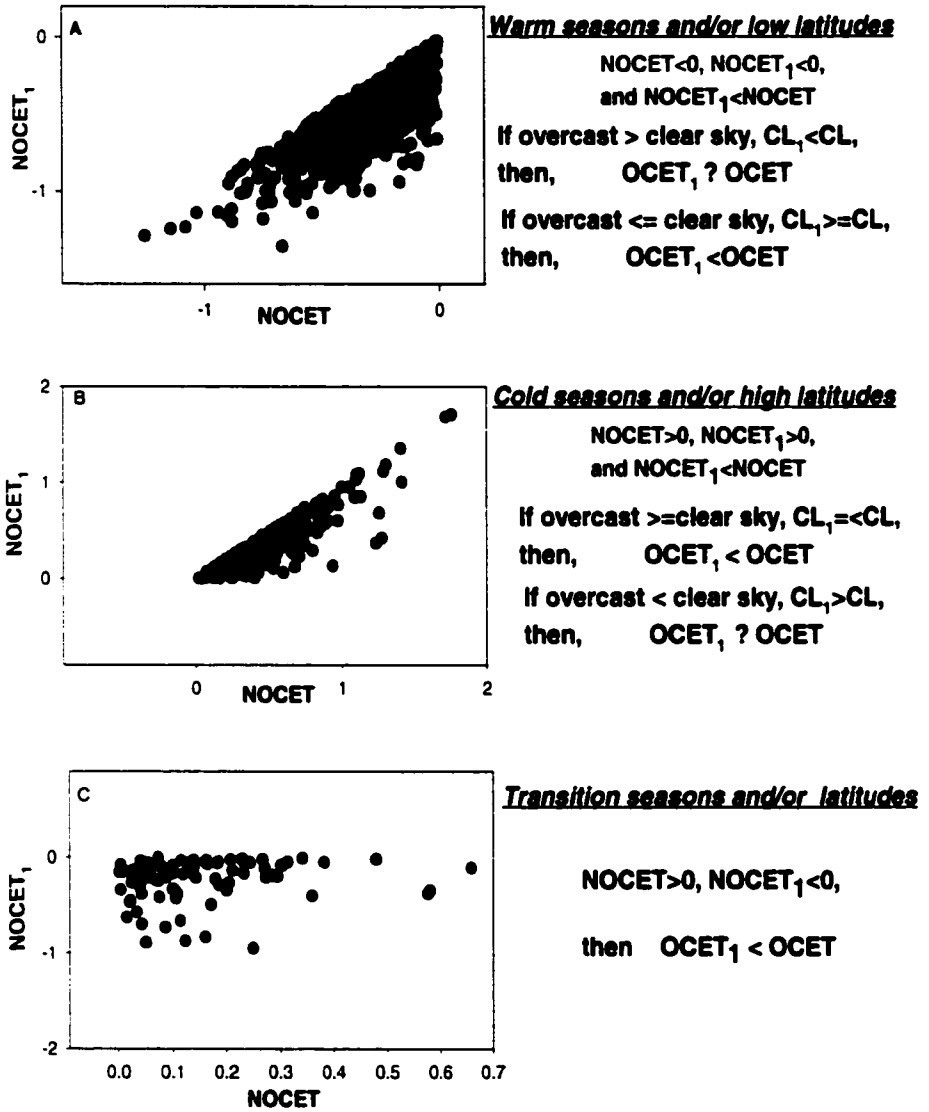


Figure B5 Relationship between daytime OCET and OCET₁.

In summary, which one is larger between OCET and OCET₁ depends not only on the time of a day, the season, and the location but also on the cloud amount frequency distribution. During nighttime, if the occurrence of overcast condition is more frequent than that of clear sky condition, the cloud-related surface warming calculated from OCET is stronger than that calculated from OCET₁. During daytime, in warm seasons and/or low latitudes, if overcast frequency is smaller than clear sky frequency, OCET₁ is more negative than OCET; in cold seasons and/or high latitudes, if overcast frequency is larger than clear sky frequency, OCET is more positively larger than OCET₁; during intermediate seasons and/or transition latitudes, OCET can be positive while OCET₁ can be negative.

Although OCET can be different from OCET₁ in terms of magnitude and/or sign, the basic physics determines OCET is similar to that determining OCET₁. For example, the nighttime surface warming calculated from OCET/OCET₁ is largely related to cloud downward infrared warming effect, though the difference in atmospheric humidity and/or cloud cover amount can lead to a difference in strength of surface warming between OCET and OCET₁; the daytime cooling calculated from OCET/OCET₁ in warm seasons is largely due to the predominance of cloud albedo cooling effect over the cloud greenhouse warming effect, though the difference in atmospheric humidity, surface heat flux, and/or cloud cover amount between OCET and OCET₁ cases can lead to a difference in strength of surface cooling between them.

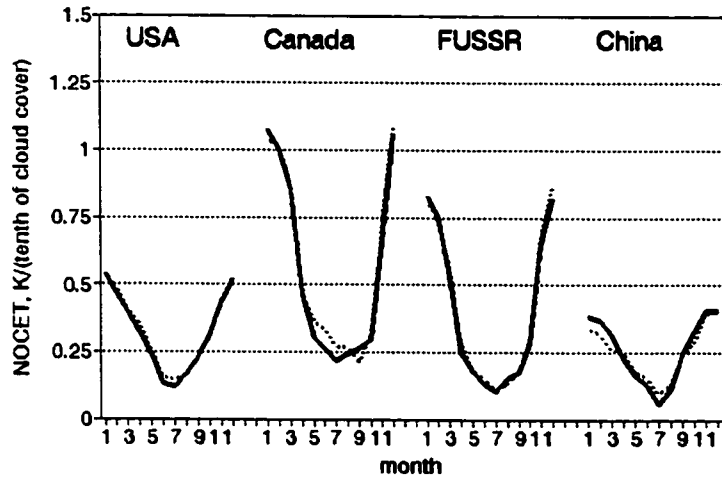
APPENDIX C

EFFECTS OF THE ACCURACY OF THE NIGHTTIME CLOUD OBSERVATIONS ON THE ESTIMATES OF THE CLOUD-TEMPERATURE RELATIONSHIP

The *in situ* nighttime cloud measurements are generally underestimated due to inadequate illumination of clouds. This could affect the estimates of nighttime OCET and NOCET, which are based on surface observations without consideration of the night cloud detection bias. Therefore, it is necessary to check the reliability of the cloud-related temperature change estimates in Chapter 5 and Chapter 6 by using the moonlight criterion suggested by Hahn et al. (1995). The application of this criterion discards about two-thirds of nighttime cloud observations, and thus prevent us from computing the year-to-year NOCET and OCET time series. This situation is particularly serious in the FUSSR and China, where only two/one nighttime measurements are available. Therefore, instead of time series of OCET (NOCET), I calculate long-term mean monthly OCET (NOCET) with and without the moonlight illumination criterion for the whole time period (e.g., from 1948 to 1993 in the contiguous U.S.). OCET (NOCET) calculated with the consideration of the illumination criterion are named OCET_m (NOCET_m).

The first plate in Fig. C1 compares the long-term countrywide NOCET and NOCET_m values. It shows that these two sets of NOCET estimates are statistically consistent with each other, and the application of the illumination criterion does not significantly affect the nighttime NOCET climatology in each of the four countries. The reason is simple. The nighttime detection bias leads to a decrease in the estimates of the difference between average and clear sky cloud cover, ΔCL , but this also decreases the estimates of the difference between surface temperature under average and "clear" sky conditions, ΔT , because some cloudy events are now wrongly classified as "clear skies". Obviously this is not the case for the OCET

A



B

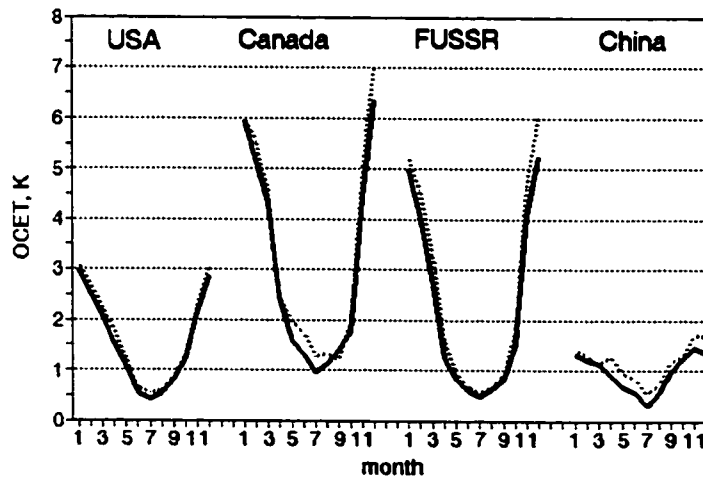


Figure C1 Comparison of two sets of long-term nighttime (A) NOCET and (B) OCET estimates. Solid lines represent standard estimates. Dashed lines represent the estimates based only on the data that conform to the moonlight criterion

estimates: the OCET_m values are systematically (but slightly) higher than the former (Fig. C1.B). The largest bias by absolute value is over the FUSSR in winter (-0.5 K or -9% of the OCET_m), and the largest bias by percentage is over China in summer (approximately -30% of the OCET_m).

APPENDIX D
CONTRIBUTION OF SURFACE AIR TEMPERATURE VARIATIONS
TO NOCET CHANGES

Climatologically the downward longwave radiation of a cloud is primarily a function of cloud cover amount and cloud base temperature. Fig. 6.6 indicates that the nighttime NOCET is well represented by specific humidity of the lowest air layer. However, cloud bases with different temperature, though associated with a same amount of cloud cover, can have different strengths of longwave warming effect (Inamdar and Ramanathan 1994), and therefore have different values of NOCET. Unfortunately we do not have cloud base temperature data. So, near surface temperature T is used as a surrogate to estimate the impact of cloud base temperature variation on NOCET.

To highlight the affect of T on NOCET, a comparison is made between $\text{NOECT-}q_{\text{clear}}$ and $\text{ROCET-}q_{\text{clear}}$. The outgoing longwave radiation from a surface with temperature T is proportional to T^4 . Here I normalize ROCET by a factor $(300/T)^4$ in order to reduce the magnitude of ROCET. The correlation between ROCET and q_{clear} during summer and autumn seasons are generally the same as those between NOCET and q_{clear} shown in Fig. 6.1, but are better than the latter during winter and spring seasons over North America and the FUSSR. In winter and spring, a larger variability of surface temperature (also cloud base temperature) in the extratropical land areas, and thus of longwave radiation, somewhat interferes with and reduces the goodness of fit of the NOCET versus humidity relationship. The variance of annual and interannual variability of surface temperature in warm seasons is low, and therefore, it produces no obvious difference between the $\text{NOCET-}q_{\text{clear}}$ and $\text{ROCET-}q_{\text{clear}}$ relationships. The use of ROCET instead of NOCET in a parameterization similar to that shown in Eqs. 6.2.2 and 6.2.3 increases the joint variance of this parameterization from 83% to 89%.

APPENDIX E

METHOD OF INSTRUMENTAL VARIABLE

The method of instrumental variable was suggested by Geary (1949) to resolve the problem of estimation of the unknown α -parameters in the linear functional relationship between stochastic variables X and Y, when each of these variables is measured/evaluated with error.

$$Y = \alpha_0 + \alpha_1 X \quad (A2)$$

The researcher has only "measurements" of Y and X: $\eta = Y + \varepsilon$ and $\xi = X + \delta$. In this situation, if $\sigma_\delta \neq 0$, the least squares method gives biased estimates of the α_1 -parameter (Kendall and Stuart 1972). A substitution of measured variables into the functional relationship (A2) above gives:

$$\eta = \alpha_0 + \alpha_1 \xi - \alpha_1 \delta + \varepsilon \quad (A3)$$

Geary (1949) suggested using additional information about the X variable that exists in a third "instrumental" variable, ζ , to estimate the unknown α -parameters in (A3). The condition of the use of this variable is that it should be significantly correlated with X but has no correlation with δ and ε :

$$\text{cov}(\delta, \zeta) = 0; \text{cov}(\varepsilon, \zeta) = 0, \text{ and } \text{cov}(X, \zeta) \neq 0 \quad (A4)$$

If these conditions are true (for example, ζ could be a second independent measurement of X) then a scalar product of ζ and (A3) will give:

$$\begin{aligned} \text{cov}(\eta, \zeta) &= \alpha_0 \text{cov}(1, \zeta) + \alpha_1 \text{cov}(\xi, \zeta) - \alpha_1 \text{cov}(\delta, \zeta) + \text{cov}(\varepsilon, \zeta) \text{ or} \\ \text{cov}(\eta, \zeta) &= \alpha_1 \text{cov}(\xi, \zeta). \end{aligned}$$

Therefore, the ratio $\text{cov}(\eta, \zeta) / \text{cov}(\xi, \zeta)$ gives an asymptotically unbiased estimate of the α_1 -parameter, which then is used to estimate the α_0 -parameter by the expression:

$$\text{avg}(\eta) - \text{avg}(\xi) \text{cov}(\eta, \zeta) / \text{cov}(\xi, \zeta),$$

where avg and cov are the mean and covariance estimates.

This approach was first employed in climatology to estimate the impact of global surface air temperature on regional climate by Vinnikov and Groisman (1979) and further applied to a climate change detection problem (Vinnikov and Groisman 1982).

REFERENCES

- Albrecht, B.A., 1989: Aerosols, cloud microphysics, and fractional cloudiness, *Science*, **245**, 1227-1230.
- Angell, J.K., 1990: Variations in the United States cloudiness and sunshine duration between 1950 and the drought year of 1998. *J. Climate*, **3**, 296-308.
- Bajuk, L.J., and C.B. Leovy, 1998: Seasonal and interannual variations in stratiform and convective clouds over the tropical Pacific and Indian Oceans from ship observations. *J. Climate*, **11**, 2922-2941.
- Barkstrom, B.R., 1984: The Earth Radiation Budget Experiment (ERBE). *Bull. Amer. Meteorol. Soc.*, **65**, 1170-1185.
- Bradley, R.S., H.F. Diaz, J.K. Eischeid, P.D. Jones, P.M. Kelly, and C.M. Goodess, 1987: Precipitation fluctuations over Northern Hemisphere land areas since the mid-19th century. *Science*, **237**, 171-275.
- Bradley, R.S., F.T. Keimig, and H.F. Diaz, 1993: Recent changes in the North American Arctic boundary layer in winter. *J. Geophys. Res.*, **98**, 8851-8858.
- Bretherton, C.S., and M.C. Wyant, 1997: Moisture transport, lower-tropospheric stability and decoupling of cloud-topped boundary layers. *J. Atmos. Sci.*, **52**, 2752-2762.
- Brown, R.D., 1997: Historical variability in Northern Hemisphere spring snow covered area. *Annals of Glaciology*, **25**, 340-346.
- Brunt, D., 1932: Notes on radiation in the atmosphere. *Quart. J. Roy. Meteor. Soc.*, **58**, 389-418.
- Cess, R.D., and Coauthors, 1991: Interpretation of snow-climate feedback as produced by 17 general circulation models. *Science*, **253**, 888-892.
- Cess, R.D., and Coauthors, 1996: Cloud feedback in atmospheric general circulation models: An update. *J. Geophys. Res.*, **101**, 12 791- 12 794.
- Cess, R.D., and Coauthors, 1997: Comparison of the seasonal change in cloud-radiative forcing from atmospheric general circulation models and satellite observations. *J. Geophys. Res.*, **102**, 16 593-16 603.
- Changnon, S.A., 1981: Midwest cloud, sunshine, and temperature trends since 1901: possible evidence of jet effects. *J. Appl. Meteor.*, **20**, 496-508.
- Charlson, R.J., S.E. Schwartz, J.M. Hales, R.D. Cess, J.A. Coagley Jr., J.E. Hansen, and D.J. Hohmann, 1992: Climate forcing by anthropogenic aerosols. *Science*, **255**, 423-430.
- Chen, T., W.B. Rossow, and Y.-C., Zhang, 2000: Radiative effects of cloud type variations. *J. Climate*, **13**, 264-268.

- Christy, J.R., R.W. Spencer, and E.S. Lobl, 1998: Analysis of the merging procedure for the MSU daily temperature series. *J. Climate*, **11**, 2016-2041.
- Chuang, C.C., J.E. Penner, K.E. Taylor, A.S. Grossman, and J.J. Walton, 1997: An assessment of the radiative effects of anthropogenic sulfate. *J. Geophys. Res.*, **102**, 3761-3778.
- Curry, J.A., 1983: On the formation of continental polar air. *J. Atmos. Sci.*, **40**, 2279-2292.
- Dai, A., I. Fung, and A.D. Del Genio, 1997: Surface observed global land precipitation variations during 1900-88. *J. Climate*, **10**, 2943-2962.
- Dai, A., K.E. Trenberth, and T.R. Karl, 1999: Effects of clouds, soil moisture, precipitation and water vapor on diurnal temperature range. *J. Climate*, **12**, 2451-2473.
- Dai, A., T.M.L. Wigley, B. Boville, J.T. Kiehl, and L. Buja, 2000: Climates of the 20th and 21st centuries simulated by NCAR Climate System Model. *J. Climate* (submitted).
- Ding, Y.-H., 1994: *Monsoons over China*. Kluwer Academic Publishers, 419pp
- Easterly, D.R., and Coauthors, 1998: Long-term observations for monitoring climate extremes in the Americas. *Climatic Change*, **42**, 285-308.
- Eskridge, R.E., O.A. Alduchov, I.V. Chernykh, P.-M. Zhai, S.R. Doty, and A.C. Polansky, 1995: A Comprehensive Aerological Reference Data Set (CARDS): Rough and systematic errors. *Bull. Amer. Meteor. Soc.*, **76**, 1759-1775.
- Fu, R., A.D. Del Genio, W.B. Rossow, and W.T. Liu, 1992: Cirrus-cloud thermostat for tropical sea surface temperature tested using satellite data. *Nature*, **358**, 394-397.
- Fu, R., A.D. Del Genio, and W.B. Rossow, 1994: Influence of ocean surface conditions on atmospheric vertical thermodynamic structure and deep convection. *J. Climate*, **7**, 1092-1108.
- Fu, R., W.T. Liu, and R.E. Dickinson, 1996: Response of tropical clouds to the interannual variation of sea surface temperature. *J. Climate*, **9**, 616-634.
- Fung, I.Y., D.E. Harrison, A.A. Lacis, 1984: On the variability of the net longwave radiation at the ocean surface. *Rev. Geophys. Space Phys.*, **22**, 177-193.
- Gandin, L.S., and Coauthors, 1976: *Statistical Structure of Meteorological Fields* (in Russian and Hungarian). Az Országos Meteorológiai Szolgálat, Budapest, 365 pp.
- Gates, W.L., 1992: AMIP: The Atmospheric Model Intercomparison Project. *Bull. Amer. Meteor. Soc.*, **73**, 1962-1970.
- Geary, R.C., 1949: Determination of linear relations between systematic parts of variables with errors of observation the variance of which are unknown. *Biometrika*, **17**, 30-59.

- Gosnell, R., C.W. Fairrall, and P.J. Webster, 1995: The sensible heat of rainfall in the tropical oceans. *J. Geophys. Res.*, **100**, 18 437-18 442.
- Groisman, P. Ya., and D.R. Legates, 1995: Documenting and detecting long-term precipitation trends: where we are and what should be done. *Climatic Change*, **31**, 601-622.
- Groisman, P. Ya., E.L. Genikhovich, and P.-M. Zhai, 1996: "Overall" cloud and snow cover effects on internal climate variables: The use of clear sky climatology. *Bull. Amer. Soc.*, **77**, 2055-2065.
- Groisman, P. Ya., E.L. Genikhovich, R.S. Bradley, and B. Sun, 1999: Trends in turbulent heat fluxes over northern Eurasia. *Interactions Between the Cryosphere, Climate and Greenhouse Gases*. IAHS Publ. 256, 19-25.
- Groisman, P. Ya., E.L. Genikhovich, R.S. Bradley, and B.M. Ilyin, 1997: Assessment surface-atmosphere interactions using the Former Soviet Union standard meteorological network data. Part II: Cloud and snow cover effects. *J. Climate*, **10**, 2184-2199.
- Groisman, P. Ya., R.S. Bradley, and B. Sun, 2000: The relationship of cloud cover to near-surface temperature and humidity: Comparison of GCM simulations with empirical data. *J. Climate*, **13**, 1858-1878.
- Groisman, P. Ya., R.W. Knight, and T.R. Karl, 2000: Heavy precipitation and streamflow in the United States: Trends in the 20th century. *Bull. Amer. Meteor. Soc.* (submitted).
- Groisman, P. Ya., T.R. Karl, D.R. Easterling, R.W. Knight, P.B. Jamason, K.J. Hennessy, R. Suppiah, Ch.M. Page, J. Wibig, K. Fortuniak, V.N. Razuvaev, A. Douglas, E. Forland, and P.-M. Zhai, 1999: Changes in the probability of heavy precipitation: Important indicators of climatic change. *Climatic Change*, **42**, 243-283.
- Groisman, P. Ya., T.R. Karl, and R.W. Knight, 1994: Observed impact of snow cover on the rise of continental spring temperature. *Science*, **263**, 198-200.
- Hahn, C.J., S.G. Warren, and J. London, 1995: The effect of moonlight on observation of cloud cover at night, and application to cloud climatology. *J. Climate*, **8**, 1429-1446.
- Hahn, C.J., S.G. Warren, and J. London, 1996: *Edited synoptic cloud reports from ships and land stations over the globe, 1982-1991*. Rep #NDP026B, 45 pp. [Available from Carbon Dioxide Information Analysis Center, Oak Ridge National Laboratory, P.O. Box 2008, Oak Ridge, TN 37831-6050]
- Hahn, C.J., and S.G. Warren, 1999: Extended edited synoptic reports from ships and land stations over the globe, 1952-1996. Environmental Science Division Publ. No. 4913, ORNL/CDIAC-123, NDP-026c, 71pp.
- Hahn, C.J., W.B. Rossow, and S.G. Warren, 2000: ISCCP cloud properties associated with standard cloud types identified in individual surface observations. *J. Climate*, (in press).

- Hartmann, D.L., K.J. Kowalewsky, and M.L. Michelsen, 1991: Diurnal variations of outgoing longwave radiation and albedo from ERBE scanner data. *J. Climate*, **4**, 598-617.
- Hartmann, D.L., M.E. Ockert-Bell, and M.L. Michelsen, 1992: The effect of cloud type on Earth's energy balance: Global analysis. *J. Climate*, **5**, 1281-1304.
- Hartmann, D.L., and M.L. Michelson, 1993: Large-scale effects on the regulation of tropical sea surface temperature. *J. Climate*, **6**, 2049-2062.
- Henderson-Sellers, A., 1989: North American total cloud amount variations this century. *Global Planet. Change*, **1**, 175-194.
- Henderson-Sellers, A., 1992: Continental cloudiness changes this century. *Geojournal*, **27.3**, 255-262.
- Henderson-Sellers, A., and P.J. Robinson, 1986: *Contemporary Climatology*. Longman Scientific & Technical, 439 pp.
- Hensen, J., M. Sato, and R. Ruedy, 1995: Long-term changes of the diurnal temperature cycle; implications about mechanisms of global climate change. *Atmos. Research*, **37**, 175-210.
- Herman, G.F., and R. Goody, 1976: Formation and persistence of summertime Arctic stratus clouds. *J. Atmos. Sci.*, **106**, 771-780.
- Inamdar, A.K., and V. Ramanathan, 1994: Physics of greenhouse effect and convection in warm oceans. *J. Climate*, **7**, 715-731.
- Isaac, G.A., and R.A. Stuart, 1996: Relationships between cloud type and amount, precipitation, and surface temperature in the Mackenzie River Valley - Beaufort Sea area. *J. Climate*, **9**, 1921-1941.
- Jones, P.D., 1994: Hemispheric surface air temperature variations: a reanalysis and an update to 1993. *J. Climate*, **7**, 1794-1802.
- Jones, P.D., S.C.B. Raper, R.S. Bradley, H.F. Diaz, P.M. Kelly, and T.M.L. Wigley, 1986: Northern Hemisphere surface air temperature variations, 1851-1984. *J. Clim. Appl. Meteorol.*, **25**, 161-179.
- Jones, C., D.E. Waliser, and C. Gautier, 1998: The influence of the Madden-Julian Oscillation on ocean surface heat fluxes and sea surface temperature. *J. Climate*, **11**, 1057-1072.
- Kagan, R.L., 1997: Averaging of meteorological field. L.S. Gandin and T.M. Smith (eds.), Kluwer Academic Publishers, 279pp.
- Kaiser, D.P., 1998: Analysis of total cloud amount over China; 1951-1994. *Geophys. Res. Lett.*, **19**, 3599-3602.

- Kalnay, E.M., and Coauthors, 1996: The NCEP/NCAR 40-year Reanalysis Project. *Bull. Amer. Meteor. Soc.*, **77**, 437-471.
- Karl, T.R., and P.M. Steurer, 1990: Increased cloudiness in the United States during the first half of the twentieth century: fact of fiction? *Geophys. Res. Lett.*, **17**, 1925-1928.
- Karl, T.R., and A.J. Koscielny, 1982: Drought in the United States: 1895-1981. *J. Climatol.*, **2**, 313-329.
- Karl, T.R., P.D. Jones, R.W. Knight, G. Kukla, N. Plummer, V. Razuvayev, K.P. Gallo, J. Lindseay, R.J. Charlson, and T.C. Peterson: 1993: Asymmetric trends of daily maximum and minimum temperature. *Bull. Amer. Meteorol. Soc.*, **74**, 1007-1023.
- Karl, T.R., and R.W. Knight, 1998: Secular trends of precipitation amount, frequency and intensity in the United States. *Bull. Amer. Meteorol. Soc.*, **79**, 231-242.
- Karl, T.R., R.W. Knight, G. Kukla, and J. Gavin, 1995: Evidence for radiative effects of anthropogenic sulfate aerosols in the observed climate record. *Aerosol forcing of climate*, R.J. Charlson and J. Heintzenberg (eds.), John Wiley & Sons Ltd., 364-382.
- Kendall, M.G., and A. Stuart, 1967: *Interence and relationship. Vol. 2, The advanced Theory of Statistics*. Charles Griffin, 690 pp.
- Kiehl, J.T., 1994: Sensitivity of a GCM climate simulation to differences in continental versus maritime cloud drop size. *J. Geophys. Res.*, **99**, 23 107-23 115.
- Klein, S.A., and D.L. Hartmann, 1993: The seasonal cycle of low stratiform clouds. *J. Climate*, **6**, 1587-1606.
- Lucas, C., E.J. Zipser, and M.A. LeMone, 1994b: Convective available potential energy in the environment of oceanic and continental clouds: Correction and comments. *J. Atmos. Sci.*, **51**, 3829-3830.
- Lucas, C., E.J. Zipser, and M.A. LeMone, 1994a: Vertical velocity in oceanic convection off tropical Australia. *J. Atmos. Sci.*, **51**, 3183-3193.
- Mitchell, J.F.B., 1989: The "greenhouse" effect and climate change. *Reviews of Geophysics*, **27**, 115-139.
- Nicholls, N., G.V. Gruza, J. Jouzel, T.R. Karl, L.A. Ogallo, and D.E. Parker, 1996: Observed climate variability and change. In *Climatic Change 1995: The IPCC Second Assessment* (eds. J.T. Houghton et al.), Cambridge University Press, Cambridge, pp. 137-181.
- Norris, J.R., 1998a: Low cloud type over the ocean from surface observations. Part I: Relationship to surface meteorology and the vertical distribution of temperature and moisture. *J. Climate*, **11**, 369-382.

- Norris, J.R., 1998b: Low cloud type over the ocean from surface observations. Part II: Geographical and seasonal variations. *J. Climate*, **11**, 383-403.
- Norris, J.R., 1999: On trends and possible artifacts in global ocean cloud cover between 1952 and 1995. *J. Climate*, **12**, 1864-1870.
- Norris, J.R., and C.B. Leovy, 1994: Interannual variability in stratiform cloudiness and sea surface temperature. *J. Climate*, **7**, 1915-1925.
- Peterson, T.C., V.S. Golubev, and P.Ya. Groisman, 1995: Evaporation losing its strength. *Nature*, **377**, 687-688.
- Phillips, T.J., 1996: Documentation of the AMIP models on the World Wide Web. *Bull. Amer. Soc.*, **77**, 1191-1196.
- Plantico, M.S., and T.R. Karl, 1990: Is recent climate change across the United States related to rising levels of anthropogenic greenhouse gases? *J. Geophys. Res.*, **95**, 16 617-16 637.
- Ramanathan, V., 1987: The role of Earth radiation budget studies in climate and general circulation research. *J. Geophys. Res.*, **92**, 4075-4095.
- Ramanathan, V., P.J. Crutzen, J. Coakley, R. Dickerson, A. Heymsfield, J. Kiehl, D. Kley, T.N. Krishnamurti, J. Kuettner, J. Lelieveld, A.P. Mitra, J. Prospero, R. Sadourny, F.P.J. Valero, and E.L. Woodbridge, 1995: Indian Ocean Experiment (INDOEX) White Paper, *C4/SIO/UCSD Publications*.
- Ramanathan, V., and W. Collins, 1991: Thermodynamic regulation of ocean warming by cirrus clouds deduced from observations of the 1987 El Nino. *Nature*, **351**, 27-32.
- Raval, A., and V. Ramanathan, 1989: Observational determination of the greenhouse effect. *Nature*, **342**, 758-761.
- Razuvaev, V.N., E.G. Apasova, and R.A. Martuganov, 1993: Daily temperature and precipitation data for 223 USSR stations. *ORNL/CDIAC-56, NDP-040, ESD Publ. No. 4194*, Carbon Dioxide Information Data Center, Oak Ridge National Lab, Oak Ridge, TN., 47 pp. + Appendices.
- Robinson, D.A., K.F. Dewey, and R.R. Heim Jr., 1993: Global snow cover monitoring: An update. *Bull. Amer. Meteor. Soc.*, **74**, 1689-1696.
- Ross, R.J., and W.P. Elliott, 1996: Tropospheric water vapor climatology and trends over North America; 1973-1993. *J. Climate*, **9**, 3561-3574.
- Ross, R.J., and W.P. Elliott. 1998: Northern Hemisphere water vapor trends. *Proc. of Ninth Symposium on Global Change Studies, Amer. Meteor. Soc.*, 11-16 January 1998, Phoenix, Arizona, 39-41.
- Rossow, W.B., and R.A. Schiffer, 1991: ISCCP cloud data products. *Bull. Amer. Meteor. Soc.*, **72**, 2-20.

- Rossow, W.B., A.W. Walker, and L.C. Garder, 1993: Comparison of ISCCP and other cloud amounts. *J. Climate*, **6**, 2394-2418.
- Rossow, W.B., and L.C. Garder, 1993: Cloud detection using satellite measurements of infrared and visible radiances for ISCCP. *J. Climate*, **6**, 2370-2393.
- Rossow, W.B., and R.A. Schiffer, 1999: Advances in understanding clouds from ISCCP. *Bull. Amer. Meteor. Soc.*, **80**, 2261-2288.
- Santer, B.D., J.J. Hnilo, T.M.L. Wigley, J.S. Boyle, C. Doutriaux, M. Firino, D.E. Parker, and K.E. Taylor, 1999: Uncertainties in observationally based estimates of temperature change in the free atmosphere. *J. Geophys. Res.*, **104**, 6305-6333.
- Serreze, M., J.E. Walsh, F.S. Chapin III, T. Ostercampf, M. Dyrgerov, V. Romanovsky, W.C. Oechel, J. Morrison, T. Zhang, and R.G. Roger: Observational evidence of recent changes in the northern high latitude environment. *Climatic Change*. (in press)
- Shinoda, T., H.H. Hendon, and J. Glick, 1998: Intraseasonal variability of surface fluxes and sea surface temperature in the tropical western Pacific and Indian Oceans. *J. Climate*, **11**, 1685-1702.
- Spencer, R.W., and J.R. Christy, 1990: Precise monitoring of global temperature trends from satellites. *Science*, **247**, 1558-1562.
- Stephens, G.L., A. Slingo, M. Webb, and I. Wittmeyer, 1994: Observations of the earth's radiation budget in relation to atmospheric hydrology. Part IV. *J. Geophys. Res.*, **99**, 18 595-18 604.
- Stokes, G.M., and S.E. Schwartz, 1994: The Atmospheric Radiation Measurement (ARM) Program: Programmatic background and design of the cloud and radiation test bed. *Bull. Amer. Meteor. Soc.*, **75**, 1201-1221.
- Stuart, R.A., and G.A. Isaac, 1994: A comparison of temperature-precipitation relationships from observations and as modeled by the general circulation model of the Canadian Climate Centre. *J. Climate*, **7**, 277-282.
- Sun, B., and P.Ya. Groisman, 1999: Cloud effects on the near surface temperature: temporal changes. *Proc. of Tenth Symposium on Global Change Studies, Amer. Meteor. Soc.*, 10-16 January 1999. Dallas, Texas, 227-281.
- Sun, B., and P. Ya. Groisman, 2000: Cloudiness variations over the former Soviet Union. *Int. J. Climatology*. (in press)
- Sun, B., P.Ya. Groisman, and I.I. Mokhov, 2000a: Intensification of convective processes in the Northern Hemisphere mid-latitudes: Evidence from changes in cloud type frequency over the United States and the former USSR. *J. Climate* (in press).

- Sun, B., P.Ya. Groisman, R.S. Bradley, and F.T. Keimig, 2000b: Temporal changes in the observed relationship between cloud cover and surface air temperature. *J. Climate* (in press).
- Thiessen, A.H., 1911: Precipitation averages for large areas. *Mon. Wea. Rev.*, **39**, 1082-1082.
- USAFETAC, 1986: *DATSAV2 Surface USAFETAC Climatic Database*. User Handbook No.4 December 1986. USAF Environmental Technical Application Center, Operating Location A, Federal Building, Asheville, NC. 6 pp.+ Appendices.
- Vinnikov, K.Ya, and A. Robock, 1996: Scales of temporal and spatial variability of mid-latitude soil moisture. *J. geophys. Res.*, **101**, 7163-7174.
- Vinnikov, K.Ya., P.Ya. Groisman, 1979: An empirical model of the present-day climatic changes. *Meteorol. Hydrol.*, **3**, 25-36 (in Russian, in English in *Soviet Meteorology and Hydrology*).
- Vinnikov, K.Ya., P.Ya. Groisman, 1982: Empirical study of climate sensitivity. *Physics of Atmosphere and Oceans*, **18**, 1159-1169.
- Vinnikov, K.Ya., P.Ya. Groisman, and K.M. Lugina, 1990: The empirical data on modern global climate changes (temperature and precipitation). *J. Climate*, **3**, 662-677.
- Wang, J., and W.B. Rossow, 1998: Effects of cloud vertical structure on atmospheric circulation in the GISS GCM. *J. Climate*, **11**, 3010-3029.
- Warren, S.G., C.J. Hahn, J. London, R.M. Chervin, and R.L. Jenne, 1986: Global distribution of total cloud cover and cloud type amounts over land, NCAR Tech. Note, NCAR/TN-273+STR, 29pp+200 maps.
- Weare, B.C., 1994: Interrelationships between cloud properties and sea surface temperatures on seasonal and interannual time scales. *J. Climate*, **7**, 248-260.
- Weare, B.C., and AMIP modeling groups, 1996: Evaluation of the vertical structure of zonally averaged cloudiness and its variability in the Atmospheric Model Intercomparison Project. *J. Climate*, **9**, 3419-3431.
- Weaver, C.P., and V. Ramanathan, 1997: Relationships between large-scale vertical velocity, state stability, and cloud radiative forcing over Northern Hemisphere extratropical oceans. *J. Climate*, **10**, 2871-2887
- Wielicki, B.A., R.D. Cess, M.D. King, D.A. Randall, and E.F. Harrison, 1995: Mission to planet Earth: Role of clouds and radiation in climate. *Bull. Amer. Meteor. Soc.*, **76**, 2125-2153.
- WMO, 1975: *Manual on the observation of clouds and other meteors*. World Meteorological Organization. Publ. 407, 155 pp.

- Woodruff, S.D., R.J. Slutz, R.L. Jenne, and P.M. Steurer, 1987: A comprehensive ocean-atmosphere data set. *Bull. Amer. Meteor. Soc.*, **68**, 1239-1250.
- Yao, M.-S., and A.D. Del Genio, 1999: Effects of cloud parameterization on the simulations of climate changes in the GISS GCM. *J. Climate*, **12**, 761-779.
- Ye, B., A.D. Del Genio, and K.-W. Lo, 1997: CAPE variations in the current climate and in a climate change. *J. Climate*, **11**, 1997-2015.
- Zhai, P.-M., and R.E. Eskridge, 1997: Atmospheric water vapor over China. *J. Climate*, **10**, 2643-2652.
- Zeng, X., and R.E. Dickinson, 1998: Effect of surface sublayer on surface skin temperature and fluxes. *J. Climate*, **11**, 537-550.
- Zhang, Y.-C., W.B. Rossow, and A.A. Lacis, 1995: Calculation of surface and top of atmosphere radiation fluxes from physical quantities based on ISCCP data sets. Part I: Methods and sensitivity to input data uncertainties. *J. Geophys. Res.*, **100**, 1149-1165.